AD-A036 435

AUTOMATIC TARGET HAND-OFF USING CORRELATION TECHNIQUES

AUBURN UNIVERSITY
ALABAMA

31 JANUARY 1977

Automatic Target Hand-Off Using Correlation Techniques

by

J. S. Boland, III, L. J. Pinson, G. R. Kano
M. A. Hennell, and E. G. Peters

Electrical Engineering Department
Auburn University
Auburn, Alabama 36830

Technical Report
February 1977

ENGINEERING EXPERIMENT STATION
Auburn University
Auburn, Alabama 36830

DISPOSITION INSTRUCTIONS

DESTROY THIS REPORT WHEN IT IS NO LONGER NEEDED. DO NOT RETURN IT TO THE ORIGINATOR.

DISCLAIMER

THE FINDINGS IN THIS REPORT ARE NOT TO BE CONSTRUED AS AN OFFICIAL DEPARTMENT OF THE ARMY POSITION UNLESS SO DESIGNATED BY OTHER AUTHORIZED DOCUMENTS.

TRADE NAMES

USE OF TRADE NAMES OR MANUFACTURERS IN THIS REPORT DOES NOT CONSTITUTE AN OFFICIAL INDORSEMENT OR APPROVAL OF THE USE OF SUCH COMMERCIAL HARDWARE OR SOFTWARE.

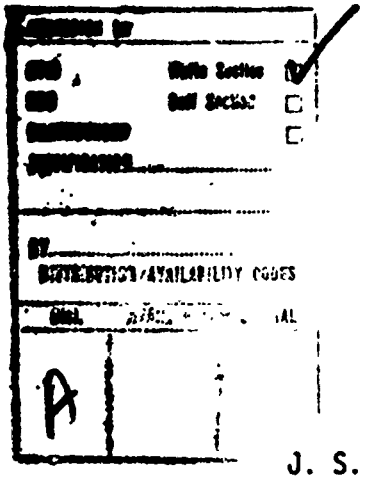

AUTOMATIC TARGET HAND-OFF USING CORRELATION TECHNIQUES

by

J. S. Boland, III, L. J. Pinson, G. R. Kane

M. A. Honnell, and E. G. Peters

Electrical Engineering Department
Auburn University
Auburn, Alabama 36830

Final Technical Report
For the Period 5 December 1975 - 31 January 1977

This research work was supported by
U.S. Army Missile Command
Redstone Arsenal, Alabama 35809
under Contract DAAH01-76-C-0396

ENGINEERING EXPERIMENT STATION
Auburn University
Auburn, Alabama 36830

31 January 1977

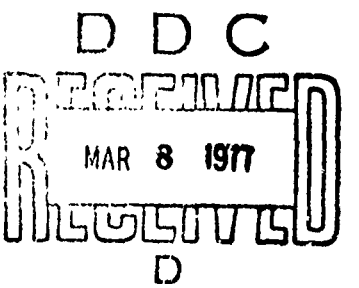

Cleared for Public Release; Distribution Unlimited

SECURITY CLASSIFICATION OF THIS PAGE (When Data Entered)

REPORT DOCUMENTATION PAGE		READ INSTRUCTIONS BEFORE COMPLETING FORM
1. REPORT NUMBER	2. GOVT ACCESSION NO.	3. RECIPIENT'S CATALOG NUMBER
4. TITLE (and Subtitle) AUTOMATIC TARGET HAND-OFF USING CORRELATION TECHNIQUES		5. TYPE OF REPORT & PERIOD COVERED Final Technical Report, 5 Dec. 1975 - 31 Jan. 1977 6. PERFORMING ORG. REPORT NUMBER
7. AUTHOR(s) J. S. Boland, III, L. J. Pinson, G. R. Kane, M. A. Honnell, and E. G. Peters		8. CONTRACT OR GRANT NUMBER(s) DAAH01-76-C-0396
9. PERFORMING ORGANIZATION NAME AND ADDRESS Engineering Experiment Station Auburn University Auburn, AL 36830		10. PROGRAM ELEMENT, PROJECT, TASK AREA & WORK UNIT NUMBERS
11. CONTROLLING OFFICE NAME AND ADDRESS Commander, U.S. Army Missile Command ATTN: DRSMI-RGC Redstone Arsenal, AL 35809		12. REPORT DATE 31 January 1977 13. NUMBER OF PAGES 148
14. MONITORING AGENCY NAME & ADDRESS(if different from Controlling Office)		15. SECURITY CLASS. (of this report) UNCLASSIFIED 15a. DECLASSIFICATION/DOWNGRADING SCHEDULE

16. DISTRIBUTION STATEMENT (of this Report)

Cleared for Public Release; Distribution Unlimited

17. DISTRIBUTION STATEMENT (of the abstract entered in Block 20, if different from Report)

18. SUPPLEMENTARY NOTES

19. KEY WORDS (Continue on reverse side if necessary and identify by block number)

Correlation, Target Hand-Off, Image Correlation

20. ABSTRACT (Continue on reverse side if necessary and identify by block number)

The problem of automatic hand-off of a target from a precision pointing and tracking system (PTS) to an imaging missile seeker is considered in this report. The approach taken is to search for the target in the seeker field of view (FOV) using the PTS video as a reference. When the target is located, the seeker line of sight is adjusted automatically such that the target is at the center of its FOV at which point the seeker tracker can lock on to the target.

DD FORM 1 JAN 73 1473 EDITION OF 1 NOV 65 IS OBSOLETE

SECURITY CLASSIFICATION OF THIS PAGE (When Data Entered)

Item 20 (Con't)

Location of the target in the seeker FOV can best be accomplished using correlation techniques. The approach taken is to consider the most accurate but yet most costly in computation time and hardware requirements. Trade-offs are then considered in order to obtain a real-time correlator (i.e., one which can compute the correlation surface at the rate of the incoming live video from the seeker). The effect of these trade-offs on correlation accuracy and other system performance criteria is given. A correlation algorithm is chosen and an implementation of this algorithm is given. An alternate implementation using an analog adder rather than a digital adder tree is recommended.

TABLE OF CONTENTS

TABLE OF CONTENTS (Con't)

LIST OF FIGURES

LIST OF FIGURES (Con't)

LIST OF FIGURES (Con't)

LIST OF TABLES

1. INTRODUCTION

Currently the U. S. Army is developing a system for the acquisition, tracking, and laser designation of military targets from helicopters. The Army is also developing terminal homing guided weapons capable of destroying designated military targets. The Army is also beginning to investigate missiles which have imaging seekers rather than laser seekers to provide guidance. This provides a true fire and forget weapon system. Very little attention has been given to-date to the problem of hand-off of a target from the acquisition system to the imaging missile seeker. This task can be accomplished by the gunner using the video display from both systems on his monitor. However, this technique is time consuming resulting in increased helicopter exposure time. As a result the U. S. Army Missile Command, Huntsville, Alabama let a contract with the Engineering Experiment Station, Auburn University to study and make a recommendation for a system to accomplish automatic hand-off of targets from designators to imaging missile seekers using correlation techniques. This report presents the result of that effort.

The overall system consists of the helicopter with pilot and gunner displays and controls, the pointing and tracking system (PTS), either integrally mounted or on the stores wing of the helicopter as shown in Figure 1, and the missiles located in a stores rack also mounted on the wing of the helicopter. The helicopter supplies power and other electronic support hardware for both systems. The pointing

and tracking system typically consists of an optics train, line-of-sight (LOS) stabilization system, day TV and forward looking infra-red (FLIR) imaging systems, manual and autotrack system, laser range finder, and associated electronics section. The imaging missile seeker could be a day TV system or a FLIR. The current advanced television seeker (ATVS) being tested by the Army [1] is composed of optical, day television camera, TV tracker, mode control, stabilization and power supply subsystems.

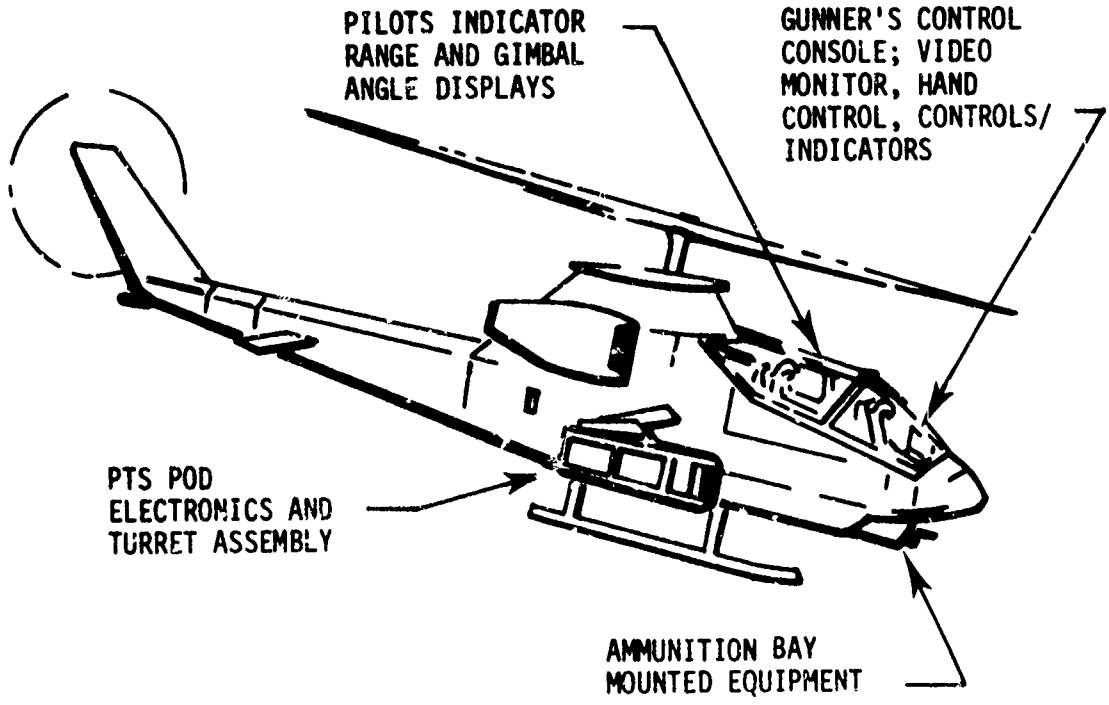

Figure 1. PTS equipment location on AH-1 helicopter.

In order to accomplish hand-off using correlation techniques, the two signals being correlated must be similar. If both the PTS and missile seeker are day TV systems sensitive in the same relative optical spectrum, correlation can be accomplished with very little signal preprocessing. However, if the two signals are dissimiliar such as from a day TV and FLIR, then correlation possibly can be accomplished but only after considerable preprocessing of the signals. For example, correlation on edges alone might work in this case. The correlator developed in this report is for two day - TV sensors. The problem of dissimilar sensors is discussed, however, in Chapter III.

A. Scope of Work

The scope of work performed under this contract was to analyze and make recommendations on the hardware and software required to be used in "handing-off" a target from a target acquisition device to an imaging missile seeker. The function of an automatic correlator is to compare the video signals from the high resolution pointing and tracking system (PTS) and from the missile seeker and to generate error signals which can be used to drive the missile seeker such that its aimpoint coincides with that of the PTS. The scope of work as written in the contract is given in the following six paragraphs for completeness.

The first phase will be to choose one or more candidate correlation approaches. This will be done by surveying the literature for information on existing correlation techniques. It is realized that some difficulty

may arise since most companies have developed correlation techniques using their own funds and therefore consider them proprietary. It is likely, however, that some information on general correlation techniques is available in the open literature.

Along with such information as is available on existing techniques, an independent solution to the "hand-off" problem will be proposed considering the variables involved (i.e., fields-of view, system resolutions, stabilization, and others). The approach will be to consider first the most accurate and complex correlation technique and propose trade-offs in Phase Three.

Since the target may not necessarily be in the seeker field of view (FOV), an algorithm will be proposed to slew the seeker TV until the target is in its FOV. Of course, it is expected that this operation will be very time consuming and should be avoided if possible. One possible alternative is to determine and store in the fire control computer boresight errors while in flight before a target is engaged. The trade-off of additional software and computer memory required by these two methods will be considered.

Phase Two, which will actually be conducted concurrently with Phase One, will consist of an investigation of the hardware and software needed for various combinations of PTS and missile seeker configurations. Consideration will be given to differing fields-of-view, scan rates, stabilization of TV cameras, boresight, and TV format (such as aspect ratio, frames per second, etc.). The contractor will consider various combinations and recommend the hardware and software necessary to implement each.

Phase Three will consist of the actual analysis of complexity of the hardware/software necessary to implement the various combinations of Phase Two. This analysis will be presented in such a way that MICOM will be able to use it to make a trade-off of the various options available (e.g., complex/versatile vs. simple/closely bounded).

In Phase Four a correlation technique, along with the system constraints, will be chosen in concert with the MICOM technical director. This decision will be based on the results of the first three phases. The hardware and software to implement this approach will be completely specified, and the correlation algorithm will be developed.

B. Organization of Report

All of the work outlined in the Scope of Work has been completed and is documented in this final report. Chapter two formulates the hand-off problem in greater detail and gives the various correlation techniques considered. As expected, all companies contacted either did not respond or gave very little detail into their correlation algorithms. As a result, the effort on this contract started with a literature search of correlation techniques, defining the most accurate but most time consuming methods, and making trade-offs in order to arrive at an implementable solution.

Chapter three goes into detail on the many correlation system considerations which had to be resolved before an implementable solution could be attained. These considerations range from the system optics,

TV sensor and TV format, electronic preprocessing, sampling rates, two system resolutions, vibration analysis, slaving of two systems before correlation, derivation of error signals to drive the seeker gimbals, and others.

Two possible implementations of the correlation algorithm are given in Chapter four. The first implementation was considered to be the state-of-the-art up until October when TRW publicly announed their 64 bit, 20 MHz bipolar correlator LSI circuit. The second implementation incorporates this TRW chip and significantly simplifies the hardware. The reason for giving both implementations is to emphasize how LSI state-of-the-art can effect the real-time correlation problem. It is known that TRW, and possibly other companies, is working on another LSI correlator chip which will simplify the implementation further or make possible an implementation which now is not feasible for real-time correlation.

Chapter five gives the conclusions and recommendations resulting from the above work. Questions which arose during the course of this work but were not answered due to lack of time or lack of simulation facilities are also given.

2. FORMULATION AND COMPARISON OF CORRELATION ALGORITHMS

In this chapter the basic correlation problem is formulated, four methods are presented to solve the problem, and finally a comparison of the four methods is given. Two of the methods are shown to be impractical at the present state-of-the-art because of computational burden.

A. Geometric Layout of PTS and Missile Seeker TV Images

For the purpose of designing a correlator, this report will consider hypothetical PTS and missile seeker day TV systems. To design a correlator for a particular PTS and missile seeker, some of the design parameters will have to be changed but the basic procedure will be identical. Consider a PTS system with a vertical narrow field of view (NFOV) of .5°, a 525 line standard TV system with 2:1 interlace, 60 Hz field rate, or 30 Hz frame rate, and a 1:1 aspect ratio. The sensor TV will be assumed to have a 2° vertical FOV with 4:3 aspect ratio, a 525 line standard TV system with 2:1 interlace 60 Hz field rate, or 30 Hz frame rate. Both systems because of vertical retrace will be considered to have 480 active TV lines.

One of the fundamental requirements for correlation using any of the methods of the next section is that the two TV images be preprocessed such that the scenes have the same spatial resolution. Since both TV systems have 480 active TV lines, the PTS will have 4 times as many lines on a given target as the missile seeker TV because of the 1:4 FOV ratio as shown in Figures 2 and 3. Since the resolution of the seeker

TV cannot be increased, the obvious solution is to decrease the PTS resolution by a factor of four. This can be accomplished by averaging the PTS video as shown in Chapter III. For the remainder of this chapter it will be assumed that the PTS image, henceforth referred to as the high resolution (HR) image, and the seeker image, henceforth referred to as the low resolution (LR) image have been preprocessed such that they have the same spatial resolution prior to application of any correlation algorithm.

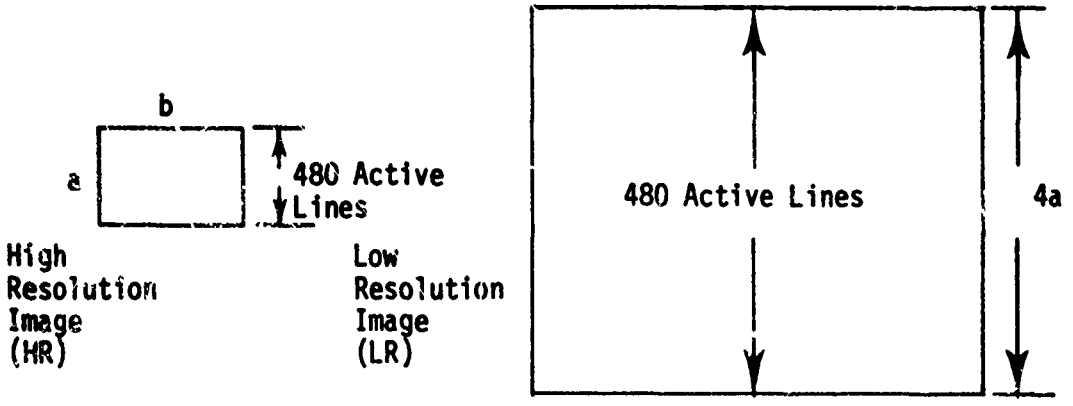

Figure 2. Target space projection of narrow & wide FOV images.

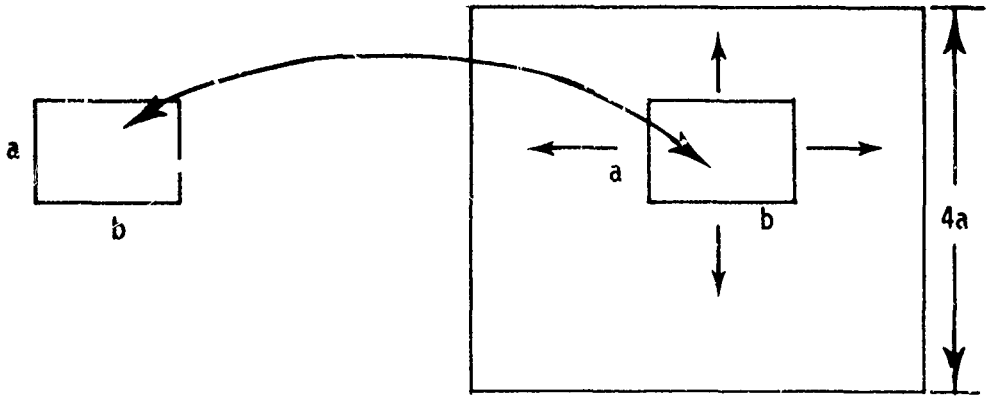

Figure 3. HR image projected onto LR image.

After the resolutions of the two images are equalized a number of correlation or matching methods can be investigated. For the remainder of this report the dimensional relationships between the two images will be as shown in Figure 4.

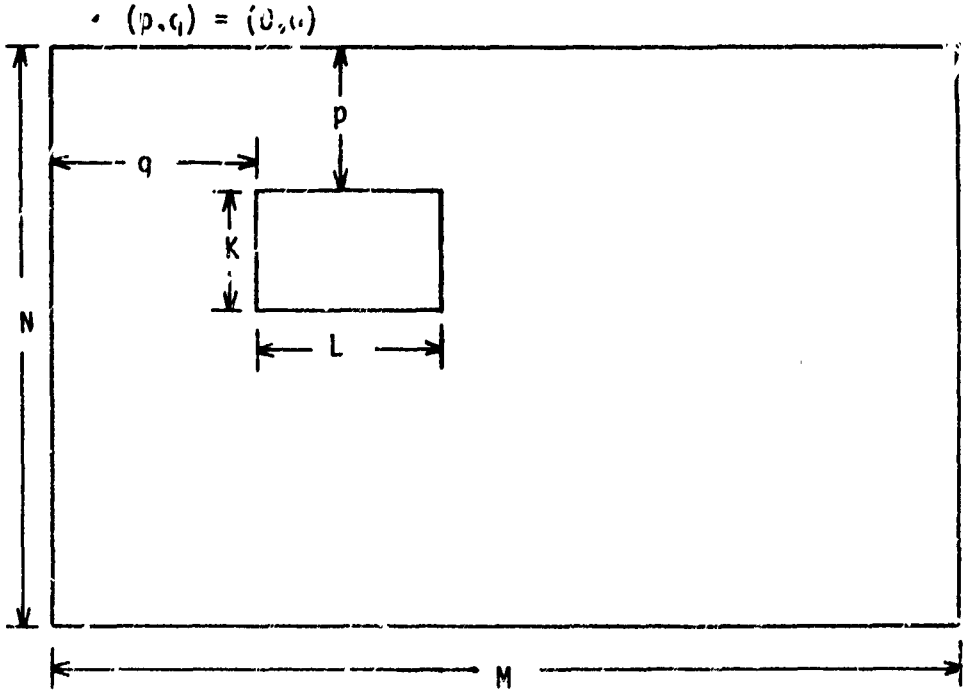

Figure 4. K x L HR image located at position (p,q) of N x M LR image.

The missile seeker image is represented by a N X M array of points. The values of N and M would be determined from a choice of sampling rate and number of TV lines of the missile seeker system. The PTS image or HR image is represented by a K X L array of points in Figure 4. This K X L array might be all or only a portion, containing the target, of the PTS image after its resolution has been changed to that of the missile seeker image. The p and q dimensions in Figure 4 give the vertical and horizontal position of the HR image in the LR image. These indices start in the upper left corner of the LR image, where p = q = 0.

B. Image Comparison Methods

For digital matching of two images a number of alternatives exist. In this section four candidate algorithms are presented and explained. A detailed comparison of these methods is given in Section C of this chapter.

1. Direct Method

The classical approach to the problem of determining where two signals match is correlation. Consider two functions $f_1(t)$ and $f_2(t)$ as shown in Figure 5. The correlation integral is defined to be

$$C(\tau) = \int_{-\infty}^{\infty} f_1(t)\, f_2(t + \tau)dt \qquad (1)$$

where τ is allowed to take on values between $-\infty$ and $+\infty$. The value of τ which maximizes $C(\tau)$ in Equation 1 is the correlation peak and is defined to be the match point between the two signals. In Figure 5 this will occur when $\tau = t_2 - t_1$. It is obvious that determining the correlation peak consists of multiplying one signal by the other signal shifted by τ and then evaluating the area under the resulting curve.

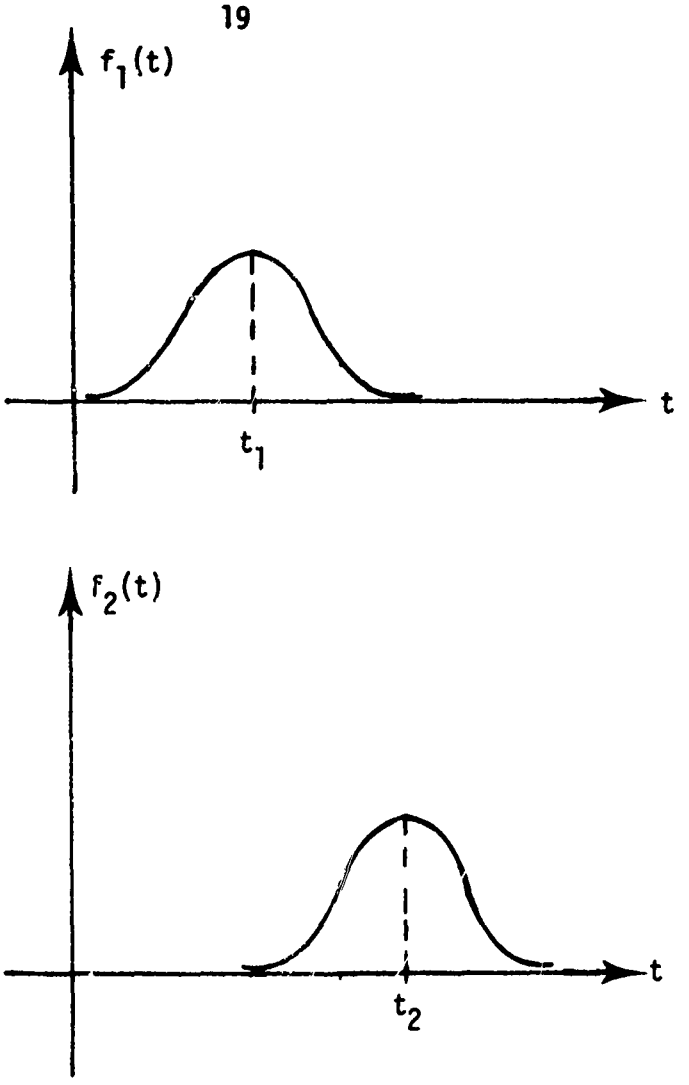

Figure 5. Two functions to be correlated.

If both signals are sampled and held, then Equation 1 can be approximated by the following equation.

$$C(p) = T \sum_{n=-\infty}^{\infty} f_1(n) f_2(n + p) \qquad (2)$$

where $f_1(n) = f_1(nT)$ and $f_2(n + p) = f_2(nT + pT)$ and T is the sampling interval. As T becomes very small, the result in Equation 2 approaches that of Equation 1 where the p which maximizes C(p) is defined as the correlation point.

The two TV images are first sampled and preprocessed to match spatial resolution and then stored in arrays. The HR image is a K X L array and the LR image is a N X M array as shown in Figure 4. Therefore a two-dimensional discrete correlation algorithm is given by

$$R(p,q) = \frac{1}{KL} \sum_{n=1}^{K} \sum_{m=1}^{L} HR(n,m)\, LR(n+p,m+q)$$

$$\text{for} \quad 0 \leq p \leq N - K$$

$$0 \leq q \leq M - L \qquad (3)$$

where R(p,q) is the correlation function, and the division by KL is a scaling factor. Equation 3 is referred to as the Direct Method in this report.

Using the algorithm of Equation 3, the selected K X L array of HR points is compared to each array of LR points of dimension K X L in the total N X M LR array. The algorithm produces the correlation array R(p,q). In most situations the maximum value of the correlation function indicates image registration or match. However, in the present case since the LR image spans a wider field-of-view, R(p,q) is actually a cross-correlation, and therefore it is possible that the maximum value of the correlation function does not indicate a target match between the HR and LR image. In order that the maximum value of the correlation function indicate target location in the LR image, both image array values need to be normalized. Once normalization is accomplished, the calculation of correlation points is insensitive to magnitude values and depends on the pattern of data points found in the K X L arrays of the LR image. Therefore, in order to use the Direct Method, image normalization must be implemented. Image normalization is

discussed in further detail in Section C of this chapter.

2. Fast Fourier Transform (FFT) Method

Because of the transform relationship between correlation and power spectral density, the cross correlation between the HR and LR images is given by

$$R(p,q) = \text{IFFT}\{|\text{FFT}[HR(n,m)]\ \text{FFT}[LR(n,m)]|\}$$

$$= \text{IFFT}\{G(k,1)\} \qquad (4)$$

where FFT [·] is the fast fourier transform, IFFT is the inverse fast fourier transform, G(k,1) is the cross power spectral density of HR and LR and R(p,q) is the cross correlation function. In Equation 4 both the HR and LR arrays have to be the same size and preferably be a power of two. To accomplish this both arrays are filled out with zeroes to form 512 x 512 arrays. The result yields 512 x 512 values of R(p,q).

3. Phase Correlation Method

A major problem in correlating two different size images is that the resultant correlation function is in fact a cross-correlation instead of the desired auto-correlation. The auto-correlation function has its maximum value for zero relative shift; this is not necessarily true for the cross-correlation function. Thus it is quite possible that the

cross-correlation function will have false peaks which are larger than the peak for zero shift. The false peak condition can occur quite easily for portions of the LR image of high brightness, especially if the smaller HR image is of lesser brightness. Therefore, the problem is one which depends on relative magnitudes of the various sub-elements of the larger image.

One technique that reduces magnitude effects in the cross-correlation function is phase correlation. The phase correlation function between the HR and LR images is given by

$$R(p,q) = \text{IFFT}\left\{\frac{\{\text{FFT}[HR(n,m)]\}\{\text{FFT}[LR(n,m]\}^*}{|\{\text{FFT}[HR(n,m)]\}\{\text{FFT}[LR(n,m)]\}^*|}\right\} \quad (5)$$

where * denotes the conjugate.

The phase correlation method is essentially a point-by-point normalization in the frequency domain of the cross-power spectrum. The same requirements on the size of the HR and LR arrays exists as for the FFT method.

4. Sequential Similarity Detection Algorithm (SSDA)

Another algorithm for determining the similarity and amount of registration between two images is known as a Sequential Similarity Detection Algorithm (SSDA). Consider a K X L HR image (reference image) and a N X M LR image. The SSDA registration surface is computed by adding the absolute value of the difference between the HR and LR pixels for each value of p and q as given by Equation 6.

$$E(p,q) = \sum_{n=1}^{k} \sum_{m=1}^{L} |HR(n,m) - LR(n+p, m+q)| \qquad (6)$$

for $0 \leq p \leq N - K$

$0 \leq q \leq M - L$

The registration point (denoted by p*, q*) is the value of p and q for which E is a minimum. The advantage of this method over the Direct Method is that subtraction circuits rather than multiplication circuits are needed for implementation. It should be pointed out, however, that the SSDA method is not a correlation technique since Equation 6 is not related to Equation 1, the correlation integral. A further comparison of these two methods is given in later sections of this report.

C. Analysis of Image Comparison Methods

1. Image Normalization

As stated in Section B of this chapter it is necessary to normalize the correlation algorithms so that false peaks are less likely to occur. False peaks can occur for the following reasons:

a. For correlation computations using the Fast Fourier Transform (FFT), the two arrays must be the same size. To accomplish this the HR array is filled in with zeroes to make it the same size as the LR array (array sizes must be a power of two). Therefore the two images being correlated are not identical which means the computation is a cross-correlation rather than an auto-correlation. There is more of a possibility for false peaks (any peak which does not correspond to correct registration) in cross-correlation than in auto-correlation.

b. The size of the target in the HR array may be slightly different from its size in the LR array. This could be caused by the ratio of the field of views (FOV) being slightly different from the assumed ratio or by the FOV ratio not being an integer number. This reduces the magnitude of the peak at the actual correlation point which could result in an erroneous decision.

c. Contrast differences in the two TV signals could cause a false peak.

d. Differences in illumination levels can cause false peaks. To illustrate this consider the Direct Method given in Equation 3. In the ideal case of exact correlation each LR pixel is exactly equal to the corresponding HR pixel

$$R(p^*, q^*) = \frac{1}{KL} \sum_{n=1}^{k} \sum_{m=1}^{L} HR^2(n,m) \tag{7}$$

where p* and q* denote the coordinates for perfect registration. For this ideal case consider a non-matching coordinate point $\hat{p}$, $\hat{q}$ where

$$LR(n+\hat{p},m+\hat{q}) = \max_{n,m} HR(n,m) = HR_{max} \tag{8}$$

Then

$$R(\hat{p},\hat{q}) = \frac{1}{KL} \sum_{n=1}^{k} \sum_{m=1}^{L} HR(n,m)HR_{max} \geq R(p^*,q^*) \tag{9}$$

It is easily seen that even in the perfect registration case, a search for the peak value of R(p,q) does not necessarily yield the correct registration point. For the Direct Method, normalization can be accomplished as follows:

$$R(p,q) = \frac{\left[\sum_{n=1}^{k}\sum_{m=1}^{L} HR(n,m)LR(n+p,m+q)\right]^2}{\left[\sum_{n=1}^{k}\sum_{m=1}^{L} HR^2(n,m)\right]\left[\sum_{n=1}^{k}\sum_{m=1}^{L} LR^2(n+p,m+q)\right]} \qquad (10)$$

This obviously involves considerable more computation time than the unnormalized Direct Method of Equation 3.

For the FFT Method, normalization can be accomplished by evaluating the IFFT of the phase correlation function as outlined in Section B-3 of this chapter.

The Sequential Similarity Detection Algorithm (SSDA) can be normalized by changing Equation 6 in Section B-4 of this chapter to

$$E(p,q) = \sum_{n=1}^{k}\sum_{m=1}^{L} |HR(n,m) - \overline{HR} - LR(n+p, m+q) + \overline{LR}(p,q)| \qquad (11)$$

for $0 \leq p \leq N-K$

$0 \leq q \leq M-L$

where $\overline{LR}(p,q)$ and $\overline{HR}$ are average shades of grey and are given by

$$\overline{LR}(p,q) = \frac{1}{KL}\sum_{n=1}^{K}\sum_{m=1}^{L} LR(n+p, m+q)$$

$$\overline{HR} = \frac{1}{KL}\sum_{n=1}^{K}\sum_{m=1}^{L} HR(n,m) \qquad (12)$$

2. Problems Associated with FFT and Phase Correlation Methods

Of the four methods presented in Section B, the FFT and Phase Correlation methods are the most difficult to implement. A number of factors involved with these two methods make them somewhat less than prime candidates for the hand-off problem. Both methods require that the input arrays be square and that the dimension should be a power of two. As shown in Section A, the HR image is preprocessed because of its smaller FOV such that it is no longer the same dimension as the LR array. Therefore it would be necessary to fill the HR array with zeroes in order to make it the same size as the LR array.

Since it is not known where the target may lie in the LR image, it is required that the entire LR array be stored when using the FFT or Phase Correlation methods. The HR image also has to be stored in memory. Additional memory is also needed for the intermediate steps of these methods. The Direct Method and SSDA methods can be used with only a small percentage of the memory needed for the FFT and Phase Correlation methods. Also, both the FFT and Phase Correlation algorithms involve, at one step, complex multiplications of two-dimensional arrays. This again would add greatly to the hardware needed for their implementation that is not needed for the direct or SSDA methods. Because of the increased amount of hardware required and the fact that the FFT and Phase Correlation methods cannot be implemented in real time, the FFT and Phase Correlation methods were eliminated as candidate algorithms.

3. Quantization of the Input Video Signals

All the algorithms discussed in Section B of this chapter require that both the HR and LR video signals be digitized. The process of digitizing continuous signals can be thought of as two separate steps. The first is sampling at discrete instants of time and the second is quantization. A discussion of the selection of an appropriate sampling rate will be given in Chapters 3 and 4 of this report. In this section the different quantizers investigated are discussed and the trade-offs used in choosing a particular quantizer are given.

The input-output relationship for the four basic quantizers considered in this section are shown in Figure 6. Figure 6 (a) is the multibit quantizer or one that has a very large number of quantization levels. Since there are many fairly inexpensive commercially available 8 bit A/D converters capable of operating at 10 MHz, they will be considered as multibit quantizers.

Figure 6 (b) gives the input-output relationship of a two level or one-bit quantizer. The weight of the output is +1 if the input is above the mean voltage level and is -1 if the input is below the mean voltage level. With this quantizer a means must be provided for finding the average shade of grey of the K X L high resolution reference image and of each of the K X L sub-arrays of the low resolution image

corresponding to each set of p and q values in Equation 3. This could be done by quantizing the images with an 8 bit A/D converter, computing the average values in the host computer, during one frame, and using these computed average values for one-bit quantization during the following frame. The average signal level is not expected to change significantly from frame-to-frame. If the average signal level does change significantly from frame-to-frame, some form of adaptive average computation should be employed. A sub-optimal but real-time implementable solution to this problem is given in Chapter 3.

Figure 6 (c) is the input-output relationship for a four level or two-bit quantizer. Assuming the mean and standard deviation of the input signal are known, there are two parameters, "a" and "v_o/σ", which can be chosen so as to minimize the variance of the estimate of R (i.e., minimize the loss in S/N ratio due to quantization).

Figure 6 (d) is the input-output relationship for a three level quantizer. The advantage of this quantizer over the two-bit quantizer is that the weighting of the products in Equation 3 are either $\pm$ 1 or 0 which leads to a simpler circuit realization. The disadvantage is that the loss in S/N ratio is greater than for the two-bit quantizer. The mean and standard deviation (rms value) of the input video must be calculated for this method.

The selection of the optimum parameters, a and v_o/σ, is made from an analysis of the degradation in the mean square S/N ratio. This analysis is presented in Section C-5 of this chapter.

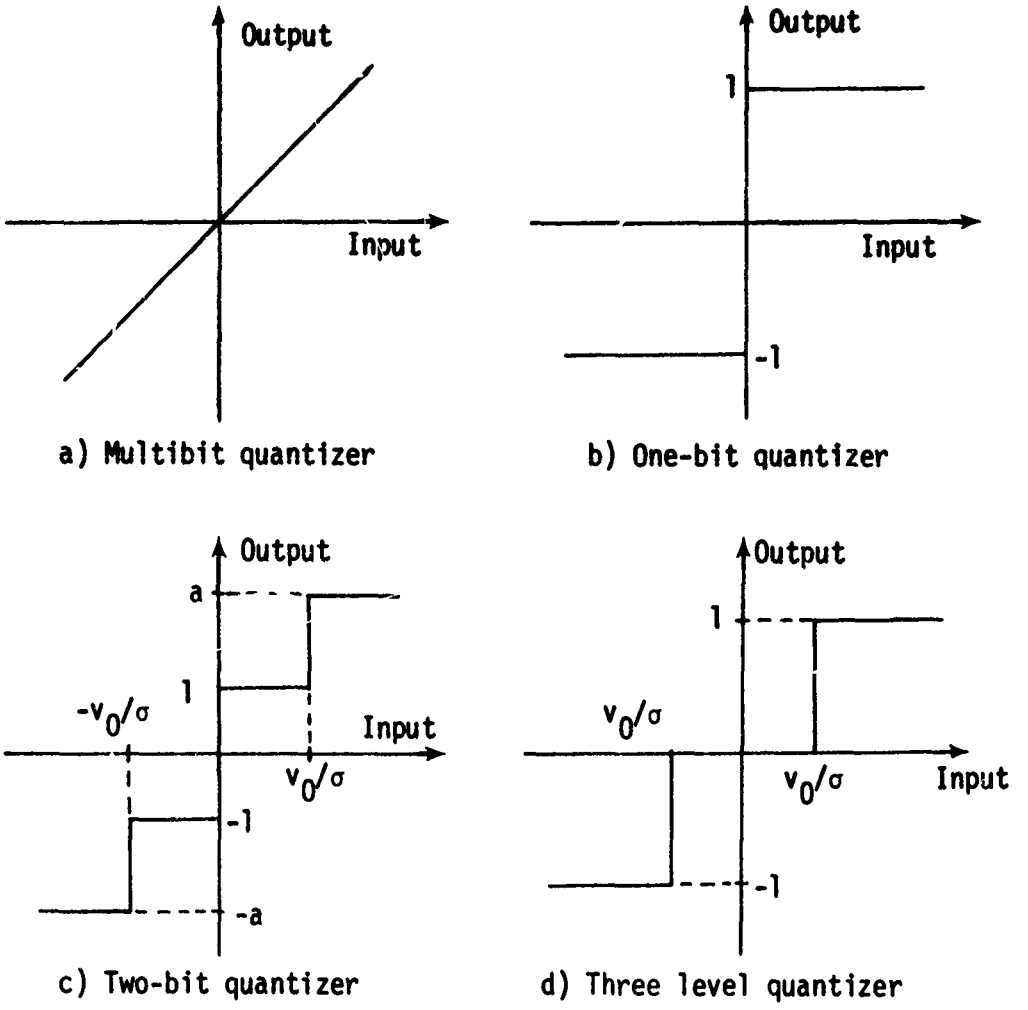

Figure 6. Quantizers

Higher order quantizers are not considered since they would require larger adders with larger computation times thereby leading to smaller arrays for real-time correlation. It will be shown in a later section that the S/N ratio gain from using a larger reference array is greater than the gain using higher-order logic in the quantizers in a smaller reference array.

4. Image Normalization Using the One-Bit Quantizer

It is shown in Section C-1 that the Direct Method requires normalization to prevent false peaks. A method of normalization is given in Equation 10. When using the transfer function shown in Figure 6 (b) to quantize both the HR and LR signals, the outputs are always ± 1. Under this situation the denominator term of Equation 10 reduces to $(KL)^2$. Then Equation 10 becomes

$$R(p,q) = \frac{1}{(KL)^2}\left[\sum_{n=1}^{k}\sum_{m=1}^{L} HR(n,m)LR(n+p,m+q)\right]^2 \qquad (13)$$

Equation 13 is the normalized direct cross-correlation expression for one-bit by one-bit quantization. The square root of Equation 13 would also be a normalized estimate of the cross correlation and is seen to be equivalent to Equation 3. Therefore the one-bit by one-bit two-dimensional correlation algorithm given by Equation 3 is normalized. Its peak value, which occurs at complete registration, is one. No additional hardware dedicated to the normalization process is required.

5. Quantization Effects on S/N Ratio for the Direct and SSDA Correlation Methods

A detailed analytical study was performed so that the effect on the mean square S/N ratio due to different quantizers being used on the HR and LR signals could be determined. The analysis was done for the

quantizers shown in Figure 6 and also for the six level quantizer shown in Figure 7.

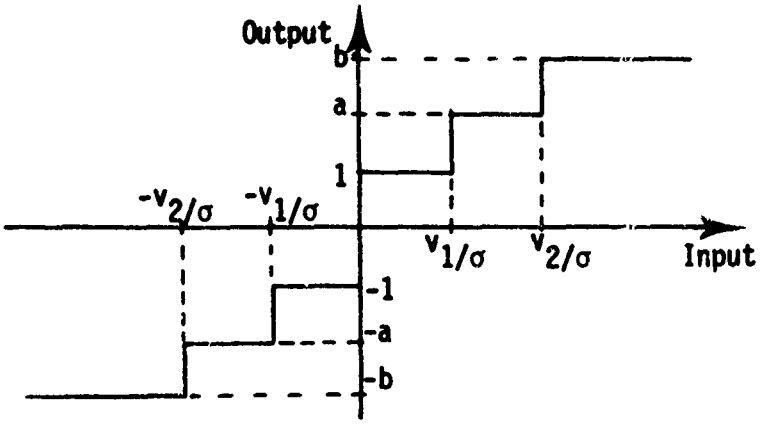

Figure 7. Six level quantizer.

In this section the variance derivations for the Direct and SSDA methods using one-bit quantization are presented. The results for the other quantizers are summarized and a comparison of the two methods is presented.

a. Direct Method

Consider the estimation of the Direct Cross-Correlation function for the first line of the high resolution image with the first line of the low resolution image as shown in Figure 8. The estimation of the

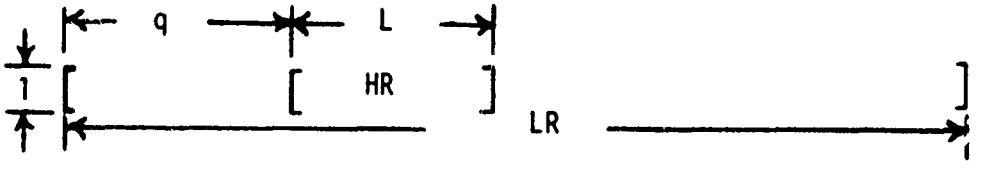

Figure 8. Layout for correlation of first line of two images.

Direct Cross-Correlation function for the first line is given by

$$\hat{R}(1,q) = \frac{1}{L} \sum_{m=1}^{L} HR(1,m)LR(1, m+q) \tag{14}$$

where HR and LR are the high resolution and low resolution images respectively. To simplify the notation, the first row designation can be dropped yielding

$$\hat{R}(q) = \frac{1}{L} \sum_{m=1}^{L} HR(m)LR(m+q) \tag{15}$$

If the sampling rate is less than or equal to the Nyquist rate, the adjacent samples can be considered to be indenendent. Therefore, except for the three or four values of q close to registration, the correlation coefficient between the two images is small (i.e., $\rho << 1$). If the two images are quantized with quantizers g_1 and g_2 respectively, then Equation 15 becomes

$$\hat{R}(q) = \frac{1}{L} \sum_{m=1}^{L} g_1[HR(m)]g_2[LR(m+q)] \tag{16}$$

The variance of this estimate is given by

$$\sigma_{\hat{R}}^2 = \left\langle \hat{R}^2 \right\rangle - \left\langle \hat{R} \right\rangle^2 \tag{17}$$

where $\langle \hat{R} \rangle$ denotes the expected value of $\hat{R}$ given by

$$\langle \hat{R} \rangle = E \left\{ \frac{1}{L} \sum_{m=1}^{L} g_1[HR(m)]g_2[LR(m+q)] \right\} \tag{18}$$

However, because of the assumed independence of the samples, Equation 18 reduces to

$$\langle \hat{R} \rangle = \frac{1}{L} \sum_{m=1}^{L} \left\langle g_1[HR(m)] \quad g_2[LR(m+q)] \right\rangle \tag{19}$$

The first term in Equation 17 can be written as

$$\langle \hat{R}^2 \rangle = \left\langle \frac{1}{L^2} \sum_{n=1}^{L} \sum_{m=1}^{L} g_1[HR(m)] g_2[LR(m+q)] g_1[HR(n)] \cdot g_2[LR(n+q)] \right\rangle \tag{20}$$

Separating the term for which n=m in Equation 20 yields

$$\langle \hat{R}^2 \rangle = \frac{1}{L^2} \sum_{m=1}^{L} \left\langle g_1^2[HR(m)] g_2^2[LR(m+q)] \right\rangle$$

$$+ \frac{1}{L^2} \sum_{\substack{n=1 \\ m \neq n}}^{L} \sum_{m=1}^{L} \left\langle g_1[HR(m)] g_2[LR(m+q)] g_1[HR(n)] g_2[LR(n+q)] \right\rangle \tag{21}$$

Consider the case where both quantizers g_1 and g_2 have an input/output relationship as shown in Figure 6(b), then Equation 19 becomes

$$\langle \hat{R} \rangle = \frac{1}{L} \sum_{m=1}^{L} \left[\int_{-\infty}^{0} \int_{-\infty}^{0} (1) f(HR,LR) d(HR) d(LR) + \int_{0}^{\infty} \int_{0}^{\infty} (1) \cdot \right.$$

$$f(HR,LR) d(HR) d(LR) + \int_{-\infty}^{0} \int_{0}^{\infty} (-1) f(HR,LR) d(HR) d(LR) +$$

$$\left. \int_{0}^{\infty} \int_{-\infty}^{0} (-1) f(HR,LR) d(HR) d(LR) \right] \tag{22}$$

where f(HR,LR) is the joint density function of the HR and LR images. If f(HR,LR) is symmetric with zero mean, then Equation 22 reduces to

$$\langle \hat{R} \rangle = \frac{1}{L} \sum_{m=1}^{L} [(1)(1/4) + (1)(1/4) + (-1)(1/4) + (-1)(1/4)]$$

or $$\langle \hat{R} \rangle = 0 \tag{23}$$

Because of the assumed independence of the samples and the input/output relationship of Figure 6(b), the first term in Equation 21 reduces to

$$\frac{1}{L^2} \sum_{m=1}^{L} (1)(1) = \frac{1}{L} \tag{24}$$

and the second term in Equation 21 becomes

$$\frac{1}{L^2} (L)(L-1) \left\langle g_1[HR] \right\rangle^2 \left\langle g_2[LR] \right\rangle^2 = 0 \tag{25}$$

Substituting Equations 23, 24, and 25 into Equation 17 yields

$$\sigma_{\hat{R}}^2 = \frac{1}{L} \tag{26}$$

Equation 26 is an expression for the variance of the estimate of R when the input is quantized into two levels. To obtain the variance of the estimate of the true correlation of the two signals, σ_ρ^2, the relationship between R and ρ must be established. If the input/output relationship for the quantized high resolution and quantized low resolution video signals are given by $g_1(HR)$ and $g_2(LR)$

respectively, where g_1 and g_2 are both as shown in Figure 6(b), then

$$R(q) = \left\langle g_1[HR] g_2[LR(q)] \right\rangle \tag{27}$$

where the HR and LR(q) signals are jointly normal with covariance μ given by

$$\mu = \left\langle HR\ LR(q) \right\rangle - \left\langle HR \right\rangle \left\langle LR(q) \right\rangle \tag{28}$$

and correlation coefficient ρ given by

$$\rho = \frac{\mu}{\sigma_{HR}\sigma_{LR}} \tag{29}$$

If $\underline{X}$ and Y are jointly normal random variables with covariance μ and the random variable Z is formed by $Z = g(\underline{X}, Y)$ where g(x,y) is an arbitrary function, then

$$E\{Z\} = E\{g(\underline{X},Y)\} = \int_{-\infty}^{\infty} \int_{-\infty}^{\infty} g(x,y) f(x,y) dxdy \tag{30}$$

where f(x,y) is the bivariate distribution function for the random variables $\underline{X}$ and Y. Price's theorem [2], [3] states that

$$\frac{\partial^n E\{g(\underline{X},Y)\}}{\partial \mu^n} = E\left\{ \frac{\partial^{2n} g(\underline{X},Y)}{\partial \underline{X}^n \partial Y^n} \right\}$$

$$= \int_{-\infty}^{\infty} \int_{-\infty}^{\infty} \frac{\partial^{2n} g(x,y)}{\partial x^n \partial y^n} f(x,y) dxdy \tag{31}$$

Applying Price's theorem with n=1 to the expression for R(q) in Equation 27 yields

$$\frac{\partial R(q)}{\partial \mu(q)} = \frac{\partial E\{g_1[HR]g_2[LR(q)]\}}{\partial \mu(q)} = E\left\{ \frac{\partial^2 g_1[HR]g_2[LR(q)]}{\partial HR\ \partial LR(q)} \right\} \quad (32)$$

and from Equation 29.

$$\frac{\partial R(q)}{\partial \rho(q)} = \frac{\partial R(q)}{\partial \mu(q)} \cdot \frac{\partial \mu(q)}{\partial \rho(q)} = \frac{\partial R(q)}{\partial \mu(q)}\ \sigma_{HR}\ \sigma_{LR} \quad (33)$$

or

$$\frac{\partial R(q)}{\partial \rho(q)} = \sigma_{HR}\ \sigma_{LR}\ E\left\{ \left(\frac{\partial g_1[HR]}{\partial HR} \right) \left(\frac{\partial g_2[LR(q)]}{\partial LR(q)} \right) \right\} \quad (34)$$

However from Figure 6(b)

$$\frac{\partial g_1}{\partial HR} = 2\delta[HR] \quad \text{and} \quad \frac{\partial g_2}{\partial LR} = 2\delta[LR] \quad (35)$$

and Equation 34 reduces to

$$\frac{\partial R(q)}{\partial \rho(q)} = \frac{1}{2\pi\sqrt{1-\rho^2}} \int_{-\infty}^{\infty} \int_{-\infty}^{\infty} 2\delta[HR]2\delta[LR]\ \mathrm{Exp}\Bigg[$$

$$- \frac{1}{2(1-\rho^2)} \left(\frac{HR^2}{\sigma_{HR}^2} - \frac{2\rho HRLR}{\sigma_{HR}\ \sigma_{LR}} + \frac{LR^2}{\sigma_{LR}^2} \right) \Bigg] d(HR)d(LR)$$

or $$\frac{\partial R(q)}{\partial \rho(q)} = \frac{2}{\pi\sqrt{1-\rho^2}} \quad (36)$$

where it has been assumed that HR and LR are jointly gaussian. For the case being considered $\rho << 1$ which leads to

$$\frac{R(q)}{\rho(q)} \tilde{=} k = \frac{2}{\pi} \tag{37}$$

From Equation 37

$$\sigma_{\hat{\rho}_{\text{One-Bit}}} \tilde{=} \sigma_{\hat{R}_{\text{One-Bit}}} \Big/ k \tag{38}$$

or

$$\sigma^2_{\hat{\rho}_{\text{One-Bit}}} \tilde{=} \frac{\pi^2}{4}\left(\frac{1}{L}\right) \tag{39}$$

using Equation 26.

If one uses the two level or one-bit quantizer with input/output relationship as shown in Figure 9 and repeats the steps given above, one finds the variance of this correlator to be

$$\sigma^2_{\hat{\rho}} = 3\left(\frac{\pi^2}{4}\right)\left(\frac{1}{L}\right) \tag{40}$$

or a variance which is exactly three times that obtained using the one-bit quantizer described by Figure 6(b). If the quantizer in Figure 6(b) quantizes to levels of $\pm n$, repeating the steps above reveals that the variance of the resulting correlator is again given by Equation 39.

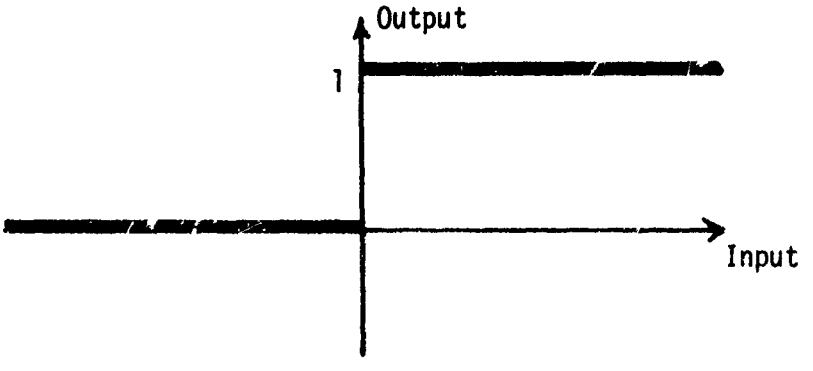

Figure 9. Alternate one-bit quantizer.

The products for the correlator described by Figure 6(b) are either -1 or +1 as shown in Figure 10(a). The correlator described by Figure 9 with an input/output table given in Figure 10(b) yields an estimate of ρ with a variance three times as large as the correlator in Figure 10(a). If one biases the output products of the correlator described in Figure 10(a) as shown in Figure 10(c), the mean of the estimate changes but the variance does not. The correlator in Figure 10(c) is therefore equivalent to that of Figure 10(a). Now if one implements the correlator in Figure 10(d), the resulting variance is the same as the correlator in Figure 10(c) but the counter can be designed to count only half as high thereby simplifying the implementation. The correlator with input/output relationship described in Figure 10(d) is easier to implement than the one described in Figure 10(a) since a ripple counter rather than an up-down counter can be used. In addition the input/output relationship described in Figure 10(d) can be realized with exclusive OR gates.

	-1	+1
-1	1	-1
+1	-1	1

a) One-bit correlator.

	0	1
0	0	0
1	0	1

b) One-bit correlator with biased input.

	-1	1
-1	2	0
1	0	2

c) One-bit correlator with biased output.

	0	1
0	1	0
1	0	1

d) One-bit correlator equivalent to (a).

Figure 10. One-bit correlator input/output tables.

b. SSDA Method

Consider the estimation of the SSDA function for the first line of the high resolution image with the first line of the low resolution image as shown in Figure 8. The estimation equation for the SSDA function is given by Equation 41 where HR and LR refer to high resolution and low resolution images respectively.

$$\hat{R}(1,q) = \frac{1}{L} \sum_{m=1}^{L} |HR(1,m) - LR(1, m+q)| \tag{41}$$

To simplify notation, the first row designation can be dropped, then Equation 41 becomes

$$\hat{R}(q) = \frac{1}{L} \sum_{m=1}^{L} |HR(m) - LR(m+q)| \tag{42}$$

Assume that the sampling rate is less than or equal to the Nyquist rate. This means that adjacent samples are almost independent for all values of q except for values near the point of registration. Therefore for all cases, except the case near registration, the correlation coefficient, ρ, is small and assumed to be much less than one.

If the two sampled lines of video are quantized with quantizers g_1 and g_2 respectively, then Equation 42 is written as

$$\hat{R}(q) = \frac{1}{L} \sum_{m=1}^{L} |g_1[HR(m)] - g_2[LR(m+q)]| \tag{43}$$

The effects of different quantization methods can be investigated by considering the cases of q for which the samples can be assumed independent. The variance of the estimate of $\hat{R}$ is given by

$$\sigma^2_{\hat{R}} = \langle \hat{R}^2 \rangle - \langle \hat{R} \rangle^2 \tag{44}$$

Assume that the quantizing functions g_1 and g_2 are given as in Figure 9. Consider first $\langle \hat{R} \rangle$, given by Equation 45.

$$\langle \hat{R} \rangle = \left\langle \left\{ \frac{1}{L} \sum_{m=1}^{L} |g_1[HR(m)] - g_2[LR(m+q)]| \right\} \right\rangle \tag{45}$$

Since the samples are independent, Equation 45 becomes

$$\langle \hat{R} \rangle = \frac{1}{L} \sum_{m=1}^{L} \langle |g_1[HR(m)] - g_2[LR(m+q)]| \rangle \tag{46}$$

Figure 11 shows the possible outcomes of the function $|g_1[HR(m)] - g_2[LR(m+q)]|$ for all combinations that the values g_1 and g_2 can possess.

$g_2[LR(m+q)]$ \ $g_1[HR(m)]$	0	1
0	0	1
1	1	0

Figure 11. Outcomes of $|g_1 - g_2|$.

Using the results of Figure 11 and expanding the expected value, Equation 46 becomes

$$\langle\hat{R}\rangle = \frac{1}{L}\sum_{m=1}^{L}\left\{\int_{-\infty}^{0}\int_{0}^{\infty}(1)f(HR,LR)d(HR)d(LR) + \int_{0}^{\infty}\int_{-\infty}^{0}(1)f(HR,LR)d(HR)d(LR)\right\} \tag{47}$$

Assuming HR and LR to be jointly gaussian and assuming independent samples, Equation 47 yields,

$$\langle\hat{R}\rangle = \frac{1}{L}\sum_{m=1}^{L}\left\{2\int_{-\infty}^{0}\int_{0}^{\infty}f(HR,LR)\,d(HR)d(LR)\right\}$$

$$\langle\hat{R}\rangle = \frac{1}{L}(L)(2)\left(\frac{1}{4}\right) = \frac{1}{2} \tag{48}$$

Therefore, the second term in Equation 44 is

$$\langle\hat{R}\rangle^2 = \frac{1}{4} \tag{49}$$

Next consider $\langle\hat{R}^2\rangle$ given by Equation 50

$$\langle\hat{R}^2\rangle = \left\langle\left\{\frac{1}{L^2}\sum_{m=1}^{L}\sum_{n=1}^{L}|g_1[HR(m)] - g_2[LR(m+q)]|\cdot |g_1[HR(n)] - g_2[LR(n+q)]|\right\}\right\rangle \tag{50}$$

Separating terms for which m=n in Equation 50 yields

$$\langle \hat{R}^2 \rangle = \frac{1}{L^2} \sum_{m=1}^{L} \left\langle \left\{ |g_1[HR(m)] - g_2[LR(m+q)]|^2 \right\} \right\rangle$$

$$+ \frac{1}{L^2} \sum_{\substack{m=1 \\ m \neq n}}^{L} \sum_{n=1}^{L} \left\langle \left\{ |g_1[HR(m)] - g_2[LR(m+q)]| \cdot \right. \right. \qquad (51)$$

$$\left. \left. |g_1[HR(n)] - g_2[LR(n+q)]| \right\} \right\rangle$$

Again using the results of Figure 11 and the assumptions made previously, Equation 51 becomes

$$\langle \hat{R}^2 \rangle = \frac{1}{L^2} \sum_{m=1}^{L} \left\{ \int_{-\infty}^{0} \int_{0}^{\infty} (1) f(HR,LR) d(HR) d(LR) + \right.$$

$$\left. + \int_{0}^{\infty} \int_{-\infty}^{0} (1) f(HR,LR) d(HR) d(LR) \right\} + \frac{1}{L^2} \sum_{\substack{m=1 \\ m \neq n}}^{L} \sum_{n=1}^{L}$$

$$\left\{ \int_{-\infty}^{0} \int_{0}^{\infty} (1) f(HR,LR) d(HR) d(LR) + \int_{0}^{\infty} \int_{-\infty}^{0} (1) f(HR,LR) d(HR) d(LR) \right\} \cdot$$

$$\left\{ \int_{-\infty}^{0} \int_{0}^{\infty} (1) f(HR,LR) d(HR) d(LR) + \int_{0}^{\infty} \int_{-\infty}^{0} (1) f(HR,LR) d(HR) d(LR) \right\} \qquad (52)$$

Equation 52 reduces to,

$$\langle \hat{R}^2 \rangle = \left(\frac{1}{L^2}\right) (L)(2) \left(\frac{1}{4}\right) + \left(\frac{1}{L^2}\right) (L)(L-1)(2) \left(\frac{1}{4}\right) (2) \left(\frac{1}{4}\right)$$

$$\langle \hat{R}^2 \rangle = \frac{1}{2L} + \frac{1}{L} (L-1) \left(\frac{1}{4}\right) = \frac{1}{4L} + \frac{1}{4} \qquad (53)$$

Substituting Equations 49 and 53 into 44 yields

$$\sigma_{\hat{R}}^2 = \frac{1}{4L} + \frac{1}{4} - \frac{1}{4} = \frac{1}{4L} \tag{54}$$

Of importance here is to find out how the mean square Signal-to-Noise (ms S/N) ratio is degraded by the use of different quantizers. The variance of the estimate of ρ, σ_ρ^2, directly reflects the degradation. The variance of ρ is found as follows.

Let

$$r(q) = E\{|g_1[HR(m)] - g_2[LR(m+q)]|\} \tag{55}$$

Assume that HR and LR have the joint gaussian density function given by Equation 56

$$f(HR,LR) = \frac{1}{2\pi\sigma_{HR}\sigma_{LR}(1-\rho^2)^{\frac{1}{2}}} \varepsilon^{-\left[\frac{1}{2(1-\rho^2)}\left(\frac{HR^2}{\sigma_{HR}^2} - \frac{2\rho HRLR}{\sigma_{HR}\sigma_{LR}} + \frac{LR^2}{\sigma_{LR}^2}\right)\right]} \tag{56}$$

Then Equation 55 is written as

$$r(q) = \frac{1}{2\pi\sigma_{HR}\sigma_{LR}(1-\rho^2)^{\frac{1}{2}}} \int_{-\infty}^{\infty}\int_{-\infty}^{\infty} |g_1[HR(m)] - g_2[LR(m+q)]| \tag{57}$$

$$\varepsilon^{-[\ldots]}\, d(HR)d(LR)$$

Using the results of Figure 11 and assuming $\rho^2 << 1$, Equation 57 becomes

$$r(q) = \frac{1}{2\pi\sigma_{HR}\sigma_{LR}} \left\{ \int_{-\infty}^{0}\int_{0}^{\infty} \varepsilon^{-\left[\frac{1}{2}\left(\frac{HR^2}{\sigma_{HR}^2} + \frac{LR^2}{\sigma_{LR}^2} - \frac{2\rho HRLR}{\sigma_{HR}\sigma_{LR}}\right)\right]} d(HR)d(LR) \right.$$

$$\left. + \int_{0}^{\infty}\int_{-\infty}^{0} \varepsilon^{-[\quad]}\, d(HR)d(LR) \right\} \qquad (58)$$

Using the expansion on ε^{X} for small χ, $\varepsilon^{X} = 1+\chi$, Equation 58 becomes

$$r(q) \cong \frac{2}{2\pi\sigma_{HR}\sigma_{LR}} \int_{-\infty}^{0}\int_{0}^{\infty} \varepsilon^{\frac{-(HR)^2}{2\sigma_{HR}^2}} \varepsilon^{\frac{-(LR)^2}{2\sigma_{LR}^2}} \left[1 + \frac{\rho(HR)(LR)}{\sigma_{HR}\sigma_{LR}}\right] d(HR)d(LR)$$

$$r(q) = \frac{1}{\pi\sigma_{HR}\sigma_{LR}} \int_{-\infty}^{0} \varepsilon^{\frac{-(HR)^2}{2\sigma_{HR}^2}} d(HR) \int_{0}^{\infty} \varepsilon^{\frac{-(LR)^2}{2\sigma_{LR}^2}} d(LR) +$$

$$\frac{\rho}{\pi} \int_{-\infty}^{0} \frac{HR}{\sigma_{HR}^2} \varepsilon^{\frac{-(HR)^2}{2\sigma_{HR}^2}} d(HR) \int_{0}^{\infty} \frac{LR}{\sigma_{LR}^2} \varepsilon^{\frac{-(LR)^2}{2\sigma_{LR}^2}} d(LR) \qquad (59)$$

Evaluating Equation 59 yields

$$r(q) = \frac{1}{\pi\sigma_{HR}\sigma_{LR}} \left(\frac{1}{2}\sqrt{2\pi\sigma_{LR}^2}\right)\left(\frac{1}{2}\sqrt{2\pi\sigma_{HR}^2}\right) +$$

$$\frac{\rho}{\pi}\left(\int_{-\epsilon}^{\frac{-(LR)^2}{2\sigma_{LR}^2}}\right)_{-\infty}^{0}\left(\int_{-\epsilon}^{\frac{-(HR)^2}{2\sigma_{HR}^2}}\right)_{0}^{\infty}$$

$$r(q) = \frac{1}{2} + \frac{\rho}{\pi}(-1+0)(0+1)$$

$$r(q) = \frac{1}{2} - \frac{\rho}{\pi}$$

or

$$\rho = \frac{\pi}{2} - \pi\, r(q) \tag{60}$$

Therefore from the relationship of Equation 60 it is shown that

$$\sigma_{\hat{\rho}}^2 = \pi^2\, \sigma_{\hat{R}}^2 \tag{61}$$

Substituting Equation 54 into 61 yields

$$\sigma_{\hat{\rho}}^2 = \pi^2 \quad \frac{1}{4L} \quad = \left(\frac{\pi}{2}\right)^2 \quad \frac{1}{L} \quad = \frac{2.467}{L} \tag{62}$$

If one uses the two level or one-bit quantizer with input/outout relationship as shown in Figure 6(b) the variance in the estimate of ρ is the same as that given in Equation 62. Therefore, if the SSDA method is to be implemented with a one-bit quantizer, the choice of quantizer depends on which is easier to implement.

c. Results of S/N Ratio Analysis for Higher Order Quantizers

The analysis of the degradation of the S/N ratio was extended for both the Direct and SSDA methods to the cases where three, four, and six level quantizers are used. As shown in Figures 6(c), 6(d), and 7, the variables v_0/σ, v_1/σ, v_2/σ, a and b are chosen such that σ_ρ^2 is minimized. Table 1 shows the results of this analysis for both the SSDA and Direct methods. The curves presented in Figure 12 show

	Direct Method		SSDA Method	
No Quantization Levels	$\sigma_\rho^2 * L$	Optimum Parameters	$\sigma_\rho^2 * L$	Optimum Parameters
2	2.467	----	2.467	----
3	1.525	$v_0/\sigma = 0.6$	1.88	$v_0/\sigma = .3$
4	1.3	$v_0/\sigma = .95$ $a = 4$	1.715	$v_0/\sigma = .5$ $a = 3$
6	1.13	$v_1/\sigma = 0.6$ $v_2/\sigma = 1.4$ $a = 3$ $b = 6$	1.613	$v_1/\sigma = .3$ $v_2/\sigma = .7$ $a = 3$ $b = 5$

Table 1. Results of S/N ratio analysis.

$\sigma_\rho^2 * L$ vs. no. of quantization levels for the two image matching methods being considered. Figure 12 clearly shows that the Direct Method yields a lower degradation in the ms S/N ratio for all quantizers except the two level quantizer. Therefore, the conclusion can be made that the SSDA method would not be implemented using the higher order quantizers if the decision were based only on degradation of the ms S/N ratio.

However, since the SSDA method can be implemented with less and faster hardware than the Direct Method when more than two levels are used, it should not be ruled out as a candidate correlation algorithm.

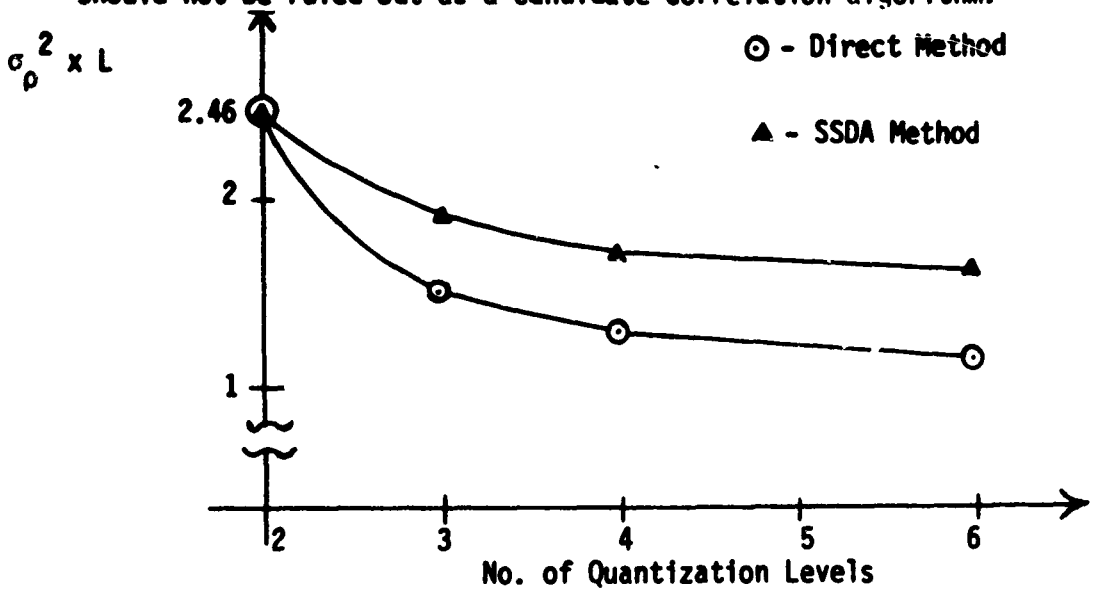

Figure 12. Comparison of the SSDA and Direct Double Summation Methods

From Table 1 and Figure 12 one can draw some conclusions about correlator design parameters (eg., reference array size, number of quantization levels, and statistical accuracy). From Table 1 the degradation in the mean square S/N ratio for both methods using any number of quantization levels is inversely proportional to the number of pixels used in the reference array (i.e., doubling the number of pixels in the reference array halves the S/N ratio degradation for a given number of quantization levels). Also from Figure 12 the degradation in the S/N ratio can be improved by increasing the number of quantization levels. However, relatively little improvement is gained by using more than four levels (2-bits) with either the Direct or SSDA

method while the hardware to implement more than four levels increases significantly. The conclusion is that a correlator using either the Direct or SSDA method should have the video pixels quantized to two, three, or four levels.

If the correlator is to operate in real time, then the sampling period of the incoming live video dictates the amount of time available for each correlation computation. However, increasing the size of the reference array and increasing the number of quantization levels (eg., from two to four levels) both require more hardware and a longer computation time. From Table 1 increasing the number of quantization levels from two to four increases the ms S/N ratio by 2.467/1.3 or 1.898 for the Direct Method and by 2.467/1.715 or 1.438 for the SSDA method. The computations, however, using four levels require more time. In fact from data books on present state-of-the-art hardware one could more than double the size of the reference array with this increased computation time using two level quantization. This increase in the size of the reference array would more than double the ms S/N ratio. Therefore, the trade-off is to make the reference array size as large as possible for real-time computation. Because of hardware considerations it is usually desirable to make each reference array dimension a power of two (i.e., 16x16, 32x32, 32x64, 64x64, etc.). If for example a 32x32 reference array in a two level correlator can be computed in real time but a 32x64 reference array can not, then one might consider using three or four levels in this 32x32 correlator if time would allow. In other

words the trade-off is to use as large a reference array as possible, then consider using more than two levels if time permits.

One additional consideration when going from two level to three or four level quantization should be pointed out. When quantizing to two levels, each KxL subarray of the LR video should be quantized to one level when above the mean and to the other level when below the mean of that KxL subarray. For each value of p and q in Equation 3 or 6 all of the KxL pixels in that subarray should be quantized about the mean of that subarray. Quantizing about some moving average mean or about the mean of the entire NxM LR image leads to errors in the correlation computation. However, since it is not practical to do this, some trade-off technique is usually devised. If a three or four level quantizer is used, then the standard deviation as well as the mean of each KxL subarray should be computed. To use any other technique to find v_0/σ in Table 1 leads to errors in the correlation computation. In fact these additional errors could be larger than the gain in going from a two level to a three or four level quantizer. The amount of error induced by inaccurate values of mean and standard deviation in the quantization is scene dependent. The conclusion is that if one uses a three or four level quantizer, care should be taken in the computation of the mean and standard deviation in order to prevent a significant loss in the S/N ratio due to inaccuracies in these computations.

6. Implementation of the SSDA and Direct Methods Using One-Bit Quantization

When both the HR and LR video are quantized to two levels, then from Table 1 the Direct and SSDA methods have the same ms S/N ratio.

In this section the implementation of the two methods using exclusive OR gates is shown to be equivalent. The conclusion is that when quantizing to two levels, the SSDA and Direct methods are equivalent. This is not the case when one or both video signals are quantized to more than two levels. In this case the SSDA method is not a true correlation technique while the Direct method is.

a. Direct Method

Consider first that the HR and LR video have zero mean and that the HR video is quantized by the input/output relationship shown in Figure 9. Then if the LR video is quantized by the input/output relationship shown in Figure 13, the correlator inputs when the input video match are given by 01 and 10 and video mismatch are given by 00 and 11 input combinations. If the output of the correlator is to be 1 when the input video match and 0 when the input video mismatch, then the input/output table is given in Figure 14 and can be implemented using an exclusive OR ($\oplus$) gate as shown in Figure 15. Implementation of the entire array is given in Chapter 4. Using this method, the peak value corresponds to registration of the two images.

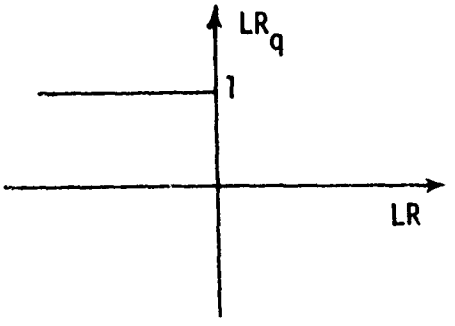

Figure 13. Reversed polarity one-bit quantizer.

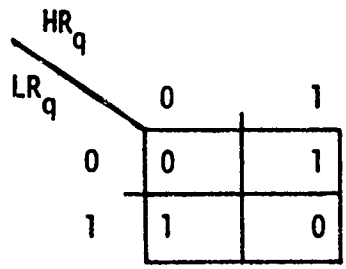

Figure 14. Input/output table for one-bit correlation.

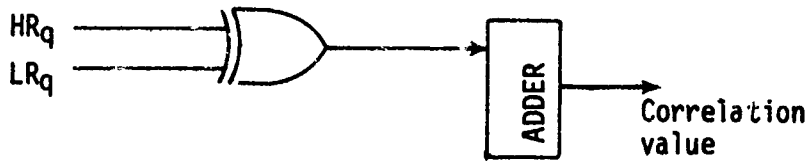

Figure 15. Exclusive-OR implementation.

b. SSDA

The SSDA implementation is similar to that given above, however the quantizer given in Figure 9 is used to quantize both signals. The outcome of the SSDA algorithm is shown in Figure 11. The states 00 and 11 now represent matched samples and 01 and 10 represent mismatch. The circuit for implementing the SSDA algorithm is the same given in Figure 15. The adder output is now an error value instead of a correlation value. Therefore the minimum value of the adder output corresponds to image registration.

In this section it has been shown that if the two images are quantized to two levels (one-bit quantization), then the Direct Method

and SSDA methods are identical. In fact, either type correlator design can be converted to the other by reversing the polarity of one of the signals before quantization and looking for a minimum if originally looking for a maximum at the output of the correlator (or vice-versa).

3. CORRELATION SYSTEM CONSIDERATIONS

The various trade-offs and other considerations which lead to the correlation implementation in Chapter 4 are presented in this Chapter.

A. Determination of Sampling Frequency

Shannon's sampling theorem says that theoretically all the information in a signal is contained in the sampled signal (and can therefore be recovered from the sampled signal) if the sampling rate is at least twice the bandwidth of the signal (B). This sampling frequency $f_s = 2B$ is usually referred to as the Nyquist rate.

Consider a 30 frame per second 525 line TV system with 4:3 aspect ratio. The number of active horizontal lines is approximately 480. If the horizontal and vertical resolution of each pixel are to be the same, then (4/3)480 = 640 samples should be taken on each TV line. The sampling rate is (4/3)(480)(525)(30) = 10.08 MHz or approximately 10 MHz. The sampling period for a 10 MHz sampler is 100 nsec. Therefore in order to design a real-time correlator each computation must be accomplished in less than 100 nsec. In other words the value of R for each p and q in Equation 3 must be computed in less than 100 nsec. However, the actual bandwidth for most 525 line black/white video signals is usually on the order of 4 MHz or slightly larger. The corresponding Nyquist rate is approximately 8 MHz. Since it is necessary to sync the sampler clock frequency to the video signal, the actual sampling rate will be slightly less than 8 MHz as explained in Chapter 4.

It should be pointed out that the recommended sampling rate of approximately 8 MHz is based entirely on system bandwidth considerations. Since sampling at a higher rate will yield relatively little gain while decreasing the available time for real time correlation, 8 MHz is seen as an upper limit on the sampling frequency. If the sampling rate is decreased in order to allow more time for real time correlation or for shift register hardware considerations as explained in Chapter 4, then what one gives up is horizontal pixel resolution. The decreased sampling rate does not effect the vertical pixel resolution since this is determined by the number of TV lines. Initial reaction to this would be to conclude that not much would be lost in correlation since as reported in [4] military targets such as tanks, personnel carriers, jeeps, etc., exhibit a larger spatial frequency content in the vertical direction than in the horizontal direction (i.e., there is more high frequency spatial content in the vertical direction than in the horizontal direction for vehicle targets). A much closer analysis given in the following section reveals that if the reference array is 32 x 64, most of the correlation is being performed on the target background and not on the target itself. Reference [4] points out that most backgrounds have greater horizontal spatial frequency content than vertical content. An obvious example of this would be forests. The effect on the accuracy of correlation if one decreases the sampling rate from approximately 8 MHz to say 5 MHz is scene dependent and was not studied under this contract. It is recommended, therefore, that the sampling rate effects on correlation be studied in any correlator technology program.

B. Area Correlator

Consider a 525 line TV system with approximately 480 active lines and a 2° vertical FOV. A standard 2.3 x 2.3 meter target would subtend 6.3 lines in the TV FOV at 5 KM, 7.9 lines at 4 KM, 10.5 lines at 3 KM, and 15.8 lines at 2 KM. If the reference array is 64 x 64 (in a full-frame correlator), then the target occupies 0.967% of the reference array area at 5 KM, 1.52% at 4 KM, 2.69% at 3KM, and 6.09% at 2 KM. Therefore, it is evident that most of the correlation is being performed on the target background and not on the target itself. If the size of the reference array is 32 x 32, then the above target area percentages would increase by a factor of four.

The results of the above paragraph can be stated in a slightly different way. If two TV lines are required to display a spatial cycle, then the highest vertical spatial frequency detectable at 5 KM is 1.34 cycles/meter, at 4 KM is 1.71 cycles/meter, at 3 KM is 2.28 cycles/meter, and at 2 KM is 3.42 cycles/meter. If the horizontal and vertical resolutions are the same (i.e., sampling at 10 MHz) then the limiting horizontal spatial frequency resolution is the same as the vertical. If the sampling rate is reduced to 7.5 MHz, then the limiting horizontal spatial frequencies detectable are 1.005, 1.28, 1.71, and 2.57 cycles/meter respectively at the above ranges. Stated another way, trees spaced every 0.75, 0.58, 0.44, and 0.29 meters apart respectively at the 5, 4, 3, 2 KM ranges could be detected when sampling at 10 MHz while trees spaced every 0.995, 0.78, 0.585, and 0.39 meters apart respectively could be detected when sampling at 7.5 MHz. The above results are summarized in Table 2.

Range kM	2.3 x 2.3 M Target size (TV lines)	Target Size in 64 x 64 Reference Array	Target Size in 32 x 32 Reference Array	Limiting Vertical Spatial Resolution cycles/meter	Limiting Horizontal Spatial Resolution f_s = 10 MHz cycles/meter	Limiting Horizontal Spatial Resolution f_s = 7.5 MHz cycles/meter
5	6.3	0.967%	3.87%	1.34	1.34	1.005
4	7.9	1.52%	6.08%	1.71	1.71	1.28
3	10.5	2.69%	10.76%	2.28	2.28	1.71
2	15.8	6.09%	24.36%	3.42	3.42	2.57

Table 2. Horizontal and vertical resolution of 2.3 x 2.3 meter target.

C. Preprocessing of Input Video

1. High Resolution Image Preprocessing

The purpose of preprocessing the HR video is to reduce the spatial resolution of the HR video to that of the LR video, a condition necessary for correlation purposes. This difference in resolution is caused by the differing fields of view (FOV), number of TV lines per frame, frame rate, aspect ratio, and sampling rate of the two TV systems. Due to size, weight, and cost constraints the FOV of the missile seeker will be W times (W>1) that of the FOV of the fine pointing and tracking system. If W is an integer, then the preprocessor averages the first W columns of the first W rows of the HR image to obtain the P(1,1) picture element (pixel) of the reference image. Then the next W columns of the first W rows are averaged to obtain the P(1,2) pixel of the reference array as shown in Figure 16. If the sampled HR video forms an A x B array, then the reference array is an (A/W) x (B/W) array. The size of a possible target in the reference array is then identical to the size of the target in the LR array. Equation 63 is the preprocessing algorithm where W is an integer.

$$P(I,J) = \frac{1}{W^2} \sum_{M=1}^{W} \sum_{N=1}^{W} HR\left[(WI - W+M), (WJ - W+N)\right] \quad \begin{matrix} 1 \leq I \leq A/W \\ 1 \leq J \leq B/W \end{matrix} \qquad (63)$$

The assumptions made in deriving Equation (63) are that both TV systems have the same frame rate, same number of TV lines per frame, same aspect ratio, are sampled at the same rate, and have linear optics. Figure 17 illustrates in block diagram form the implementation of Equation 63. The hardware implementation is presented and discussed in Chapter 4.

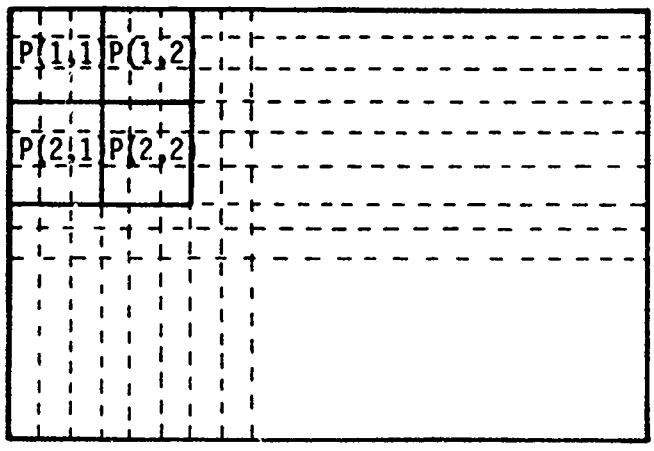

Figure 16. Preprocessing of HR image where W = 3.

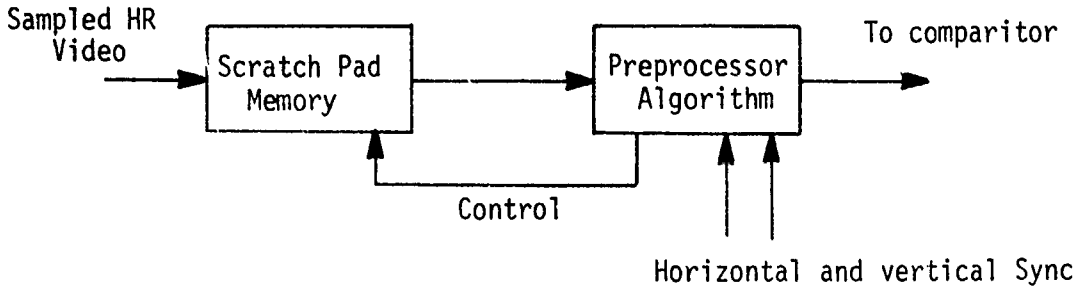

Figure 17. Block diagram of preprocessor.

If W is not an integer, the preprocessing algorithm is more complex. Making the same assumptions about the two TV systems as made previously and defining

$$U = \text{smallest integer} \leq (I - 1)W + 1$$

$$V = \text{smallest integer} \leq (J - 1)W + 1$$

$$X = \text{smallest integer} \leq IW$$

$$Y = \text{smallest integer} \leq JW$$

the preprocessing algorithm becomes:

$$P(I,J) = \frac{1}{W^2}\left\{ \sum_{M=U+1}^{X} \sum_{N=V+1}^{Y} HR(M,N) \right.$$

$$+ \sum_{N=V+1}^{Y} \left[\left[U - (I-1)W\right] HR(U,N) + \left[IW - X\right] HR(X+1,N) \right]$$

$$+ \sum_{M=U+1}^{X} \left[\left[V - (J-1)W\right] HR(M,V) + \left[JW - Y\right] HR(M,Y+1) \right]$$

$$+ \left[U - (I-1)W\right] \left[\left[V - (J-1)W\right] HR(U,V) + \left[JW - Y\right] HR(U,Y+1) \right]$$

$$\left. + \left[IW - X\right] \left[\left[V - (J-1)W\right] HR(X+1,V) + \left[JW - Y\right] HR(X+1,Y+1) \right] \right\} \qquad (64)$$

Figure 18 illustrates the pixel averaging where W = 3.25. The algorithm in Equation 64 can be checked by looking at the P(2,2) element in Figure 18.

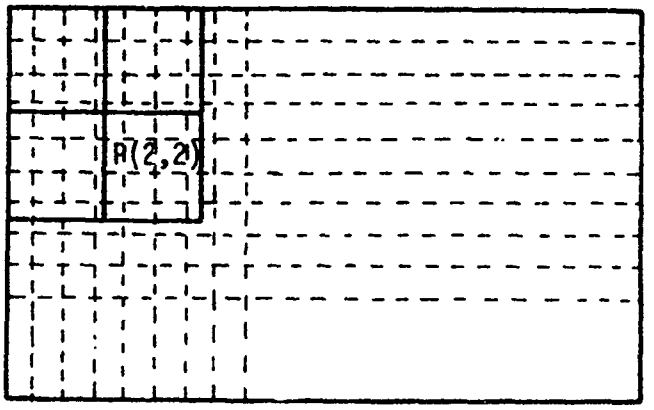

Figure 18. Preprocessing where W = 3.25.

The possibility that the last column and last row of P(I,J) elements turn out to have less than W x W elements of the HR array is of no concern since only the 32 x 32 or 32 x 64 P(I,J) elements centered about the desired target will be used in the correlation algorithm. The important factor is to have the spatial resolution of the preprocessed HR array identical to the spatial resolution of the LR array.

In Equation 64, W is the scale factor by which the resolution of the fine pointing and tracking system TV image must be reduced. The scale factor is due only to differing FOV and is the same in both the horizontal and vertical directions because of the assumptions made about the two TV systems. The effect on Equation 64 of removing these restrictions will now be investigated.

a. Number of TV lines per frame.

If the number of TV lines in the HR image is twice the number of lines in the LR image and all other factors are the same including the FOV, then the vertical resolution of the HR image is twice the LR image and the horizontal resolution is half. The reduction of horizonal resolution is caused by the fact that the image beam is scanning twice

as fast in the HR image which causes each pixel width to be twice as long when sampling at the same rate. This could be corrected by sampling the HR image at twice the rate of the LR image.

Let W_H refer to the horizontal scale factor and W_V refer to the vertical scale factor between the HR and LR systems. Then if the ratio of the number of TV lines in the LR to the HR images is W_1 and all other parameters are identical, the contribution of the different number of lines to W_H is W_1 and to W_V is $1/W_1$.

b. Aspect Ratio

If the LR image has a 4:3 aspect ratio and the HR image has a 1:1 aspect ratio and all the other parameters are identical, then the vertical spatial resolutions of the two sampled images are the same but the horizontal spatial resolution of the HR image is 4/3 that of the LR image. The reason for this is that with linear optics the LR horizontal line is looking at a total scene which is 4/3 wider than the HR scene. However since the scan rate and sampling rates are the same, then each pixel in the LR image covers 4/3 as much horizontal target area as the HR image. Therefore the horizontal spatial resolution of the HR image is 4/3 greater than the LR image.

In general if the aspect ratios of the LR and HR images are P_1 and P_2 respectively where $P_1/P_2 = W_2$, then the contribution of the differing aspect ratios to W_H is W_2 and to W_V is 1.

c. Frame rate

If the frame rate of the LR image is 30 frames/sec and of the HR image is 15 frames/sec and all other parameters are equal, then the horizontal spatial resolution of the HR image is twice that of the LR

image and the vertical spatial resolutions are the same. This is caused by the fact that the beam is scanning twice as fast in the LR system thereby causing the spatial width of each pixel to be double that of the HR image when the sampling rates are identical.

In general, if the ratio of the frame rates of the LR to HR system is W_3 and all other parameters are identical, then the contribution of the differing frame rates to W_H is W_3 and to W_V is 1.

d. Sampling Rate

By an analysis similiar to that given in (a) - (c) above, if the ratio of the sampling rates of the HR to LR TV images is W_4 and all other parameters are identical, then the contribution of the different sampling rates to W_H is W_4 and to W_V is 1.

e. Field of View

If the ratio of the LR to HR fields of view is W_5 and all other parameters are identical, then the contribution of the different FOV's to W_H is W_5 and to W_V is W_5.

f. General Spatial Resolution Matching Equation

If all of the parameters in (a) through (e) above are considered at once, the total horizontal and vertical spatial resolution scale factors are given by

$$W_H = W_1 W_2 W_3 W_4 W_5$$

$$W_V = W_5/W_1 \qquad (65)$$

Defining

$$\begin{aligned} U &= \text{smallest integer} \leq (I-1)W_V + 1 \\ V &= \text{smallest integer} \leq (J-1)W_H + 1 \\ X &= \text{smallest integer} \leq IW_V \\ Y &= \text{smallest integer} \leq JW_H \end{aligned} \tag{66}$$

the preprocessing algorithm given in Equation 64 can be placed in the more general form given below.

$$\begin{aligned} P(I,J) = \frac{1}{W_H W_V} \Bigg\{ & \sum_{M=U+1}^{X} \sum_{N=V+1}^{Y} HR(M,N) \\ & + \sum_{N=V+1}^{X} \Big[[U - (I-1)W_V]\, HR(U,N) + [IW_V - X]\, HR(X+1,N) \Big] \\ & + \sum_{M=U+1}^{Y} \Big[[V - (J-1)W_H]\, HR(M,V) + [JW_H - Y]\, HR(M,Y+1) \Big] \\ & + [U - (I-1)W_V] \Big[[V - (J-1)W_H]\, HR(U,V) + [JW_H - Y]\, HR(U,Y+1) \Big] \\ & + [IW_V - X] \Big[[V - (J-1)W_H]\, HR(X+1,V) + [JW_H - Y]\, HR(X+1,Y+1) \Big] \Bigg\} \end{aligned} \tag{67}$$

2. Low Resolution Image Preprocessing

Since the mean value used for quantizing each KxL sub-array in the LR image is different, it is felt that all of the preprocessing can best be handled digitally. This section presents the optimal and sub-optimal techniques used to find the mean value and to quantize the pixels of each KxL sub-array for the two level quantization case.

Optimally for each value of p and q. in Equation 3 and Figure 4 the K x L pixels should be quantized about the mean video level of that sub-array. This could be done by storing K lines of the low resolution video in say 4 or 5 bit memory, computing the average value of each K x L sub-array as each new pixel is added, then quantizing all K x L pixels about the mean for each value of p and q. It is felt that this method is far too time and power consuming for the amount of accuracy gained. Several sub-optimal trade-offs will now be presented.

Since the mean video level is not expected to change appreciably from frame to frame, one method of reducing the real-time computational burden is to use the mean video level of each sub-array computed from the previous frame. This method, however, requires additional memory and additional host computer load.

A second possibility would be to quantize about the same mean for each sub-array until the mean changes by more than some precomputed amount at which time that entire K x L sub-array would be requantized about the new mean. This method, however, still requires the hardware to requantize an entire K x L sub-array.

A third possiblity is to store the previous K lines of digitized video in 4 or 5 bit memory, compute the average value of each K x L sub-array as a new pixel is digitized, and requantized only the last column of the array about the new mean. This would require only K comparators rather than KL comparators. The average can be computed by storing the sum of each column in shift registers. When a new pixel is added, the first column sum is subtracted from the total and the column containing the new pixel is added to the total.

A fourth possibility is to use the method of the previous paragraph but quantize only the added pixel about the new mean leaving all other quantized values the same. This would require only one comparator. Using this method only the lower right pixel in the K x L array would be quantized exactly as shown in the solid area of Figure 19. If the mean video is assumed to vary linearly with distance from this pixel, then the upper left pixel has the largest error for this value of p and q. The fifth and more accurate method on the average would be to compute the quantization level of the marked pixel by computing the mean level of the dashed K x L array as shown in Figure 19. This would mean a delay in each correlation computation of approximately K/2 lines plus L/2 sample intervals.

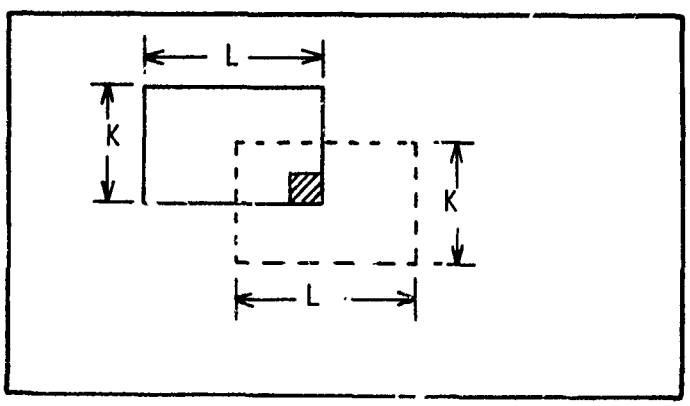

Figure 19. Method for pixel quantization.

The sixth possibility is to quantize about the average of the HR reference. It is felt that this method, while being by far the easiest to implement, would lead to too many false registration points and would be unacceptable.

A further study involving typical military scenes is needed to determine which of the above trade-offs is the best to implement. Without the benefit of this study, method five is recommended and an implementation is suggested in Chapter 4 of this report.

3. Effect of Quantization about Incorrect Mean

As pointed out in the previous section, one of the sources of error in the two level by two level (one-bit by one-bit) correlator is quantization about an incorrect mean. The effect on the mean square signal/noise ratio of quantizing an entire array about the same incorrect mean is presented in this section. The effect on the ms S/N ratio of quantizing each pixel about differing incorrect means is not presented. However, the results can be used as an upper bound if one uses the maximum expected mean error in the resulting curves.

Consider the HR and LR images quantized respectively with the quantizers shown in Figure 20. These quantizers represent an error in quantizing around the wrong dc level of the HR and LR images. Although the above quantizers assume that the HR and LR signals are zero mean, this does not necessarily have to be true. For HR and LR signals that are not zero mean the dc error due to quantization would be given by $\Delta X_1 = X_1 - \overline{HR}$ and $\Delta X_2 = X_2 - \overline{LR}$.

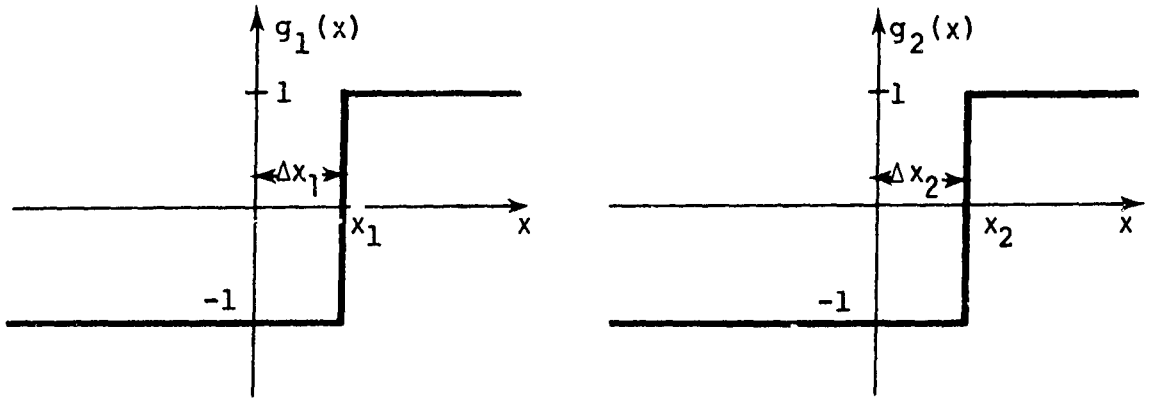

Figure 20. Quantizers for the HR and LR images.

a. Direct Method

Consider the first line of video

$$R(1,q) = \frac{1}{M} \sum_{m=1}^{L} HR(1,m)\ LR(1,m+q) \tag{68}$$

Dropping the row 1 notation and quantizing the HR and LR signals as shown in Figure 20 yields

$$\hat{R}(q) = \frac{1}{L} \sum_{m=1}^{L} g_1\ [HR(m)]\ \ g_2\ [LR(m+q)] \tag{69}$$

The variance in the estimate of $\hat{R}$ is

$$\sigma_{\hat{R}} = \langle \hat{R}^2 \rangle - \langle \hat{R} \rangle^2 \tag{70}$$

where

$$\langle \hat{R} \rangle = E\left\{ \frac{1}{L} \sum_{m=1}^{L} g_1[HR(m)]\ g_2[LR(m+q)] \right\} \tag{71}$$

and

$$\langle \hat{R}^2 \rangle = E\left\{ \left[\frac{1}{L} \sum_{m=1}^{L} g_1[HR(m)]\ g_2[LR(m+q)] \right]^2 \right\} \tag{72}$$

Assuming sample pair independence, a gausian distribution of the HR and LR signals, and evaluating the resulting expectation integrals yields

$$\sigma_{\hat{R}}^2 = \frac{1}{L} \left\{ 1 - 16\ \mathrm{erf}^2\ \left(\frac{x1}{\sigma}\right)\ \mathrm{erf}^2\ \left(\frac{x2}{\sigma}\right) \right\} \tag{73}$$

Using Price's Theorem to evaluate $r(\tau)$ where ρ is the correlation coefficient between HR and LR yields

$$\frac{dr}{d\rho} = \sigma^2 < \left(\frac{\partial g_1}{\partial HR}\right)\left(\frac{\partial g_2}{\partial LR}\right) > \tag{74}$$

Evaluating the partials in Equation 74 by inspection of Figure 20, assuming a jointly gaussian distribution for the HR and LR signals and evaluating yields the following relationship between σ_ρ^2 and $\sigma_{\hat{R}}^2$.

$$\sigma_\rho^2 = \left(\frac{\pi}{2}\right)^2 e^{\frac{x_1^2}{\sigma^2}} e^{\frac{x_2^2}{\sigma^2}} \sigma_{\hat{R}}^2 \tag{75}$$

Substitution of Equation 73 into 75 yields the desired effect of the incorrect mean on the ms S/N ratio.

$$\sigma_\rho^2 = \frac{1}{L}\,\frac{\pi^2}{4}\, e^{\left(\frac{x_1}{\sigma}\right)^2} e^{\left(\frac{x_2}{\sigma}\right)^2} \left\{1 - 16\,\mathrm{erf}^2\left(\frac{x_1}{\sigma}\right)\mathrm{erf}^2\left(\frac{x_2}{\sigma}\right)\right\} \tag{76}$$

b. SSDA Method

The registration function for the SSDA method is given by

$$R(q) = \frac{1}{L} \sum_{m=1}^{L} |HR(m) - LR(m+q)| \tag{77}$$

Going thru an analysis similiar to that used for the Direct Method yields the identical result for σ_ρ^2 given in Equation 76. This was expected, however, since the two methods have been shown to be equivalent in the one-bit by one-bit case.

Figure 21 shows a parametric set of curves depicting the change in σ_ρ^2 for various values of $(\frac{x_1}{\sigma})$ and $(\frac{x_2}{\sigma})$. The dotted curve in Figure 21 shows the effect on σ_ρ^2 if the dc errors in the quantizers are equal. If both x_1 and x_2 are zero (i.e., no error in the mean), then $\sigma_\rho^2 \times L = 2.467$ which is the result obtained in Table 1. As can be seen from Figure 21 the variance is essentially insensitive to small dc errors but grows very rapidly for errors in the mean above 0.4σ.

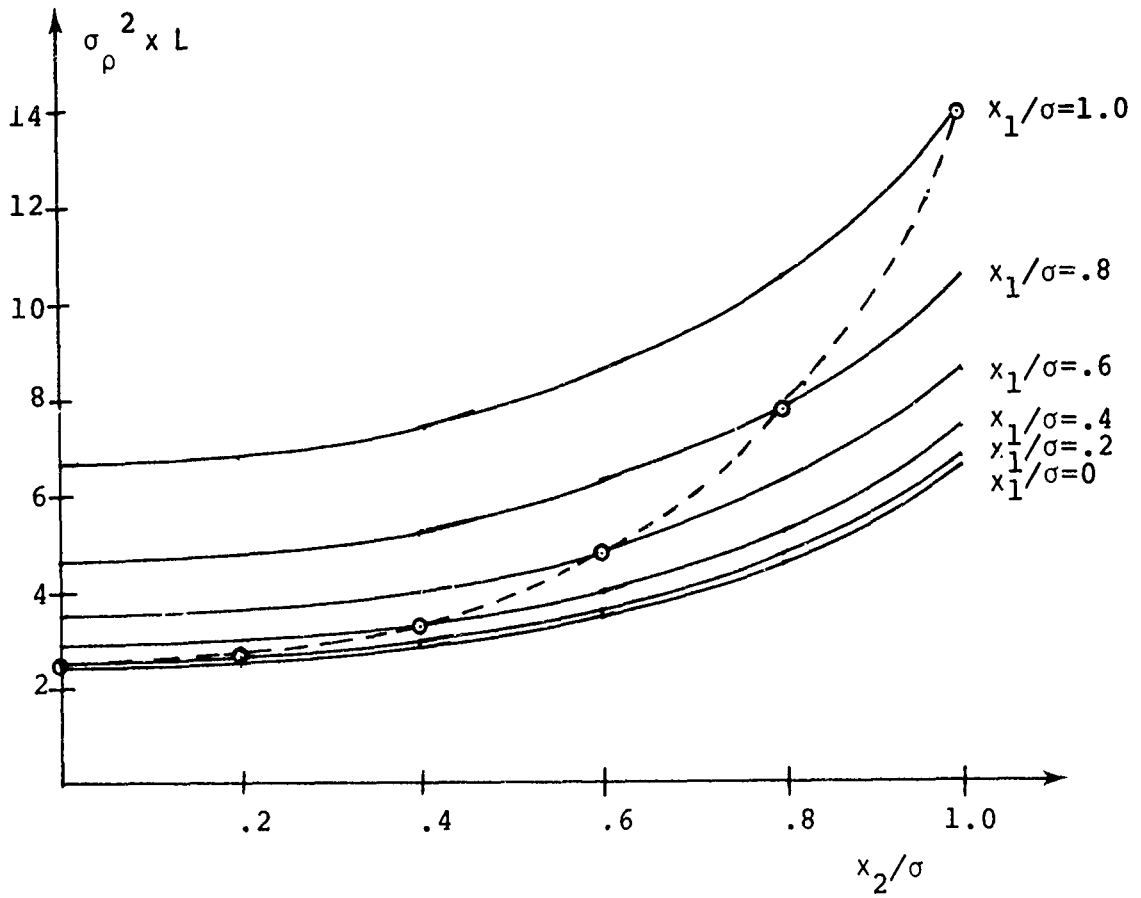

Figure 21. Effect of dc quantization level on the variance in the estimate of ρ

4. Preprocessing for Differing Sensor Characteristics

When trying to accomplish target hand-off between two systems, it is very important for the two sensors to have similiar characteristics. This of course is the reason for the necessity for the algorithm which equalizes the spatial resolution of the two images as given in Section C-1 of this chapter. It is also very important for the spectral characteristics of the two sensors to be the same since correlation can be accomplished only if the two video signals are almost the same. If one sensor covers a wider frequency spectrum than the other, an optical filter might possibly be used during correlation to cause the two spectral responses to be the same. If the two sensors have completely different spectral responses, such as one sensitive in the visible spectrum and one in the infrared spectrum, then correlation would be difficult to accomplish due to the difference in signal characteristics. However one possibility in this case would be to preprocess the video such that only the edges are used for correlation. This is a possibility since even if there is a contrast reversal between the two signals, the edges in the FOV should be approximately the same.

Preprocessing of the HR and LR arrays concerns changing the form of the data so that a better registration between the two can be obtained. In most of the literature that has been surveyed this task is referred to as outlining, edge detection, or boundary mapping. These methods are used mainly for cases in which the two images are acquired at different times or the images come from different types of sensors. The first of these reasons is not applicable to the present system under

study. It is quite possible that for the system under study the images could be produced from different types of sensors. In this situation the data representation of the ground scene from the two sensors might be different. Then some type of preprocessing of the data, such as boundary mapping could be employed.

Reference [5] describes a method by which boundary maps are produced from the raw data. Essentially this method calculates the differential change in magnitude from one data point to the next. It does this for both X and Y directions away from the point being examined. The algorithm then decides if the point being examined represents the boundary of a region or not. If it is a boundary, then that location is assigned a value of 1. If it is not a boundary point, a 0 is assigned to the location. Once a boundary map is produced for the entire image, a correlation can be performed using boundaries of objects in the image instead of all the raw data from the image.

If the data received from the HR and LR imaging systems are of different forms (such as would occur with different sensor characteristics) then the method of boundary maps or edge detection would warrant further investigation. Implementation of any of these methods, however, requires additional hardware and computation time.

D. Vibration Analysis

The effect of LOS jitter of the PTS and missile seeker systems on the correlation algorithm accuracy is investigated in this section. From talks with MICOM engineers the jitter of the seeker LOS should be less

than 100 μrad rms and is the value used in this section. The LOS jitter of the PTS system has been demonstrated to be less than 30 μrad for at least one system. These values are the total rms jitter due primarily to disturbances from the helicopter at 11, 22, 33, and 44 Hz.

The primary effect of LOS jitter on the correlation algorithm is to cause a distortion in the stored video scene. For example, if the jitter is causing the LOS to move downward during the sampling and storage of a 32 x 64 element video array, then the 32nd line may actually be looking at the scene the equivalent of several TV lines below where it should be thus causing a stretching distortion. If the LOS is moving up due to jitter, then the 32nd line may actually be looking at the scene the equivalent of several TV lines above where it should be thus causing a compressing distortion. The problem is further complicated by the fact that one video image may be compressed and the other stretched by the jitter. The net effect on the correlation algorithm is to cause a smaller correlation peak which can be modeled by a reduction in the signal-to-noise ratio

In the calculations which follow both TV systems are considered to be 525 line systems with 480 active TV lines (the remaining 45 lines are used in the vertical retrace), and to have 60 half-frames per second or 30 full frames per second (2:1 interlace) with a 4/3 aspect ratio. For a sampling rate of 7.5 MHz the low resolution image will be digitized into a 240 x 480 element array during the first half-frame and 240 x 480 element array during the second half-frame. If the correlator is designed such that correlation values are calculated as data comes in, then correlation is being performed during each half-frame (i.e., the 32 rows used in the

correlator all come from the same half-frame). Therefore, the total time elapsed from the first sample in each 32 x 64 array used in the correlation algorithm to the last will be the time required to sample 31 complete lines plus 64 samples of the following line.

$$T_R = \frac{31 + (64/480)}{525 \times 30} = 0.00197 \text{ seconds} \tag{78}$$

As stated previously the LOS jitter is predominately at 11, 22, 33, and 44 Hz. If one assumes that the 100 μrad rms jitter is all at 44 Hz, the worst possible condition for correlation, then the greatest angular disturbance which the LOS would have in 0.00197 seconds would be twice the value of the 44 Hz sinewave evaluated at t = .00197/2 seconds.

$$\Delta\phi_{max} = 2(141.4)\ \sin[2\pi 44(0.000986)]$$

or

$$\Delta\phi_{max} = 76.16\ \mu\text{rad} \tag{79}$$

If the seeker vertical FOV is 2°, then each TV line is scanning 72.7 μrad if one assumes 480 active TV lines. Therefore the maximum movement of the LOS from the first to the last sample taken for each computation of R would be slightly over one line. Since correlation in the half-frame correlator is being performed by using alternate lines of the full frame, it is felt that this amount of movement will not cause a significant problem. A more detailed analysis could be obtained by modeling this LOS movement with an additive noise source which would degrade the S/N ratio.

Next consider the case where correlation is performed using 16 lines from one half-frame and 16 lines from the succeeding half-frame. The 32 x 64 correlator then operates on 64 samples from each of these lines. The total time required to sample the data used for each computation of R is

$$T_R = \frac{15 + 64/480}{525 \cdot 30} + \frac{1}{60} = 0.0176 \text{ seconds} \qquad (80)$$

which is more than half a cycle of a 44 Hz waveform. Therefore, the total movement could be as much as the peak-to-peak LOS jitter or 282 μrad. This represents approximately 3.89 TV lines. Even if all of the jitter is at 11 Hz, the maximum angular movement would be 162 μrad which is over 2 TV lines. Using the full-frame correlator the correlation peak would be reduced more than for the half-frame correlator. The net effect of the LOS jitter is a larger reduction in the S/N ratio for a full-frame correlator than for a half-frame correlator.

Table 3 shows the maximum possible angular vibration in μrad and its equivalent in TV lines if a 100 μrad rms jitter in the seeker LOS is considered to be concentrated at 11, 22, 33, or 44 Hz. The data for a 32 x 64 element correlator operating on each half-frame respectively and for the same correlator operating on a full-frame are given. From the data in Table 3 it is obvious that a 32 x 64 correlator operating on successivie half-frames is much less sensitive to LOS jitter than a full-frame correlator. The half-frame correlator is also simpler to implement since data does not have to be stored from one half-frame to the next.

Frequency	Half-Frame Correlator		Full-Frame Correlator	
Hz	$\Delta\phi_{max}$ μ rad	Equivalent TV Lines	$\Delta\phi_{max}$ μ rad	Equivalent TV Lines
11	20	0.27	162	2.22
22	40	0.54	265	3.64
33	59	0.81	282	3.86
44	78	1.07	282	3.86

Table 3. Angular disturbances in seeker LOS due to jitter.

Next consider a PTS system with a vertical FOV of 0.4°. With this system five lines of video must be averaged in order to equalize the size of the target in the two FOVs. Therefore the elapsed time between first and last sample will be

$$T_R = \frac{(5 \times 32\text{-}1) + (64/480)}{525 + 30} = 0.01 \text{ seconds} \tag{81}$$

If one assumes that the 30 μrad of jitter is all at 44 Hz, then the largest angular disturbance which the LOS would have in .01 seconds would be

$$\Delta\phi_{max} = 2(\sqrt{2})\ (30)\sin[2\pi 44(.005)]$$

or (82)

$$\Delta\phi_{max} = 83.35 \text{ μrad}$$

For a vertical FOV of 0.4°, each TV line, assuming 480 active lines, scans 14.5 μrad. Since each five successive lines of the PTS video are averaged, the $\Delta\phi_{max}$ is slightly more than one TV line when averaged. The net effect of LOS jitter on the PTS is therefore seen to be approximately the same as the effect on the seeker system.

E. Derivation of ΔX and ΔY Misalignment in LR Image

After the correlation array, R(p,q), has been calculated, it is desired to move the missile seeker LOS such that the target is in the center of the LR FOV. In order to do this the misalignment in both the X and Y directions must be determined. The position of the target in the LR image can be determined by performing a search of the R(p,q) correlation array for a maximum in order to identify the registration points p* and q*.

The geometrical layout of the HR and LR images is shown in Figure 22. The p and q counters start in the upper left corner of the LR image. This designates the starting placement of the HR image in the LR image for the calculation of the R(p,q) array.

Figure 22 also shows a possible location of the HR Image which produced a maximum value of R(p,q) over all possible p and q. It is desired that image registration take place in the center of the LR image. The K x L array of LR image points around the center is shown in Figure 23 along with the geometric definitions of ΔX and ΔY. The displacements ΔX and ΔY represent values by which the LR camera must be

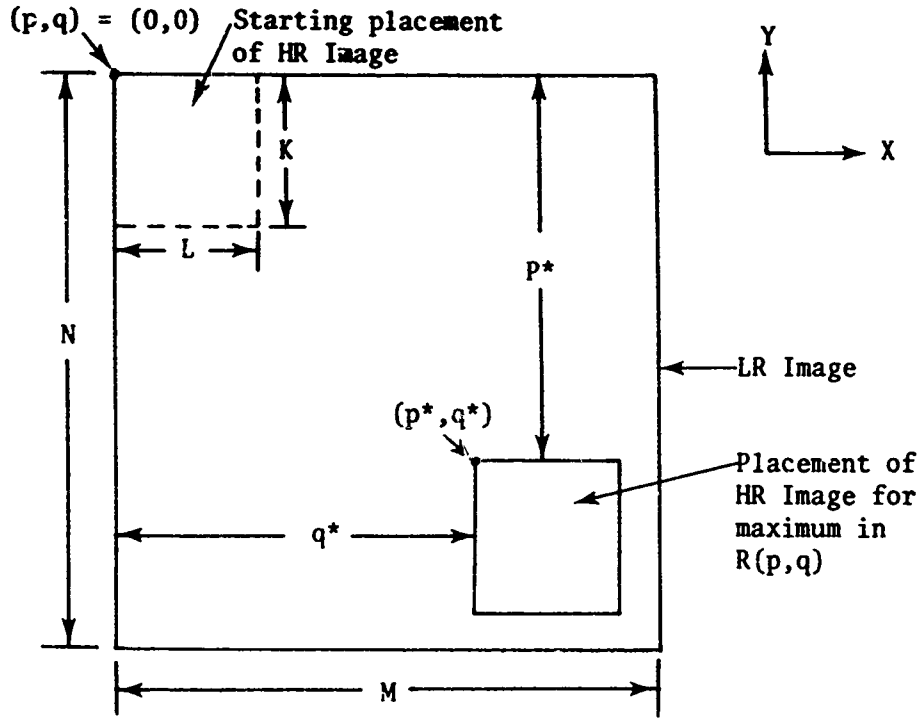

Figure 22. Image layout identifying p* and q*.

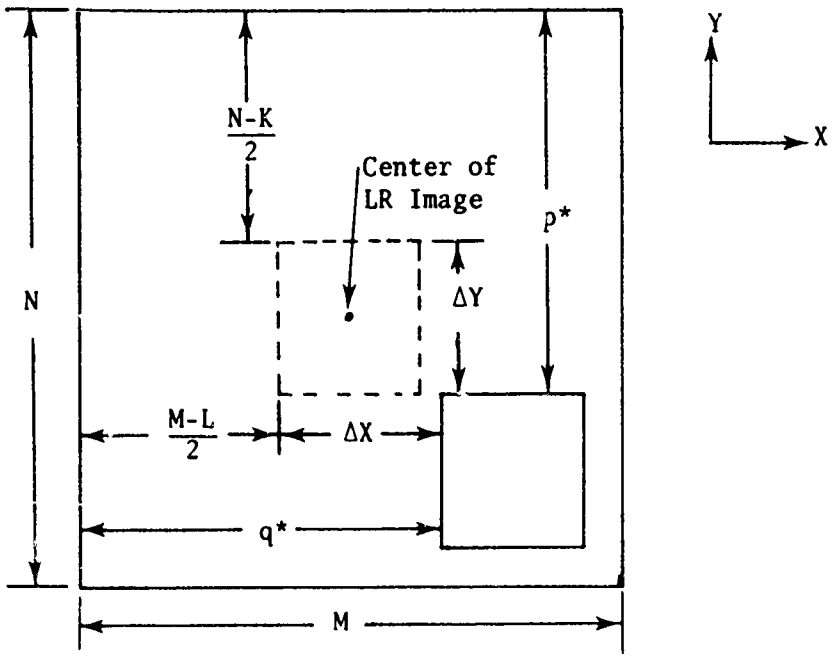

Figure 23. Image layout showing ΔX and ΔY.

shifted so that the maximum value of R(p,q) will occur at the center of the LR image. It is desired that

$$p^* = \frac{N - K}{2} \tag{83}$$

and

$$q^* = \frac{M - L}{2} \quad , \tag{84}$$

Using this reasoning ΔX and ΔY can be calculated using the following equations:

$$\Delta X = q^* - (\frac{M-L}{2}) \tag{85}$$

and

$$\Delta Y = (\frac{N-K}{2}) - p^*. \tag{86}$$

The ΔX and ΔY in Equations 85 and 86 are expressed in terms of pixel elements. The angular errors $\Delta\phi_X$ and $\Delta\phi_Y$ in a seeker with a FOV of 2°, 480 active TV lines in this FOV and 480 samples per line are

$$\Delta\phi_X = \frac{\Delta X}{480} \times 2°, \text{ in degrees} \tag{87}$$

$$\Delta\phi_Y = \frac{\Delta Y}{480} \times 2°, \text{ in degrees} \tag{88}$$

These angular errors can be used to torque the seeker gimbals such that the target is in the center of the FOV.

F. Threshold Effects on Probability of False Registration and Detection Probability

The following analysis develops the concepts of the probability of false registration (i.e., the probability that two images are chosen as registered when they in fact are not) and the probability of detection (i.e., the probability that two images are chosen to be registered given that they are in fact registered). Each of these probabilities is given in terms of the threshold for deciding if registration is achieved and the input SNR for both images.

For simplicity and because other considerations indicate its desirability, the following is developed for a 1-bit by 1-bit (2-level by 2-level) correlator using either the Direct Double Summation Method or the Sequential Similarity Detection Algorithm. Previous comparisons have shown these two methods to be identical statistically for the 1-bit quantization case.

The following assumptions are inherent in the development.

1. Signal and noise levels at each pixel are independent of each other and of signal and noise levels from any other pixel.

2. The noise at any pixel is zero mean Gaussian for both the HR and LR images.

3. The rms noise level is constant ($\sigma_{n_{HR}}$) for each pixel of the HR image and a different constant ($\sigma_{n_{LR}}$) for each pixel of the LR image.

4. The signal levels for the HR and LR images have mean values $\overline{HR}$ and $\overline{LR}$ respectively for the pixels within each image. It is of course realized that $\overline{LR}$ may change as p and q (the shift values) change; however for a given correlation computation $\overline{LR}$ is a constant.

5. The signal plus additive noise from HR and LR images are subjected to 1-bit quantization as represented by g_1 and g_2 in Figures 24 and 25.

The only possible outputs for a one-bit implementation are zero or one for comparison of a LR pixel with a HR pixel. Therefore, for implementation of a K by L array correlation, the correlation magnitude takes on values ranging from 0 to KL in integer steps. The obvious questions which arise and the answer of which is the purpose of this section is: "How close to the maximum value of KL must a given correlation be to indicate registration? What are the consequences of chosing a particular threshold for a decision on registration of the HR and LR images?"

Under the assumptions outlined above we can write the probability density functions for the noise in any pixel of the HR and LR images for a given shift value (p,q).

$$f_{n_{HR}}(n_{HR}) = \frac{1}{\sqrt{2\pi}\sigma_{n_{HR}}} e^{\frac{-n_{HR}^2}{2\sigma_{n_{HR}}^2}} \tag{89}$$

$$f_{n_{LR}}(n_{LR}) = \frac{1}{\sqrt{2\pi}\sigma_{n_{LR}}} e^{\frac{-n_{LR}^2}{2\sigma_{n_{LR}}^2}} \tag{90}$$

At pixel (n,m) in the HR image and pixel (n+p, m+q) in the LR image we have signal plus noise as follows:

$$r_{HR} = r_{HR}(n,m) = HR(n,m) + n_{HR}(n,m) \tag{91}$$

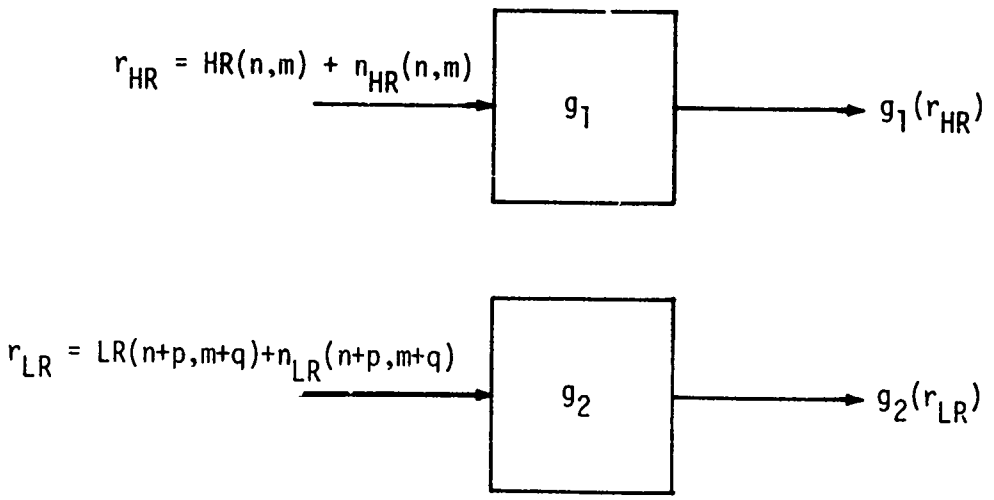

Figure 24. Quantized signal plus noise.

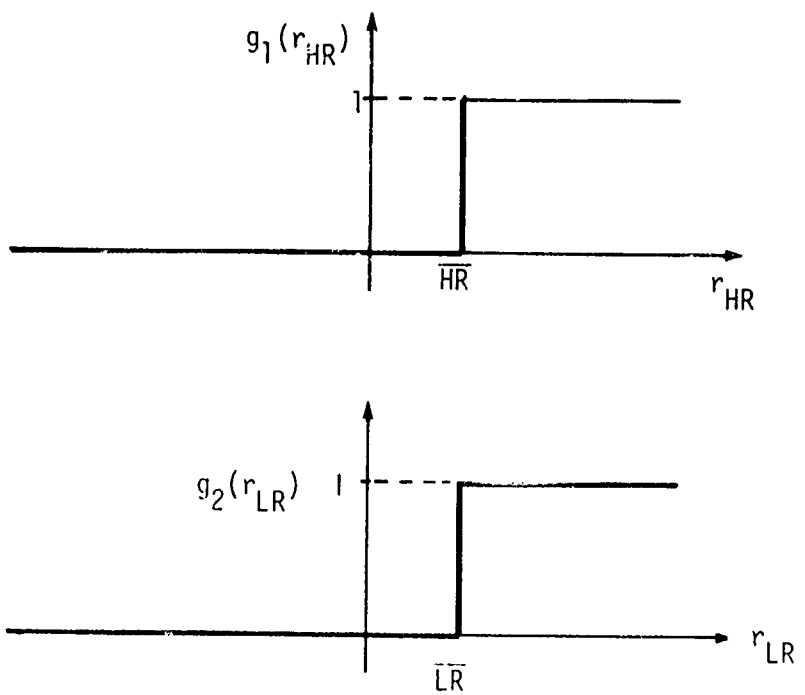

Figure 25. Quantizer characteristics.

$$r_{LR} = r_{LR}(n+p,\ m+q) = LR(n+p, m+q) + n_{LR}(n+p,\ m+q) \tag{92}$$

where r_{HR} and r_{LR} are to be quantized and compared logically and the output summed for KL pixels as shown in Figure 26.

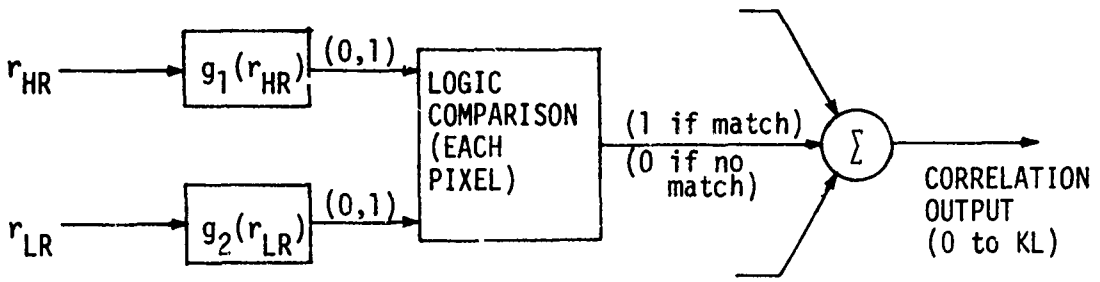

Figure 26. Correlation technique.

From the quantizers g_1 and g_2 we have the rules <u>for no noise</u>

$$g_1 = \begin{cases} 1 \text{ if } HR > \overline{HR} \\ 0 \text{ if } HR < \overline{HR} \end{cases} \tag{93}$$

$$g_2 = \begin{cases} 1 \text{ if } LR > \overline{LR} \\ 0 \text{ if } LR < \overline{LR} \end{cases} \tag{94}$$

If noise is included, the rules become <u>with noise</u>

$$g_1 = \begin{cases} 1 \text{ if } HR+n_{HR} > \overline{HR} \\ 0 \text{ if } HR+n_{HR} < \overline{HR} \end{cases} \tag{95}$$

$$g_2 = \begin{cases} 1 \text{ if } LR+n_{LR} > \overline{LR} \\ 0 \text{ if } LR+n_{LR} < \overline{LR} \end{cases} \tag{96}$$

Clearly there are four hypotheses that can be postulated for the outputs of the two quantizers in terms of the inputs. The hypotheses are:

$$\begin{aligned} H_{HR0} &- \text{the input HR} < \overline{HR} \text{ (choose } g_1=0) \\ H_{HR1} &- \text{the input HR} > \overline{HR} \text{ (choose } g_1=1) \\ H_{LR0} &- \text{the input LR} < \overline{LR} \text{ (choose } g_2=0) \\ H_{LR1} &- \text{the input LR} > \overline{LR} \text{ (choose } g_2=1) \end{aligned} \tag{97}$$

These hypotheses can be chosen with no error by a simple threshold circuit if no noise is present. If noise is present, there are possibilities for error in the choices. This error is dependent on the signal levels, the noise statistics and the number of pixels used in a given correlation computation.

The correlation output is then compared with a threshold value, N_0, to determine if the images are registered. If the correlation output is greater than N_0, the images are chosen to be registered. Since N_0 is a parameter which must be chosen, its effect on expected errors must be known. Specifically its effect on false alarm and detection probabilities must be known.

1. False Alarm

False alarm occurs when the logic comparison indicates registration of the image with a particular LR image when in fact the two are different. The probability of false alarm is best examined by considering the probability of false alarm for each comparison of an HR and an LR pixel

pair. Defined for each pixel pair, the false alarm probability is simply the probability that the HR and LR pixels are chosen matched given that they are different. However, since the HR and LR images can be different (not registered) without requiring that all KL pixels be different between the two images, consideration must be given for the probability of matched pixel pairs within non-registered images. This consideration requires an additional assumption about the probabilities of pixel pairs being matched or mis-matched given that the images are different. Fortunately, based on fundamental arguments supported by the method of quantizing about the mean value for each image, these assumed probabilities are easily obtained.

Since the relation of total number of chosen pixel matches to the threshold N_0 is really what determines false registration probability, it is necessary to examine the probability of choosing pixels as matched given that the images are different. Clearly this has two parts: 1. probability of [choosing pixels matched|pixels matched| images different], and 2. probability of [choosing pixels matched| pixels different|images different].

If the individual pixels for different images are assumed to be independent of each other, then a "0" or "1" is equally likely at any given quantization step. This should be true for any symmetric probability density functions of the HR and LR intensities since quantization is about the mean value in each image. With this assumption, it can be shown that for each pixel pair comparison, the probability of false alarm is independent of the image signal-to-noise ratios.

The probability of false alarm for the ith pixel pair comparison is

$$P_i[E] = [M_{HR}M_{LR} + (1-M_{HR})(1-M_{LR})] \cdot P[\text{pixels match}|\text{different images}] + [(1-M_{HR})M_{LR} + M_{HR}(1-M_{LR})] \cdot P[\text{pixels different}|\text{images different}] \quad (98)$$

where:

$$M_{HR} \triangleq \int_{-\infty}^{SNRHR} \frac{1}{\sqrt{2\pi}} e^{-\frac{\beta^2}{2}} d\beta$$

$$M_{LR} \triangleq \int_{-\infty}^{SNRLR} \frac{1}{\sqrt{2\pi}} e^{-\frac{\beta^2}{2}} d\beta$$

SNRHR = HR image signal-to-noise ratio
SNRLR = LR image signal-to-noise ratio.

Under the assumption stated above P[pixels match|images different] = P[pixels different|images different] = $\frac{1}{2}$ and $P_i[E] = \frac{1}{2}$; for all SNRHR and SNRLR.

If all KL pixels are considered, we find that if N is the number of false alarms in KL pixels then the probability density function for N is given by

$$P_N[E] = \binom{KL}{N} a^{N_b(KL-N)} \quad (99)$$

where $P_N[E]$ is the probability of exactly N false alarms and obeys the familiar binomial probability law

where $\binom{KL}{N} = \frac{(KL)!}{N!(KL-N)!}$ (100)

is the binomial coefficient and gives the number of possible combinations of KL pixels with N false alarms, and

$a = P_i[E]$ = probability of false alarm on each pixel pair

$b = 1 - P_i[E]$.

If a threshold value of N is chosen, i.e. $N = N_0$, such that if $N \leq N_0$ for any given correlation computation the decision is to reject the hypothesis that the images are alike, then a probability of false registration can be found as a function of N_0 from

$$P_{FA}[N_0] = \text{Probability } [N > N_0 | \text{images different}]$$

or

$$P_{FA}[N_0] = 1 - \sum_{N=0}^{N_0} \binom{KL}{N} a^N b^{(KL-N)} \tag{101}$$

For KL large, the binomial probability law is approximately gaussian which gives

$$P_{FA}(N_0) \simeq 1 - M\left(\frac{N_0 - (KL)a + \frac{1}{2}}{(KL)ab}\right) \tag{102}$$

where

$$M(x) = \int_{-\infty}^{x} \frac{1}{\sqrt{2\pi}} e^{-\frac{\beta^2}{2}} d\beta.$$

Probability of false alarm is plotted versus threshold, N_0, for KL = 2048 in Figure 27 and for KL = 1024 in Figure 28.

2. Detection

Detection or correct registration occurs when the HR and LR images are correctly chosen to be identical; that is, they are chosen matched given that they are matched. Similar to the development for false alarm, it is convenient to start with a single pixel pair comparison to derive the statistical behavior of correct registration.

The major difference between the probabilities for false alarm and detection lies in the fact that when the HR and LR images are registered, the probability that pixel pairs match should be higher than it was for the unlike images examined in the false alarm treatment. Furthermore, this difference in probability of match and mismatch for each pixel pair results in the probability being dependent on signal-to-noise ratio's of the two image signals.

The probability of choosing a pixel pair matched given that the HR and LR images are registered is

$$P_i[C] = [M_{HR}M_{LR} + (1 - M_{HR})(1 - M_{LR})]$$

$$\cdot P[\text{pixels match} \mid \text{images same}]$$

$$+[(1 - M_{HR})M_{LR} + M_{HR}(1 - M_{LR})]$$

$$\cdot P[\text{pixels mismatch} \mid \text{images same}] \qquad (103)$$

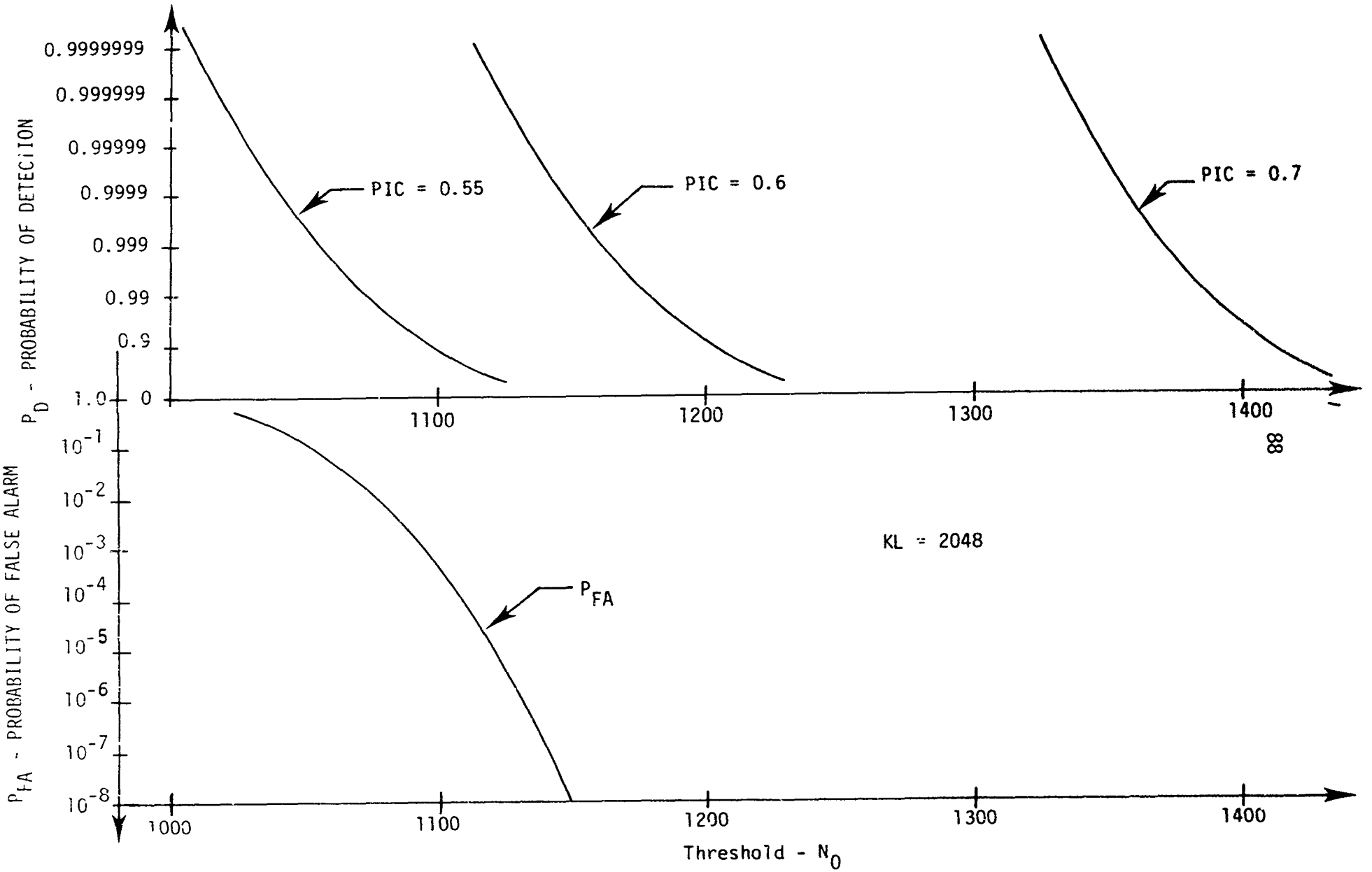

Figure 27. Detection and false alarm probabilities versus decision threshold (KL=2048).

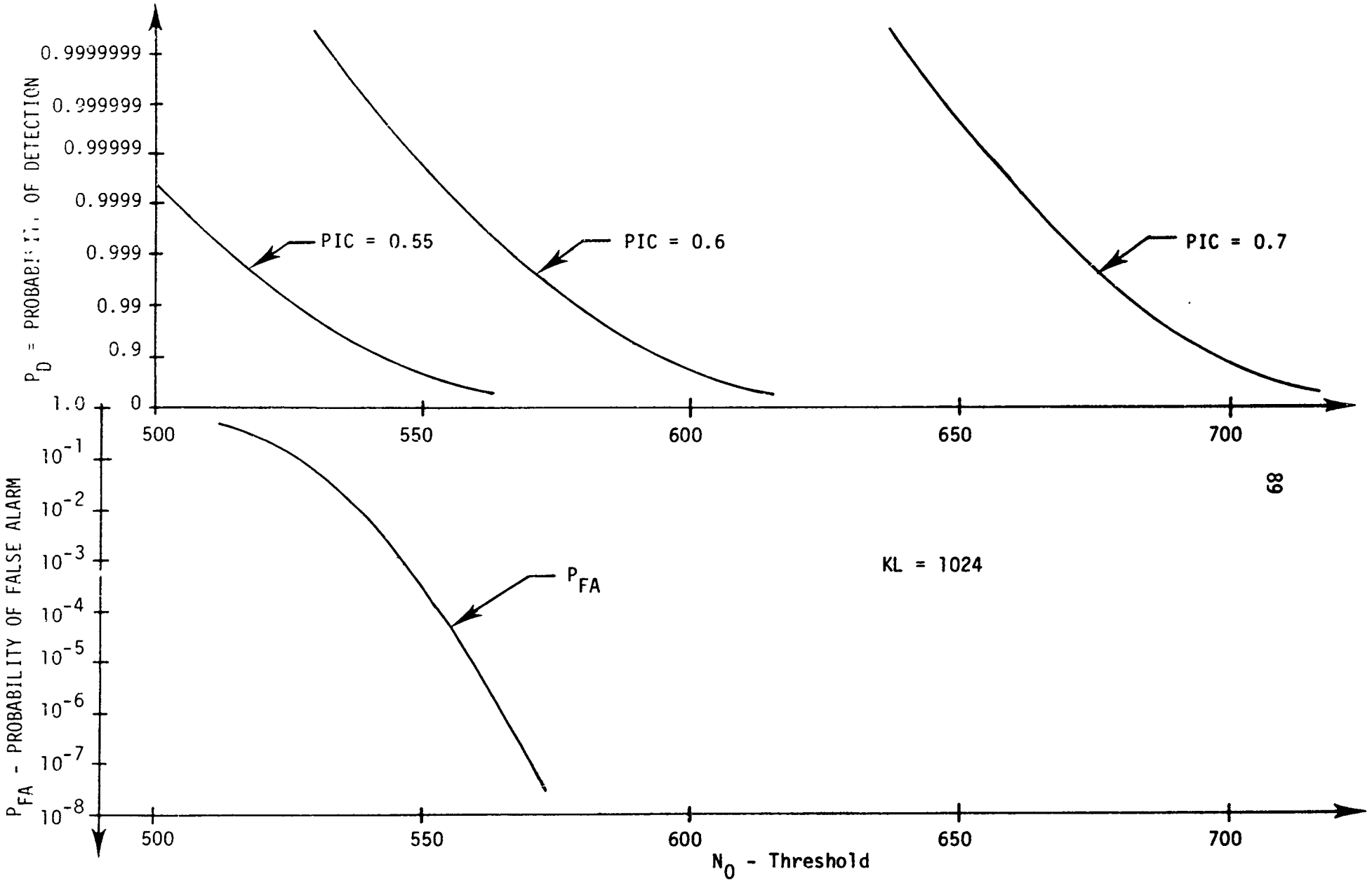

Figure 28. Detection and false alarm probabilities versus decision threshold (KL=1024).

or if we define the error probability

$$\varepsilon \triangleq P[\text{pixels mismatch} | \text{images same}]$$

then

$$P_i[C] = [M_{HR}M_{LR} + (1 - M_{HR})(1 - M_{LR})]\ (1-\varepsilon)$$

$$+[(1 - M_{HR})M_{LR} + M_{HR}(1 - M_{LR})]\ \varepsilon\ . \qquad (104)$$

For the ideal case, $\varepsilon = 0$, each HR and LR pixel pair will match so that additive noise is the only error source. However, for practical sensors, there is a finite probability that pixel pairs will mismatch due to different spectral responses, non-linearities and other error sources. Thus it is important to examine the effects of non-zero values for ε. Since M_{HR} and M_{LR} are dependent on signal-to-noise ratios SNRHR and SNRLR of the respective video signals, then as indicated by Equation 104 the probability of choosing a single pixel pair as being matched, given that the two images are alike, is dependent on the three parameters SNRHR, SNRLR and ε.

Once the value for $P_i[C]$ is established then the total detection probability as a function of the threshold, N_0, can be determined. If all KL pixels are considered, we find as with the false alarm problem that if N is the number of pixels chosen as matched, then the probability density function for N is again binomial.

$$P_N[C] = \binom{KL}{N} c^N\ d^{(KL-N)} \qquad (105)$$

And the probability of detection is the probability that N will be greater than N_0, or

$$P_D[N_0] = \text{Probability } [N > N_0 | \text{images alike}]$$

$$P_D[N_0] = 1 - \sum_{N=0}^{N_0} \binom{KL}{N} c^N d^{(KL-N)} \qquad (106)$$

where

$$c = P_i[C]$$

$$d = 1 - P_i[C]$$

Clearly, P_D is a function of KL, N_0 and $P_i[C]$ which in turn depends on SNRHR, SNRLR and ε. Figure 27 shows P_D versus threshold, N_0, for KL = 2048 data points and for three worst case values of $P_i[C]$. (NOTE: $P_i[C]$ is listed as PIC on all figures).

A value of PIC = 0.5 gives exactly the same curve for P_D as is shown for P_{FA}. This could occur only if we assume a value of $\varepsilon = 0.5$. This is highly unlikely since it says, that even though the images are alike, there is at best a 50-50 random chance that individual pixel pairs match between the two images. If the sensor characteristics are so different that $\varepsilon \leq 0.5$ is possible, then there is no need to waste effort trying to correlate the two images. Figure 28 shows similar curves for P_D with KL = 1024.

As an example of what the curves in Figures 27 and 28 mean consider that it is desired that a high P_D be attained while keeping the number of false detections to one per second. The number of false detections is given by

$$N_{FD} = P_{FA} \cdot N_p N_q \cdot F\, T_m$$

where:

N_p = number of shift values "p" for which correlation is computed

N_q = number of shift values "q" in the other direction

F = frame rate (frames/sec)

T_m = total mission time (1 sec)

$$N_{FP} = P_{FA} \cdot [640-64][480-32] \cdot 30$$

$$1 \simeq 8(10^6)P_{FA} \qquad (107)$$

which requires $P_{FA} \leq 1.2(10^{-7})$. Then from Figure 27 this P_{FA} corresponds to a threshold of $N_0 \simeq 1140$.

Projecting up to the P_D curve for PIC = 0.55 indicates a detection probability of less than 0.3 which is unacceptable. For PIC = 0.6 the value of P_D is greater than 0.9999. Evaluation of this result says that if a false alarm rate of one per second is to be achieved then to maintain high detection probability, SNRHR, SNRLR and ε must be such that PIC > 0.55 and preferably $\geq$ 0.6.

The relationship between P_D and P_{FA} is shown more clearly in Figure 29 where N_0 is the common variable which has been removed. Improvement in performance is represented by movement of the curves diagonally upward from the coordinate center.

Incidentally, a false alarm rate of one per second is the case where one false registration occurs out of $\sim 8(10^6)$ correlations. This is the number of real time correlations computed per second for a

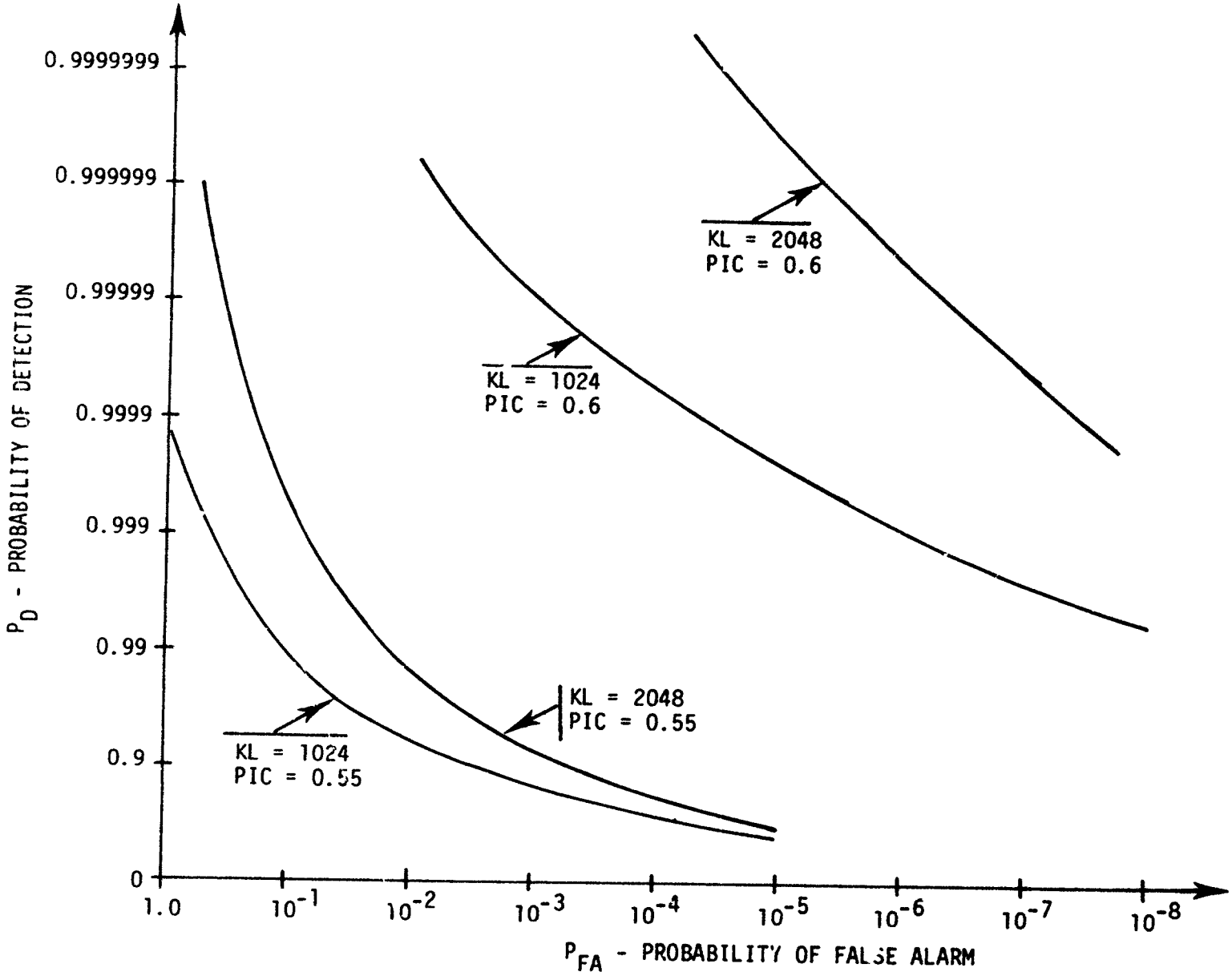

Figure 29. Probability of detection versus probability of false alarm; parameter dependence.

32 x 64 reference array and a 480 x 640 low resolution image at standard TV frame rates.

Since the above results are so strongly dependent on PIC a parametric analysis of PIC is of value.

The effect of ε on the value of PIC is shown in Figure 30 for four discrete values of ε as a function of signal-to-noise ratio. For convenience in plotting, only values corresponding to equal SNR for the video signals are shown. The figure shows that ε has a profound effect on the maximum attainable value of PIC which is reached asymptotically as the signal-to-noise ratios increase. In each case, the maximum achievable value of PIC is $1-\varepsilon$, and is achieved only as the two video SNR's increase.

Since the HR image SNR and the LR image SNR will most likely vary independently of each other, it is of interest to examine the effect of different SNR's on PIC. Figure 31 illustrates this effect for a fixed value of $\varepsilon = 0.1$. As in Figure 30 the absolute maximum attainable PIC is $1-\varepsilon$; however, it is not reached unless both video SNR's are greater than 3. The point made by Figure 31 is that for optimum detection probability, both images should have a SNR of at least three. Only partial compensation is achieved by one video signal having very high SNR if the other video signal has SNR significantly less than 3.

To summarize briefly, the above analysis indicates that for signal-to-noise ratios which can reasonably be expected from electro-optic sensors ($\sim$3), even for a worst case assumption about sensor characteristic mismatch ($\varepsilon = 0.4$), for the 32 x 64 reference array size

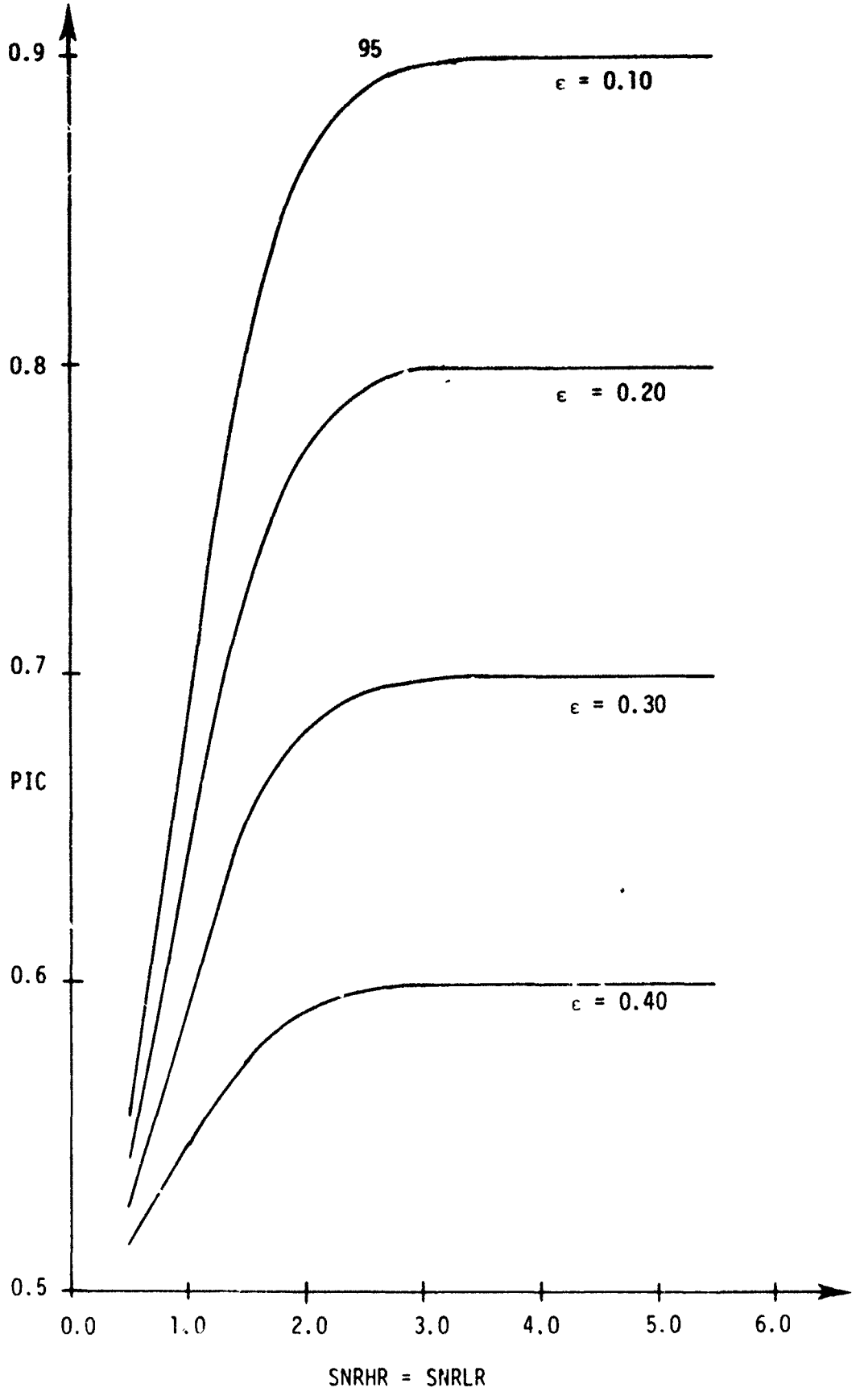

Figure 30. Effect of SNR and pixel mismatch probability, ε, on probability of a correct decision for each pixel.

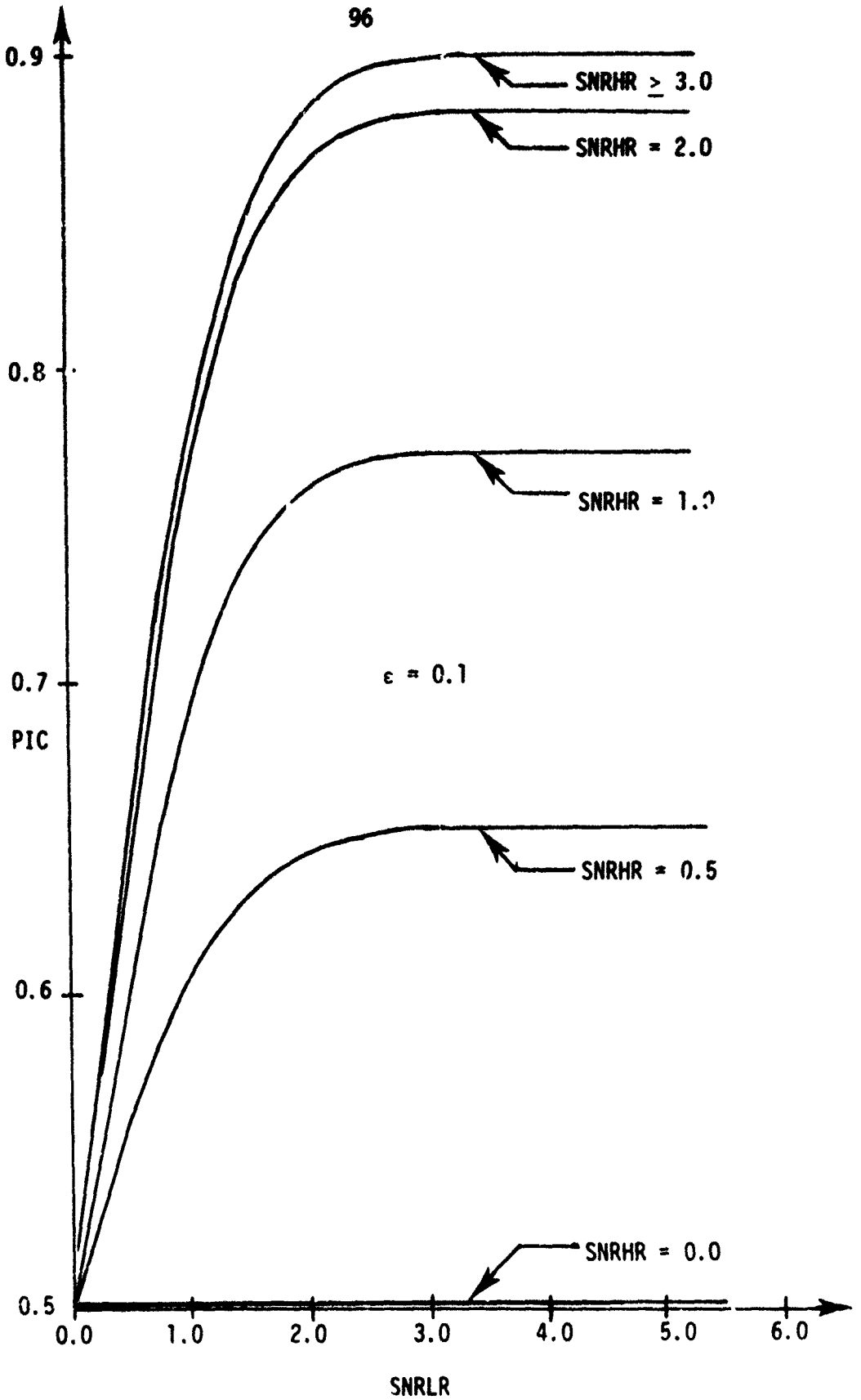

Figure 31. Effect of different video SNR on probability of making correct decision for each pixel.

a threshold can be set which will ensure low false alarm rate and high detectior probability. It should be stated that the above analysis is based on a one-look correlation for each shift value. Multiple-look correlation, that is, computing the correlation function for a given shift value several times and using a decision based on the multiple correlations, will provide even better performance statistically. However, since multiple correlations in real time would require parallel processors, increased processing speed or reduced data array size, that technique can be eliminated for practical reasons. More than adequate statistical performance should be achievable with the one-look real-time correlation technique.

G. Target Not in Seeker FOV

Due to inaccurate boresight alignment or to movement of the missile within its stores rack, there exists the possibility that the target will not be within the seeker FOV. If the correlation coefficient does not exceed the threshold value during n consecutive TV fields, the decision is made to slew the seeker TV LOS in a search pattern to find the target. The value of n is a design parameter which should be studied in a technology program. A value of from one to four would be an adequate range for such a study.

Figure 32 illustrates two possible search patterns. Figure 32(a) shows a search pattern which searchs for the target over an area which is nine times the area of the original search area in eight discrete steps of the seeker LOS. Figure 32(b) shows a search pattern which searchs for the target over an area which is four times that of the

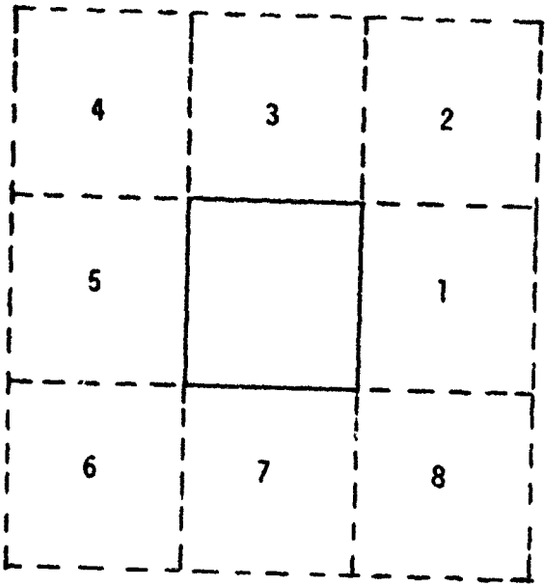

(a)

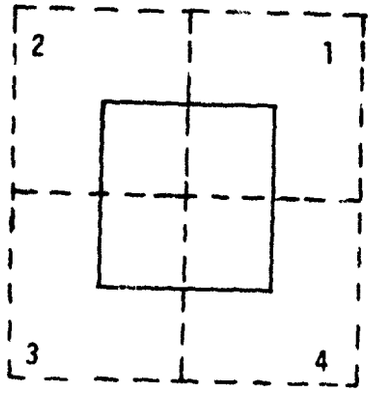

(b)

Figure 32. Search patterns for missile seeker.

original area in four discrete steps. Search pattern 32(b) would require less than half the time as search pattern 32(a) if say the target is in the last possible dotted square. Due to recent experiments conducted at MICOM where the missile seeker was slaved to the PTS, it is felt that the search pattern of Figure 32(b) will be adequate (i.e., the probability of finding the target in search pattern 32(b) is quite high). However, in a technology program, tests should be conducted to determine the optimal search pattern (that is one that yields a high enough probability of finding the target in the least possible time). Another reason for choosing search pattern 32(b) is because of the inaccuracies of the correlation algorithm around the edges of the FOV. Since the edges of the original FOV in Figure 32(b) are well within the search pattern FOVs, the possibility of missing the target due to edge effect is reduced. If one uses the search pattern of Figure 32(a), there exists the possibility of not finding the target at all even though it is within the original FOV but close to an edge.

The correlation values are ignored during the slewing of the seeker LOS. When the LOS stops, if after n TV fields the correlation does not exceed the chosen threshold, the LOS is advanced to the next search area. If after completely searching all areas the threshold is not exceeded, the gunner would be flashed a signal to this effect whereupon he can re-initiate the process if he desires.

4. IMPLEMENTATION

The system required to implement either of the correlation and location functions presented in Chapter 3 will consist primarily of hardware to perform the correlation operation itself. The speed of operation of the entire system will be limited by speed considerations in the correlator. The correlation activity consists of a comparison activity (absolute difference, equivalence ($\oplus$) or multiplication) followed by a summation operation. In order to speed the summation process, an adder tree is employed. The number of layers of addition and hence the speed of the adder tree is a function of the fan-in or number of branches on each layer of the tree as well as the propagation delay of the logic used to implement the tree. It is of major importance that maximum fan-in be employed whenever possible. Digital implementations treat addition as a binary operation. Therefore, the number of layers in the adder tree is directly related to $\log_2 N$ where N is the number of functions to be summed. Dramatic speed increases will be obtained by increasing the fan-in. A later section will illustrate this phenomenon. The method of presentation will be to discuss the various components of Figure 33 by first examining correlation techniques followed by discussion of the various support components.

A. Implementation of One-Bit by One-Bit Real-Time Correlator

In this section the logic design for a one-bit by one-bit correlator is considered. The objective is to find the largest reference array which can be handled in real time subject to a variety of constraints such as logic family, power requirements, etc. It has been

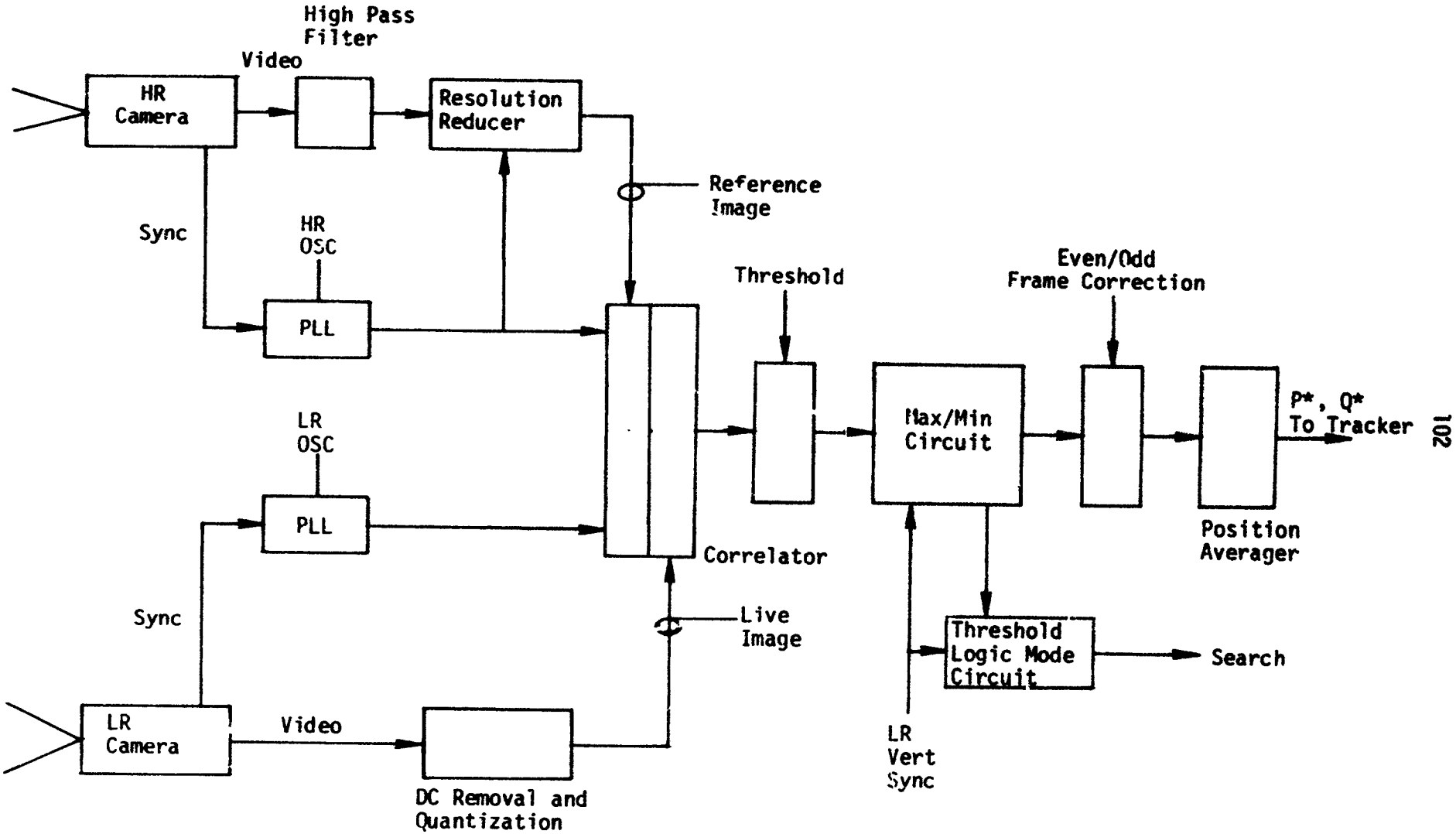

Figure 33. Block diagram of correlator hand-off system.

shown that each value in the $\hat{R}$ correlation matrix must be found in about 133 nsec when sampling the incoming video at 7.5 MHz. Two logic families will be investigated: ECL and TTL Schottky. No slower logic families can meet the computational speed requirement for even the smallest reference array. The technique employed is to use an exclusive-OR or an exclusive-NOR circuit to perform difference or multiplication respectively and then to sum these correlation elements with an adder tree.

Figure 34 is the logic diagram for a 12 by 1 correlator. One can think of this as one column in an array correlator. The inputs to the exclusive-OR gates are quantized one-bit signals. Figure 35 shows how 16 of these correlators can be combined to yield a 12 x 16 element correlator. The circuit type, packaging, power, and propagation times are given in the Figures below the appropriate blocks. All M x L correlators can be designed in the same way. The 12 x 16 correlator was chosen for illustrational purposes.

Table 4 is a summary of total packaging and power requirements, and total propagation delay for several reference array sizes using ECL and TTL logic. The largest real-time correlator using ECL logic is seen to be 48 x 64. The largest array using TTL logic is less than 12 x 16 and is not shown since this is unacceptable. One can observe from Table 4 that the ECL logic is about twice as fast as the TTL logic for a given array size. However, the total power requirement is about twice as great for the ECL logic as for the TTL logic. Since the number of packages is about the same, the physical size of the correlators should be about the same unless heat sinks are necessary for the ECL correlator.

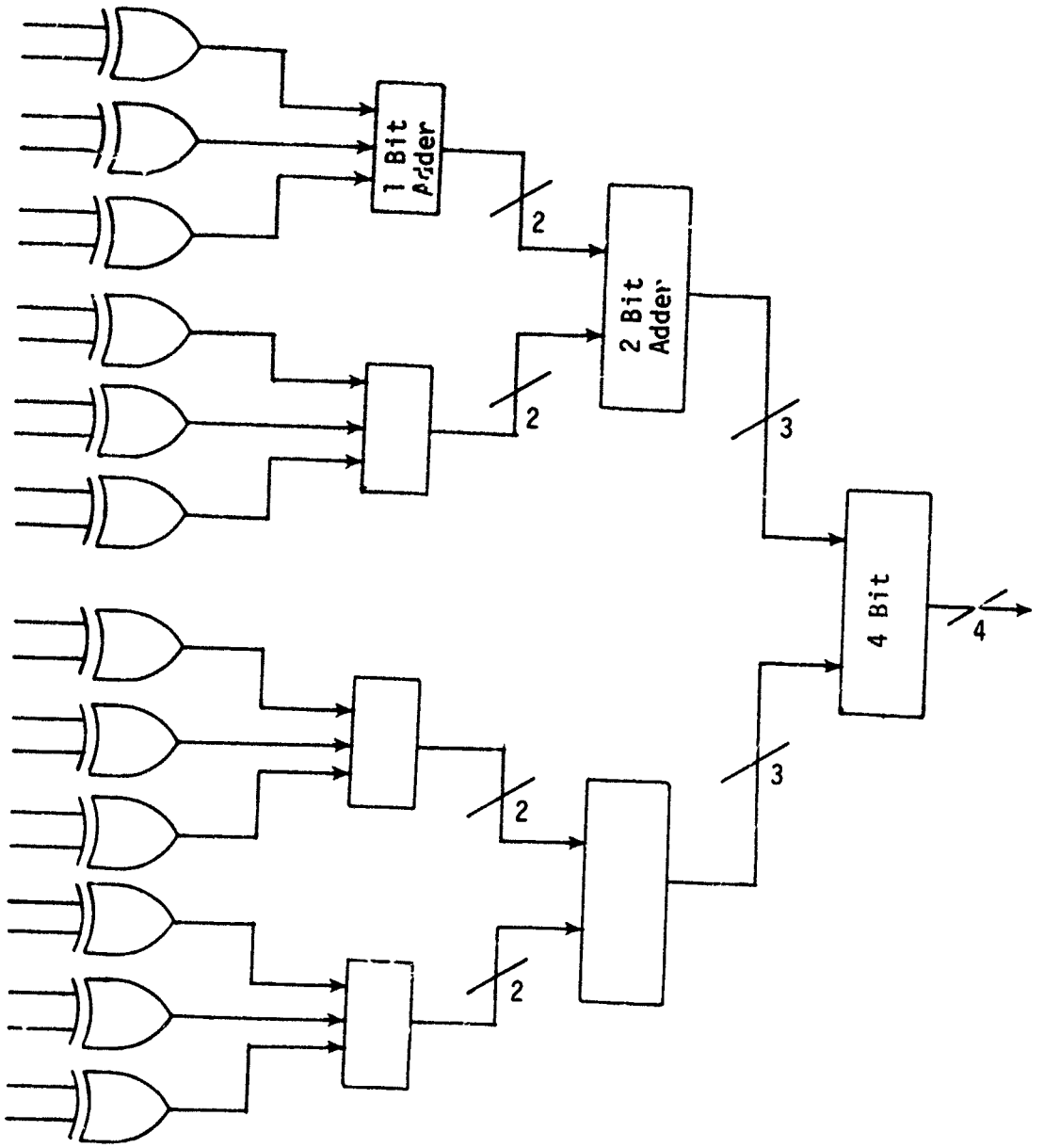

MC10107	MC10180	MC10182	MC10181
4 pkg	2 pkg	2 pkg	1 pkg
480 MW	720 MW	1150 MW	600 MW
2.5 NS	4.5 NS	7.5 NS	6.5 NS

Figure 34. Logic for 12 x 1 correlator

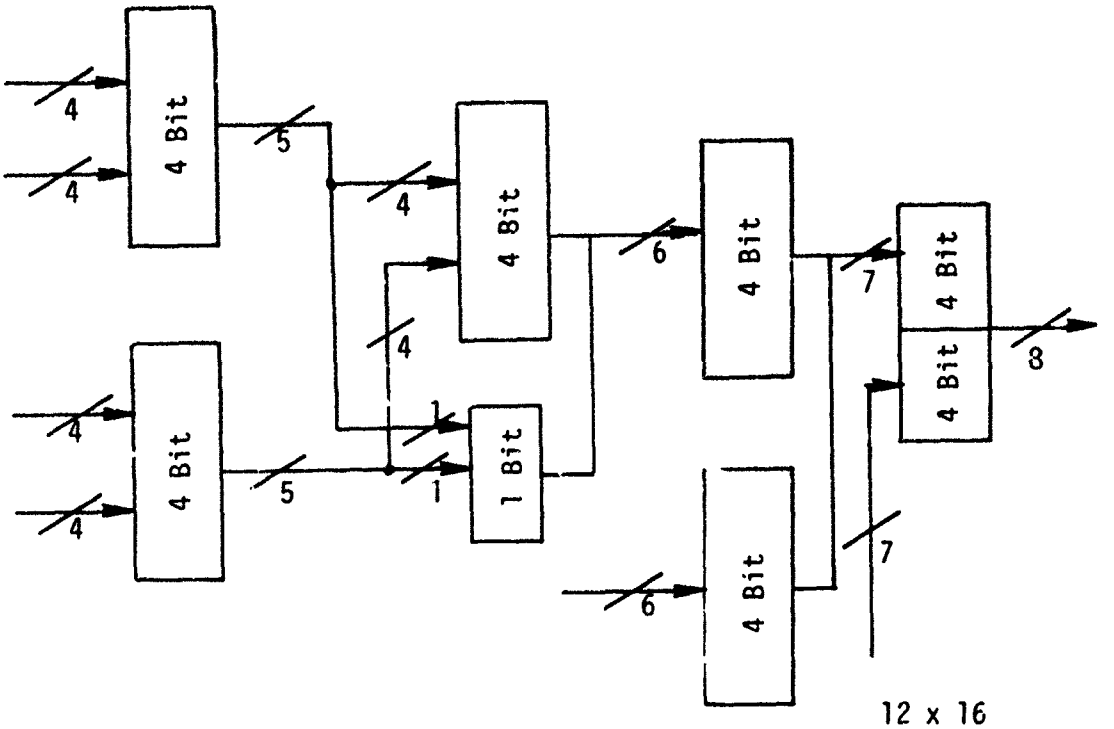

1/4 ckt	1/4 ckt	1/2 ckt	12 x 16 Correlator Output
MC10181	MC10181, MC10180	MC10181	MC10181
3 pkg	6 pkg	4 pkg	2 pkg
4800 NW	3120 MW	2400 NW	1200 NW
6.5 NS	11 NS	13 NS	13 NS

Figure 35. Extension of Figure 34 to produce a 12 x 16 correlator.

	ECL			TTL		
Array Size	Pkg	Power	Delay	Pkg	Power	Delay
8 x 12	82	29 W	51 ns	74	15 W	114 ns
12 x 16	166	59 W	64 ns	150	30 W	139 ns
16 x 24	366	120 W	77 ns	304	61 W	164 ns
24 x 32	671	239 W	90.5 ns	611	123 W	189 ns
32 x 48	1345	480 W	108.5 ns			
48 x 64	2696	964 W	126.5 ns			

Table 4. Comparison of ECL vs. TTL logic correlators.

It is possible to extend the hardware in a simple way to encompass larger arrays with little increase in hardware complexity. The basic design of all the fast correlators is a multiply circuit and an adder tree. In the one-bit case it is possible to "hang" additional multiply circuits on the adder tree without effecting the propagation times considerably. The full adder is in fact a ternary function. Figure 36 shows the logic diagrams for a 15 x 1 correlator. Figure 37 is the extension of Figure 36 that produces a 15 x 16 correlator. This basic block is iterated in space to form the various array sizes listed in Table 5.

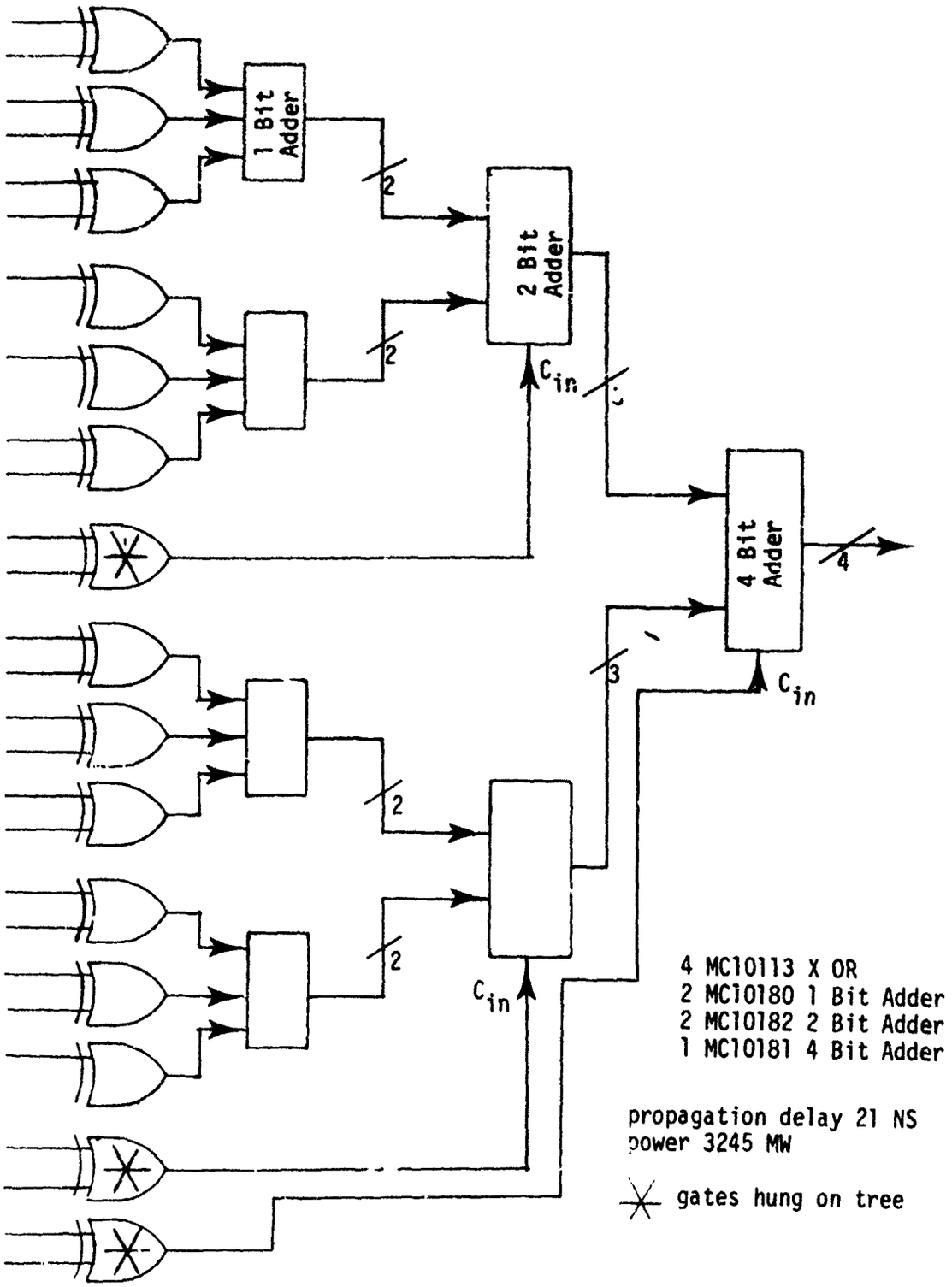

Figure 36. Logic diagram for a 15 x 1 one-bit correlator.

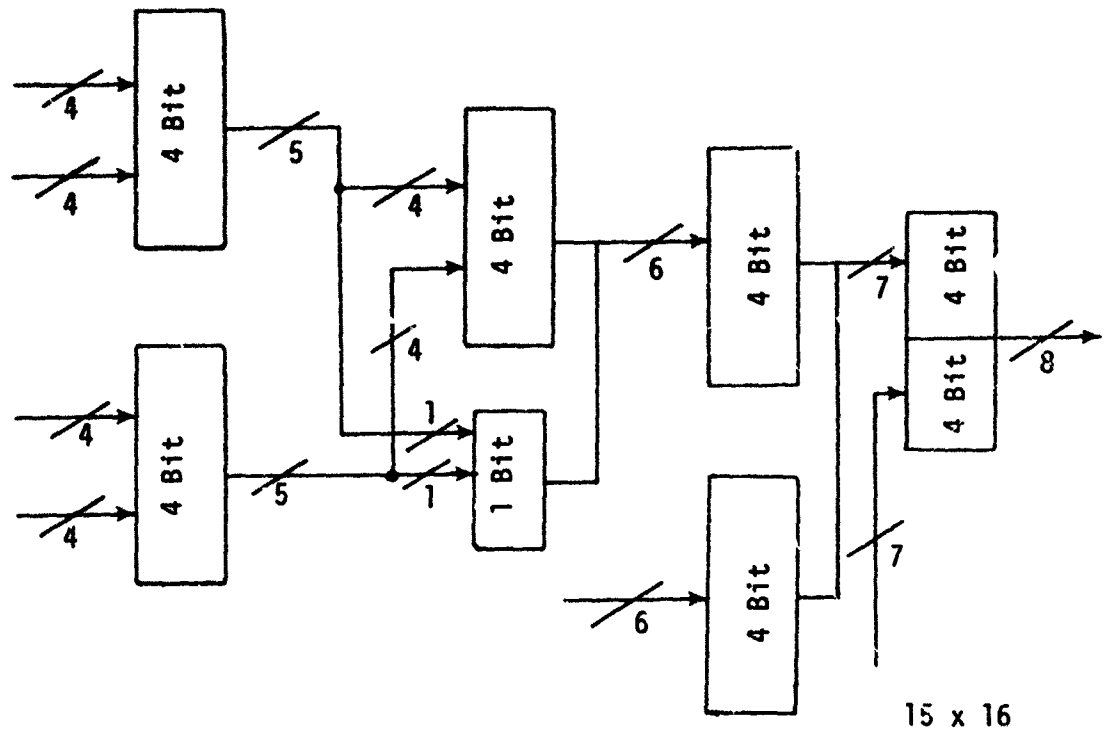

1/4 ckt	1/4 ckt	1/2 ckt	15 x 16 Correlator Output
MC10181	MC10181, MC10180	MC10181	MC10181
8 pkg	6 pkg	4 pkg	2 pkg
4800 NW	3120 MW	2400 NW	1200 NW
6.5 NS	11 NS	13 NS	13 NS

Figure 37. Extension of Figure 36 to produce a 15 x 16 correlator.

ECL			
Array Size	Pkg.	Power	Delay
15 x 16	166	59w	64NS
16 x 30	366	120w	77NS
30 x 32	671	239w	90.5NS
32 x 60	1345	480w	108.5NS
60 x 64	2696	964w	126.5NS

Table 5. One-bit by one-bit correlator using ECL logic.

It appears unlikely that a complete ECL implementation would be practical due to the large power requirement. In this section we will first describe an implementation based on low power Schottky TTL-logic. Since this logic family is not fast enough to do an addition of 2048 (32 x 64) one-bit numbers in anything approaching 133 ns, it is necessary to perform the computation in pieces. This technique is called pipelining. During a given time interval the 'pipe' may be computing Part 1 of Item 3, Part 2 of Item 2 and Part 3 of Item 1; at the next time step computation is performed on Part 1 of Item 4, Part 2 of Item 3, Part 3 of Item 2. A new result is generated at each time interval but for any specific data item the time required is the product of the basic time interval and the number of sections of pipe (see Figure 38). The Schottky pipe version illustrated on the accompanying pages (Figure 39) requires approximately 1600 packages and 300 Watts for a 32 x 64 array.

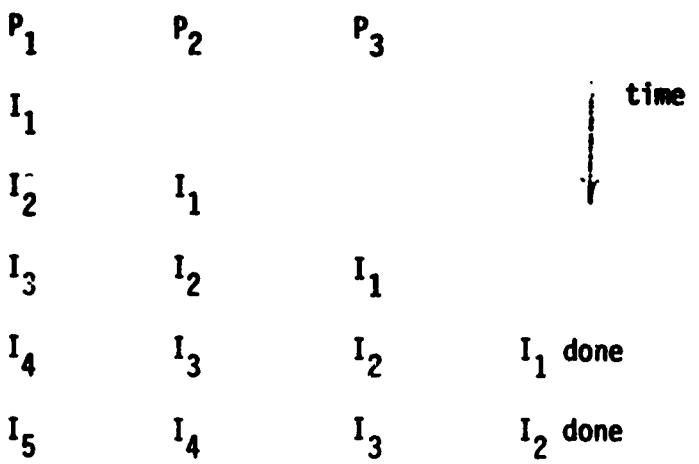

Figure 38. Items in pipe.

The pipe delay in each of the three sections of pipe is 132 ns. Memory required in addition to that contained in the correlator itself is assumed to be a charged coupled device since this will provide the necessary speed with very low power consumption. Bubble memories may become practical in this application as well. Assuming a picture image P x Q with R points devoted to horizontal retrace and sync, and a correlation array K x L, from Figure 40 we observe that the delay required is (Q + R - L) for each row. Using CCD (charge coupled array) power dissipation at 10 MHz is about 20 μW/BIT. Therefore total power dissipation is $20 \times 10^{-3} K(Q + R - L)$ milliwatts.

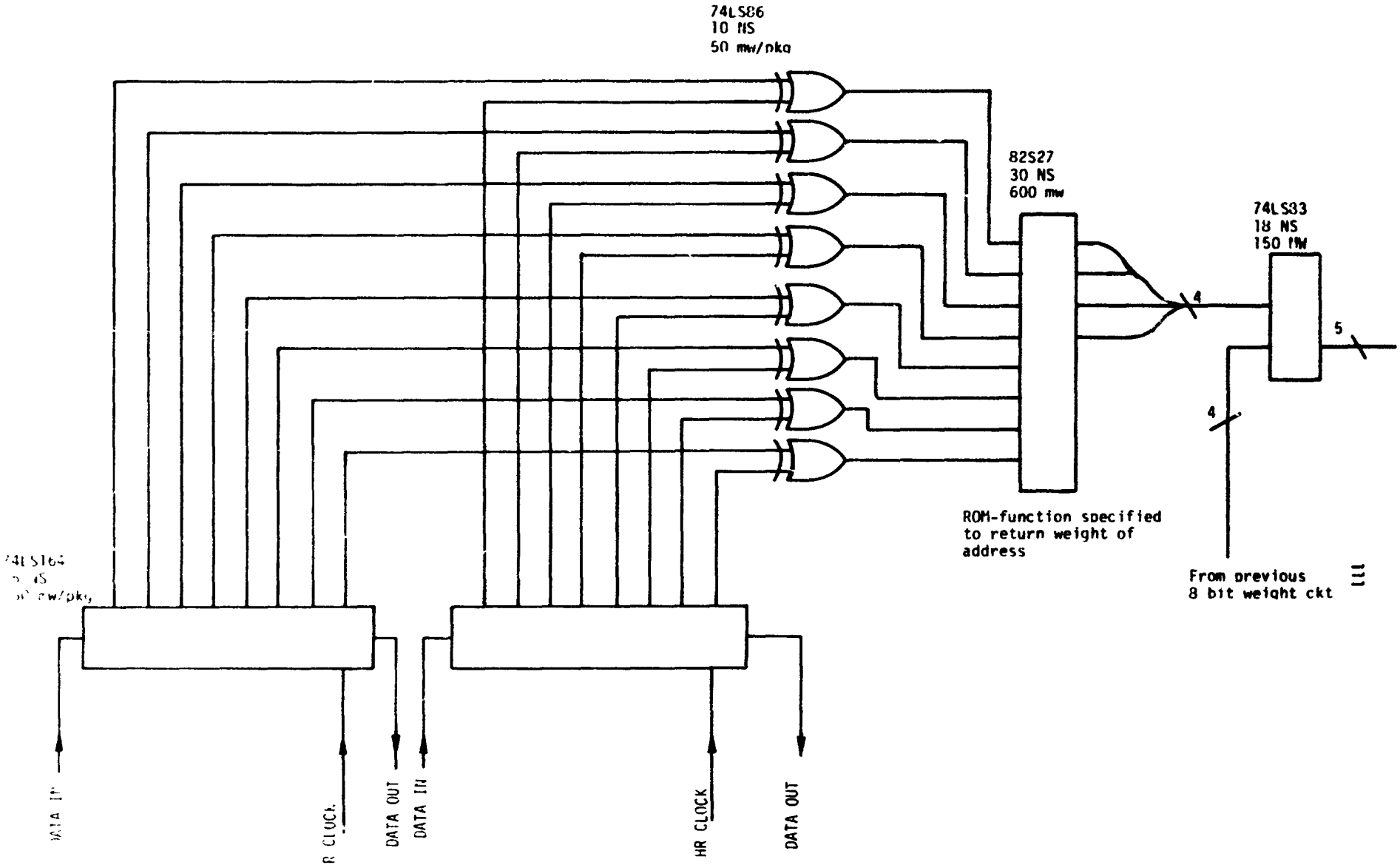

Figure 39 (Part 1). Correlator and adder tree.

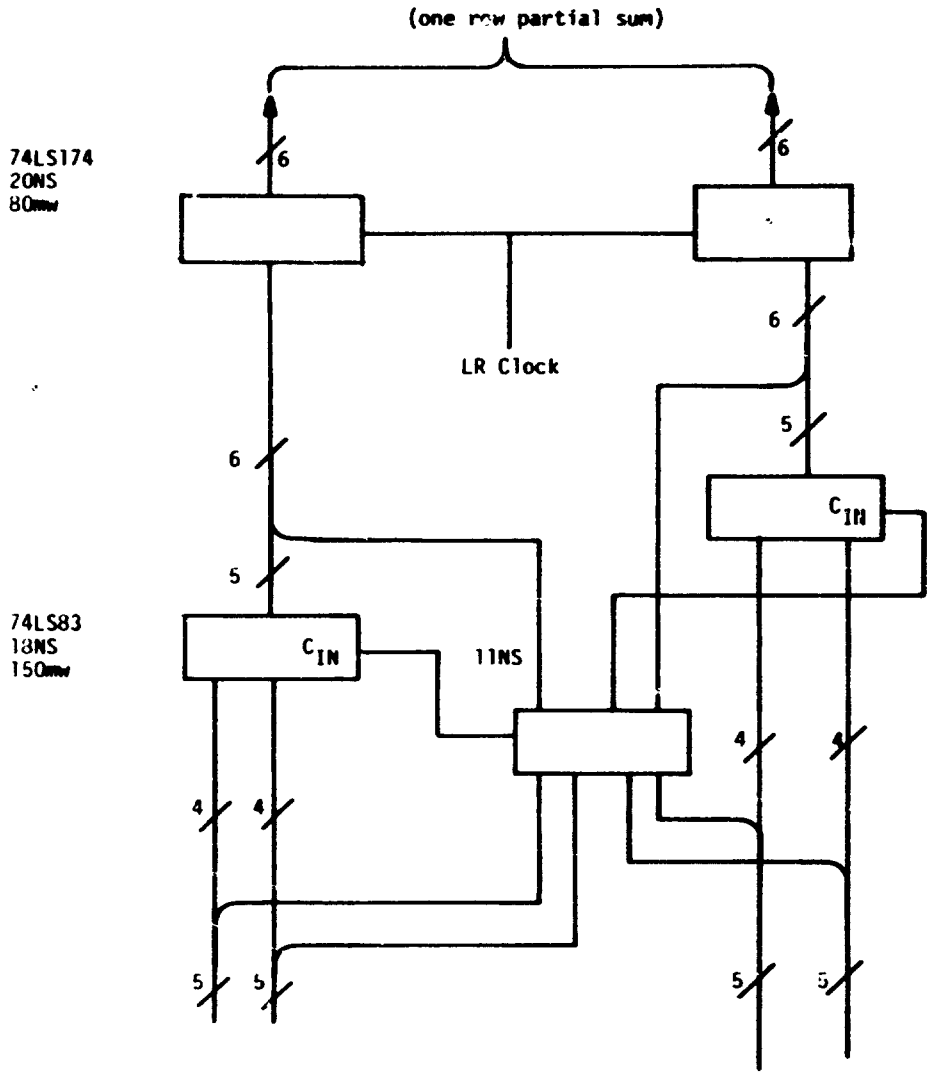

1 of 32 sections

First Piece of Pipe

	Component	Power
2	74LS174	160mw
4	74LS83	600mw
8	82S27	4800mw
16	74LS86	800mw
16	74LS164	2400mw
pkg 46		8760mw

132 NS propagation delay

Total all sections

1472 pkg 280 watts

Figure 39 (Part 2). Correlator and adder tree.

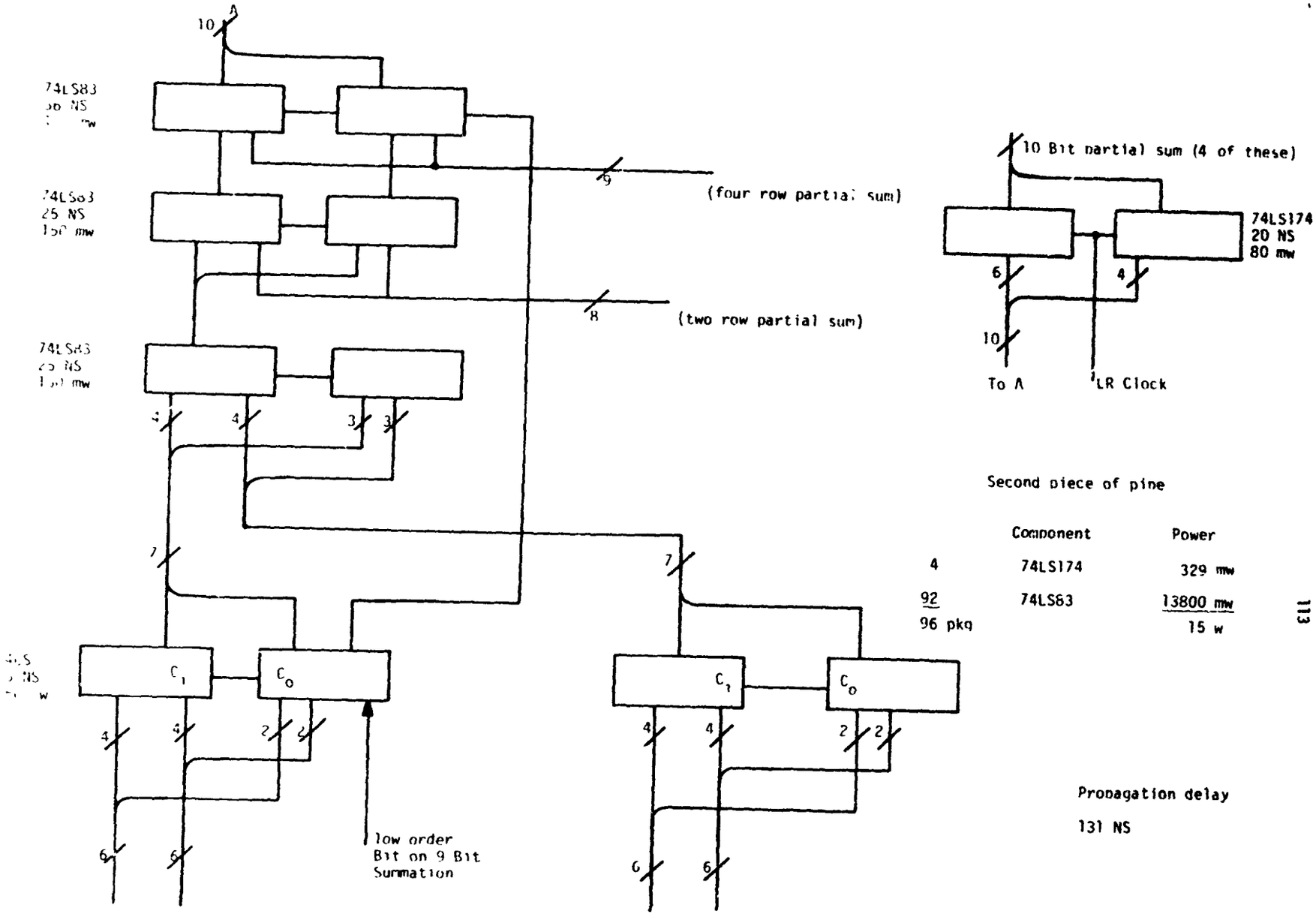

Second piece of pine

	Component	Power
4	74LS174	329 mw
92	74LS83	13800 mw
96 pkg		15 w

Propagation delay

131 NS

Figure 39 (Part 3). Correlator and adder tree.

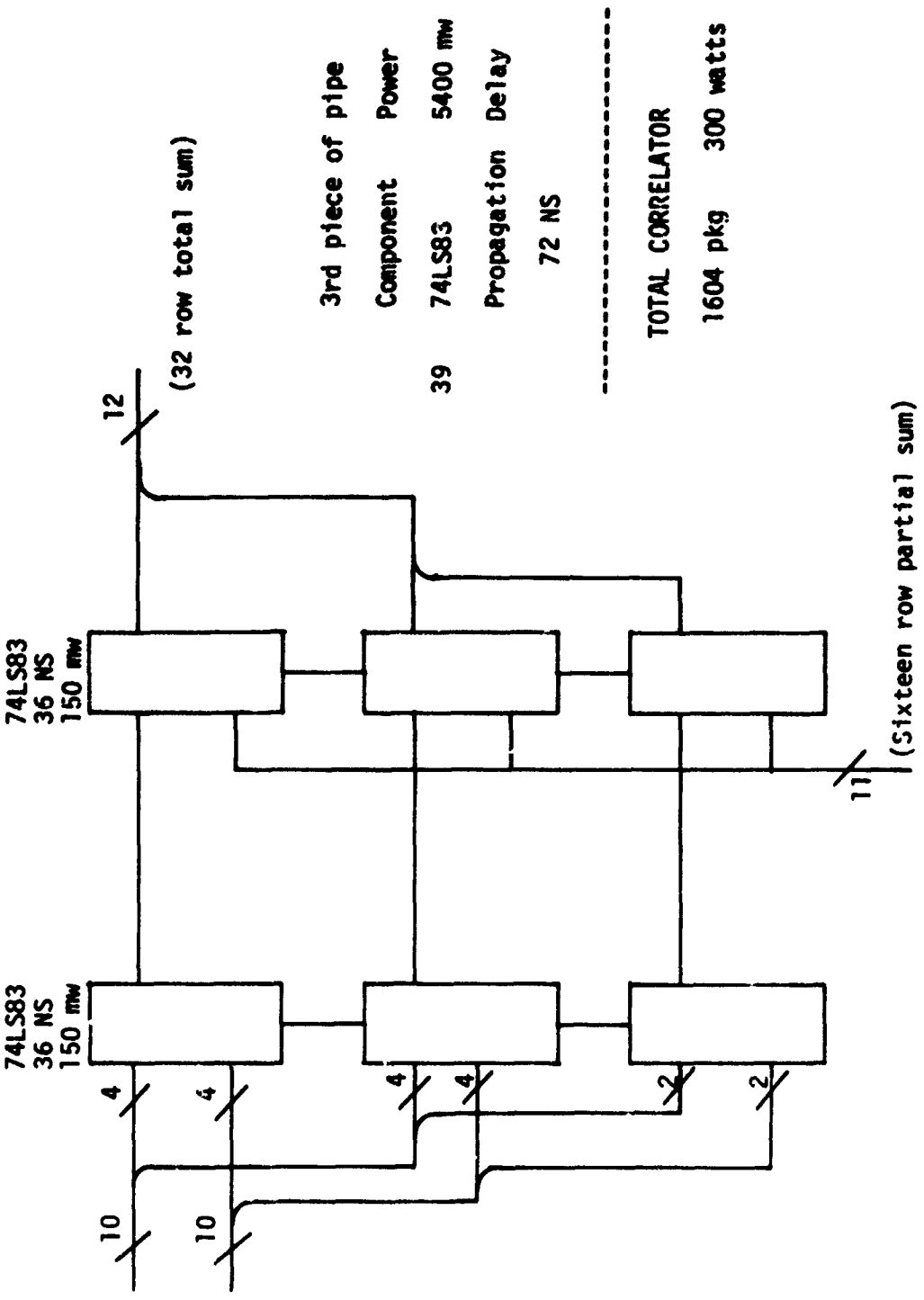

Figure 39 (Part 4). Correlator and adder tree.

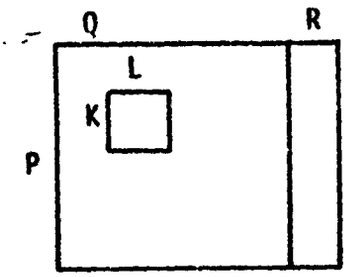

(Q + R - L) Bits each row

K(Q + R - L) Bits total

Figure 40. Memory requirement for correlation computation.

Another problem involving the one-bit by one-bit correlator concerns the removal of the DC component of the LR image. This forms a support component in the system block design. The following is a discussion of a sub-optimal technique that accomplishes the removal of the DC digitally. Referring to Figure 41, in approximating the level about which to quantize pixel A the value of pixel B must be known. Pixel B lags A by (K/2)(Q+R) + l/2 sample intervals. The column containing pixel B is used to determine

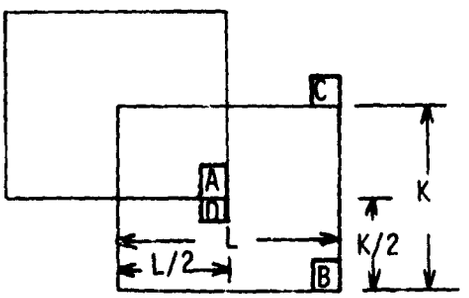

Figure 41. Method of computing mean video level.

L mean values and then is not used until Q + R - L events later. Data Item C must be removed from the column sum after K(Q + R) events. The resulting algorithm is presented as Figure 42. If we assume a 3 bit quantization of the picture, then 3 x [K x (Q + R) + L/2] + 14 x (Q + R + L) bits of memory are required As before, using Q + R = 476, K = 32, L = 64, 53,352 bits are required. Power dissipation is approximately 1.5 watts for the memory array using CCD. Clocking and interface logic could increase this number significantly.

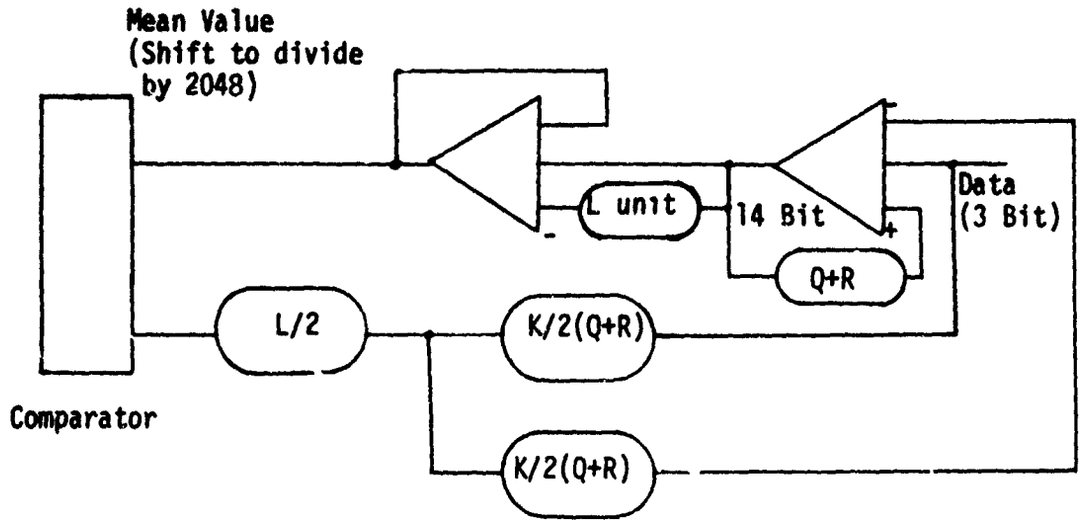

$$3x\ (K(Q + R) + L/2)$$
$$+\ 14x\ (Q + R + L) \quad \text{Bits of memory}$$

Figure 42. Mean video computation and quantizer.

The use of half-frame correlation (i.e., non-interlaced images) serves to reduce the hardware memory requirements. In order to achieve reasonable computational speeds through the adder tree, the circuit is divided into sections (i.e., pipelined). With interlacing, one of the final stages of the pipe sums results delayed from the previous half-frame. Because this delay requires considerable memory and because of the effects of vibration discussed earlier, it is recommended that a half-frame correlator be implemented, thus, effecting a cost, space and power saving.

The maximizing circuit is quite simple and is shown in Figure 43 . The position counter is also used in the edge correction problem. The picture is dimensioned as in Figure 44 . Notice that both the horizontal and vertical blanking intervals are indicated by a one in the most significant bit of each counter. The retrace intervals have been adjusted to ensure this simple hardware implementation. The final construction may require that sample rates be adjusted to achieve this effect.

The mean value of the image needed for quantization near the edges is difficult to calculate because part of the K X L subarray extends into the horizontal retrace region or vertical retrace region as shown in Figure 45. The dc component of these areas that depend on values outside the field of view can be calculated by substituting a binary noise source for the retrace voltage. One possible implementation is shown in Figure 46. This will preclude the possibility of false contrast changes near the edge by smearing the edge so that it always appears gray.

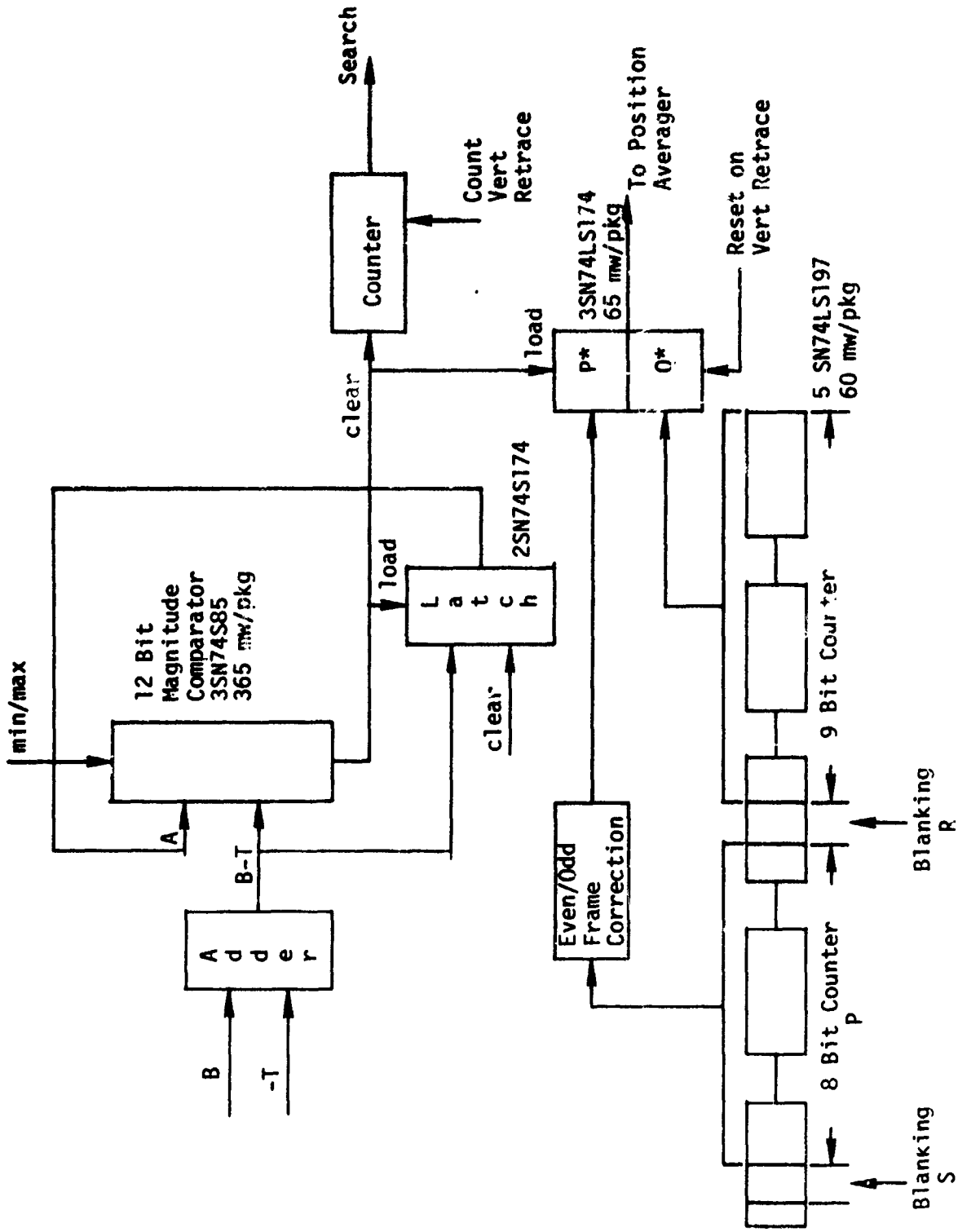

Figure 43. Circuit for computing the maximum (i.e., the registration point).

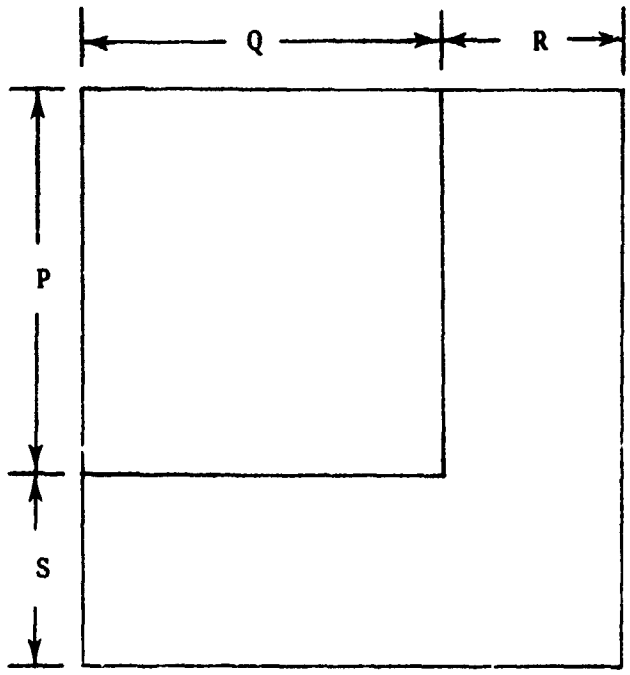

P x Q is single scan picture area

For example 256 x 512

R and S are horizontal and vertical blanking intervals

For example (P + S) x (Q + R) could be 320 x 576

Figure 44. Picture size (P x Q) with horizontal and vertical retrace R and S.

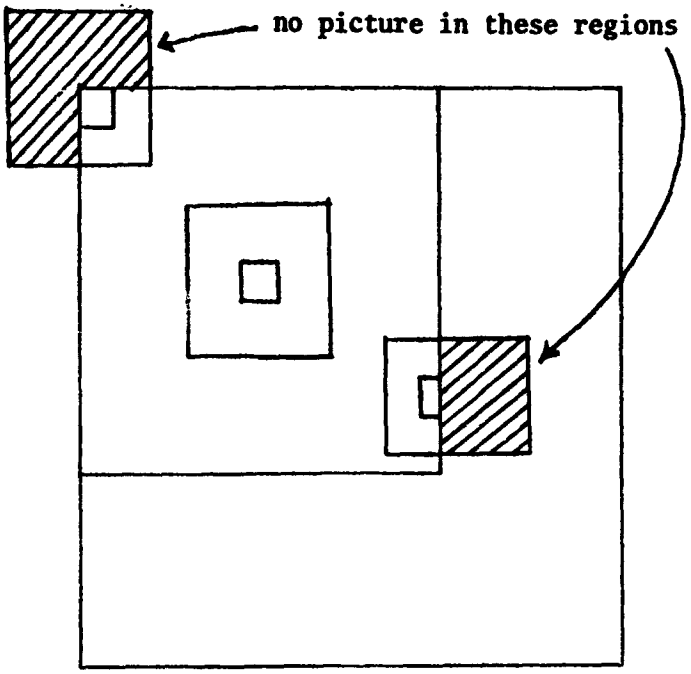

Figure 45. Retrace (Edge) effects on quantization.

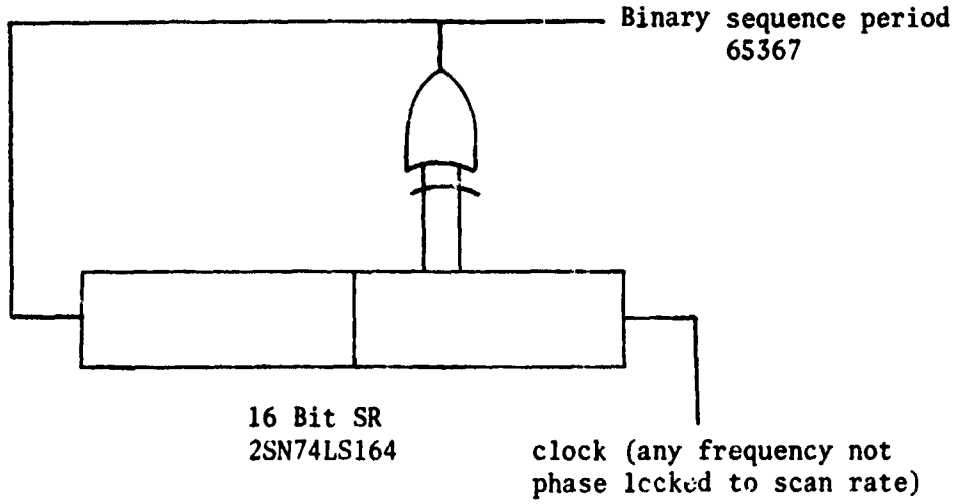

Figure 46. Binary noise source generator.

The high resolution image contains far too much data to be used in the correlation. This data is reduced by computing a spatial average using Equation 67 where W_H and W_V are assumed to be integers. The components of the spatial averaging are then sampled to reduce the data. Figure 47 illustrates the hardware for such a reduction. The digital approach uses MOS or CCD shift registers for delay. The precision of the HR image is assumed to be 3-bits. A binary adder with a register acting as accumulator forms the desired sums. The sum of 25 3-bit numbers will not exceed 256 or 8 bits in precision. The Divider is a 2048 x 1 ROM. 3x4, 3x5, 4x3, 4x4, 4x5, 5x3, 5x4, 5x5 horizontal and vertical reductions in the aspect ratios can be handled. The ROM, also causes the 3-bit precision of the image to be quantized to 1-bit.

The horizontal and vertical blanking signals are used to force the magnitude comparator in the peak detecting circuit to ignore the correlation values computed during horizontal and vertical retrace. Since the correlator is designed to run free, these correlation values must be ignored during retrace. The circuit used to accomplish this is shown in Figure 48. Also illustrated is a method for selecting either minimum or maximum. If B is to be larger than A to track maximum, then the blanking should force B > A.

B. Block Diagram of 32 x 64 Array Correlator System

A detailed block diagram of a total correlator system has been drawn by incorporating all of the block diagrams of the previous figures. The correlation system is designed around the XOR implementation. The block diagram

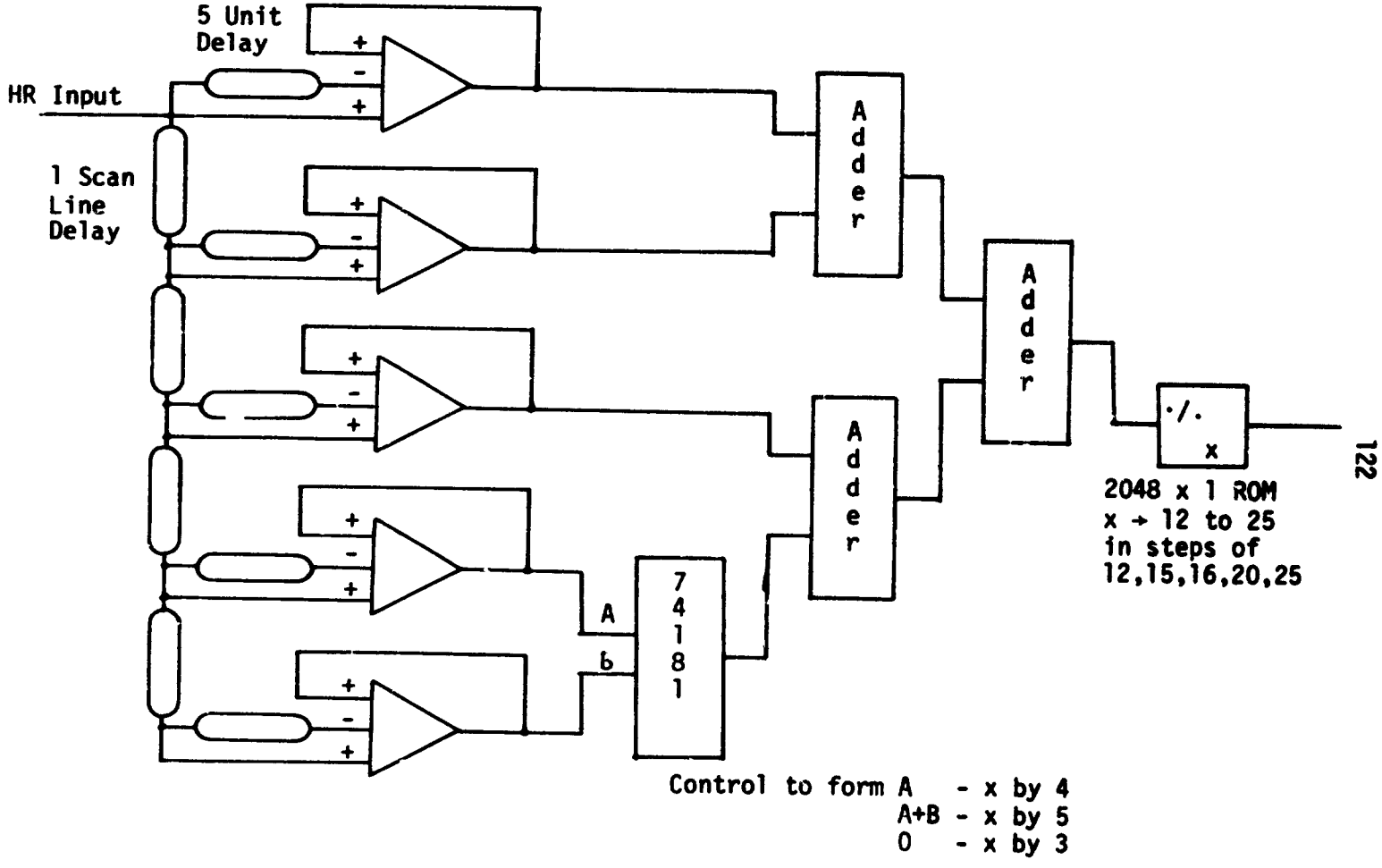

Figure 47. Averaging circuit for resolution reduction of HR video.

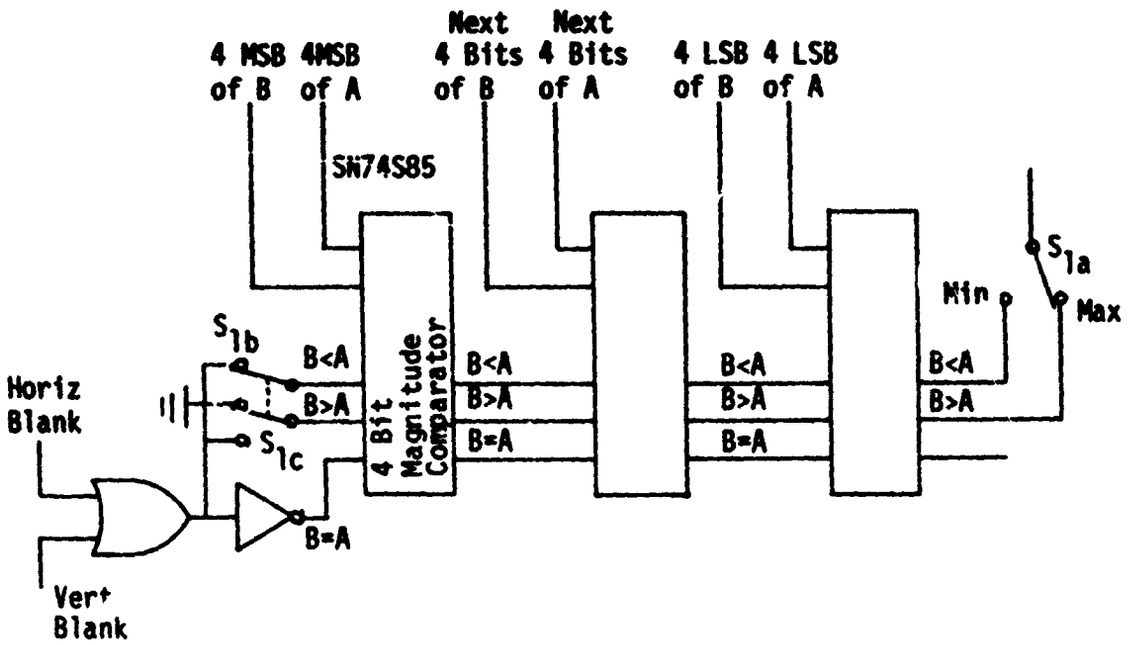

Figure 48. Blanking circuits for correlator during horizontal and vertical retrace.

also shows the pre-processing that is done on both the HR and LR video signals assuming an adjustable FOV ratio between the two and also shows how the processed signals are clocked into the correlator.

The completed implementation is shown in Figure 33. A more detailed representation is shown in fold out Figure 49. It is important to remember that the diagrams represent potential ways of implementing the desired design and are presented as a feasibility demonstration. A practical implementation might not employ identical techniques. The following discussion treats the blocks in Figure 33 as a system. The component functions were treated separately earlier in this chapter. The high

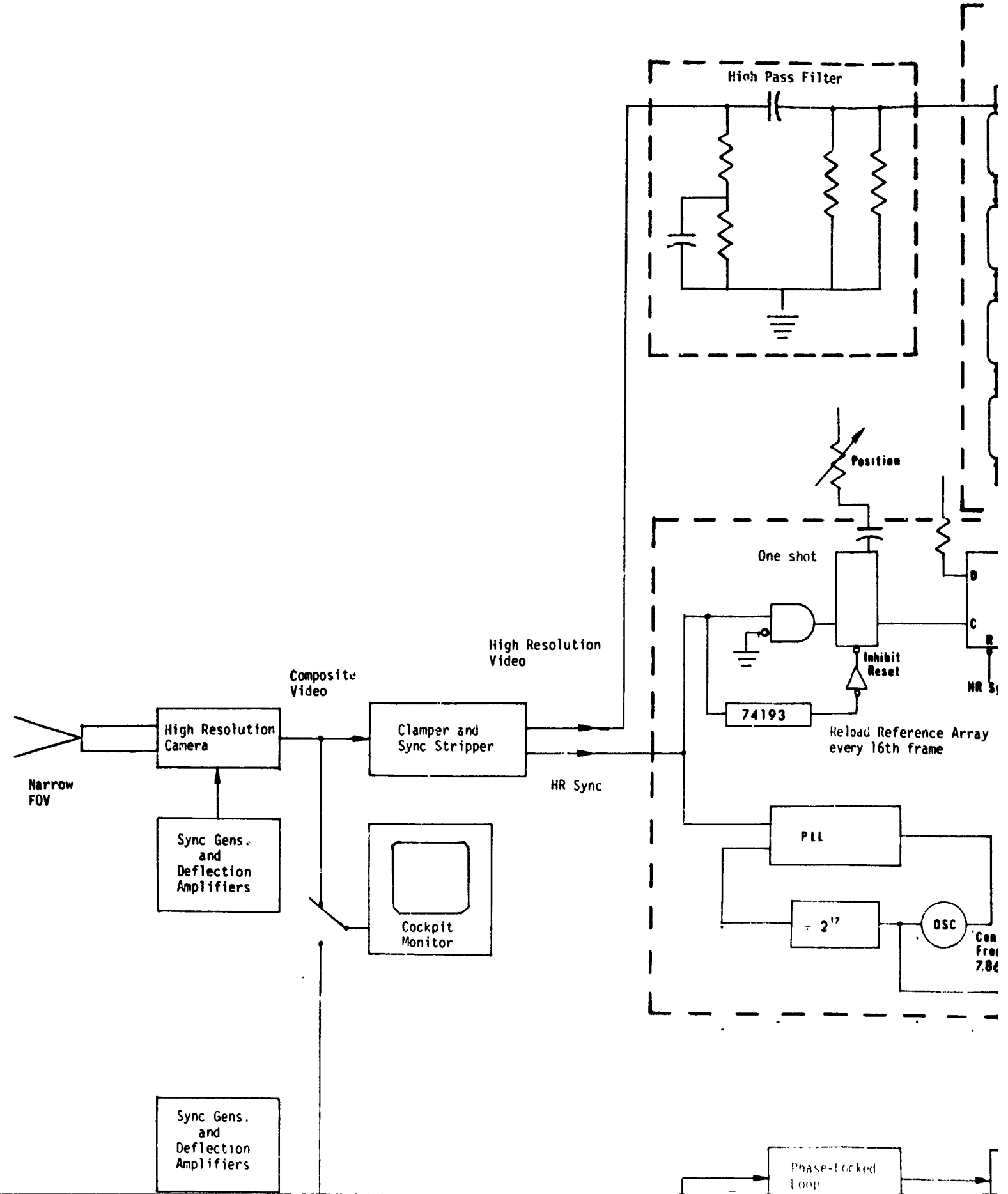
High Pass Filter
Position
One shot
D
C
Inhibit
Reset
74193
Reload Reference Array
every 16th frame
High Resolution
Video
Composite
Video
High Resolution
Camera
Clamper and
Sync Stripper
Narrow
FOV
HR Sync
Sync Gens.
and
Deflection
Amplifiers
Cockpit
Monitor
PLL
÷ 2^17
OSC
Sync Gens.
and
Deflection
Amplifiers
Phase-locked
Loop

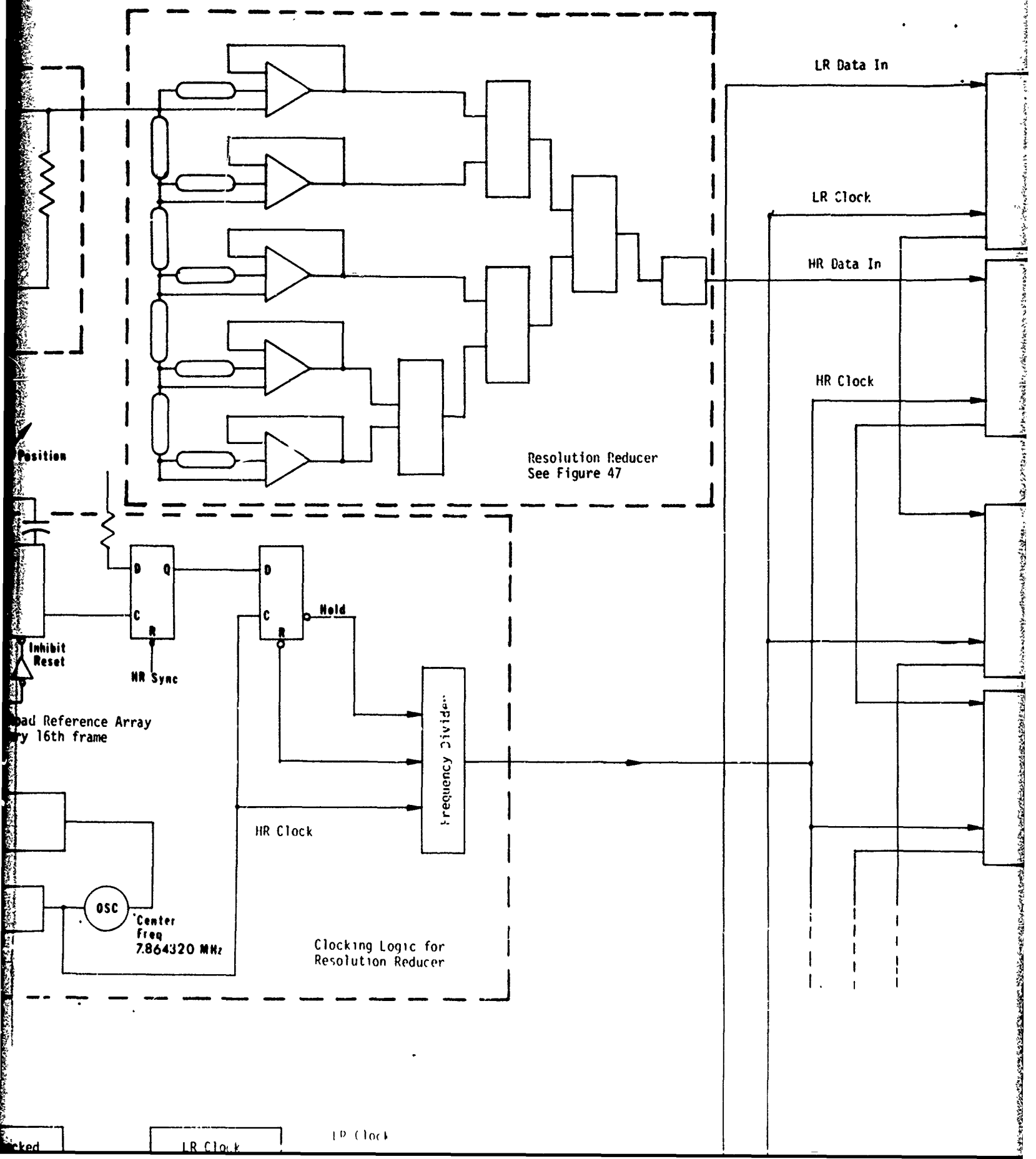
LR Data In
LR Clock
HR Data In
HR Clock
Position
Resolution Reducer
See Figure 47
D
Q
C
R
Hold
Inhibit
Reset
HR Sync
ad Reference Array
y 16th frame
Frequency Divider
HR Clock
OSC
Center
Freq
7.864320 MHz
Clocking Logic for
Resolution Reducer
LR Clock

C

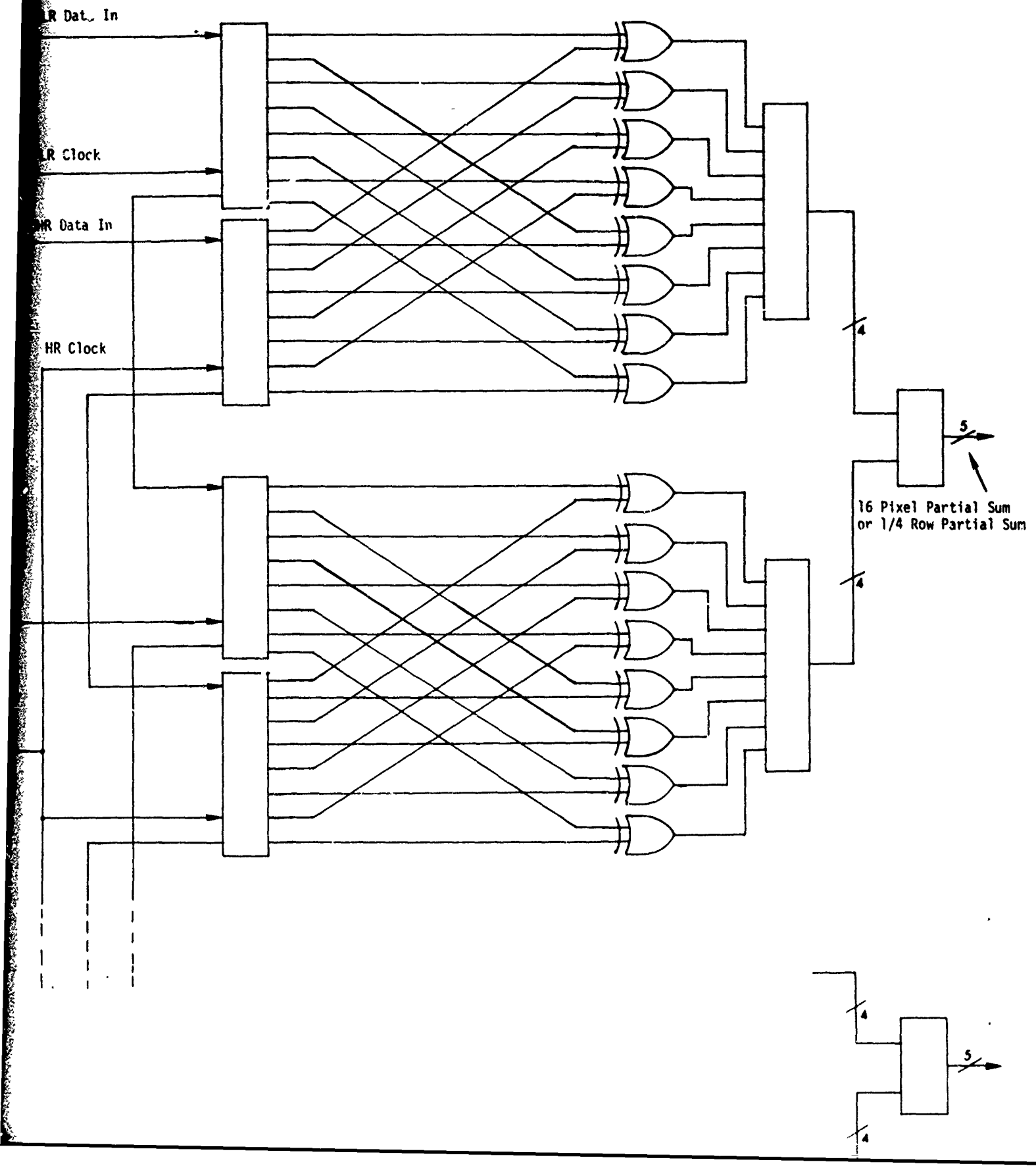
LR Data In
LR Clock
HR Data In
HR Clock
4
5
16 Pixel Partial Sum
or 1/4 Row Partial Sum
4
4
5
4

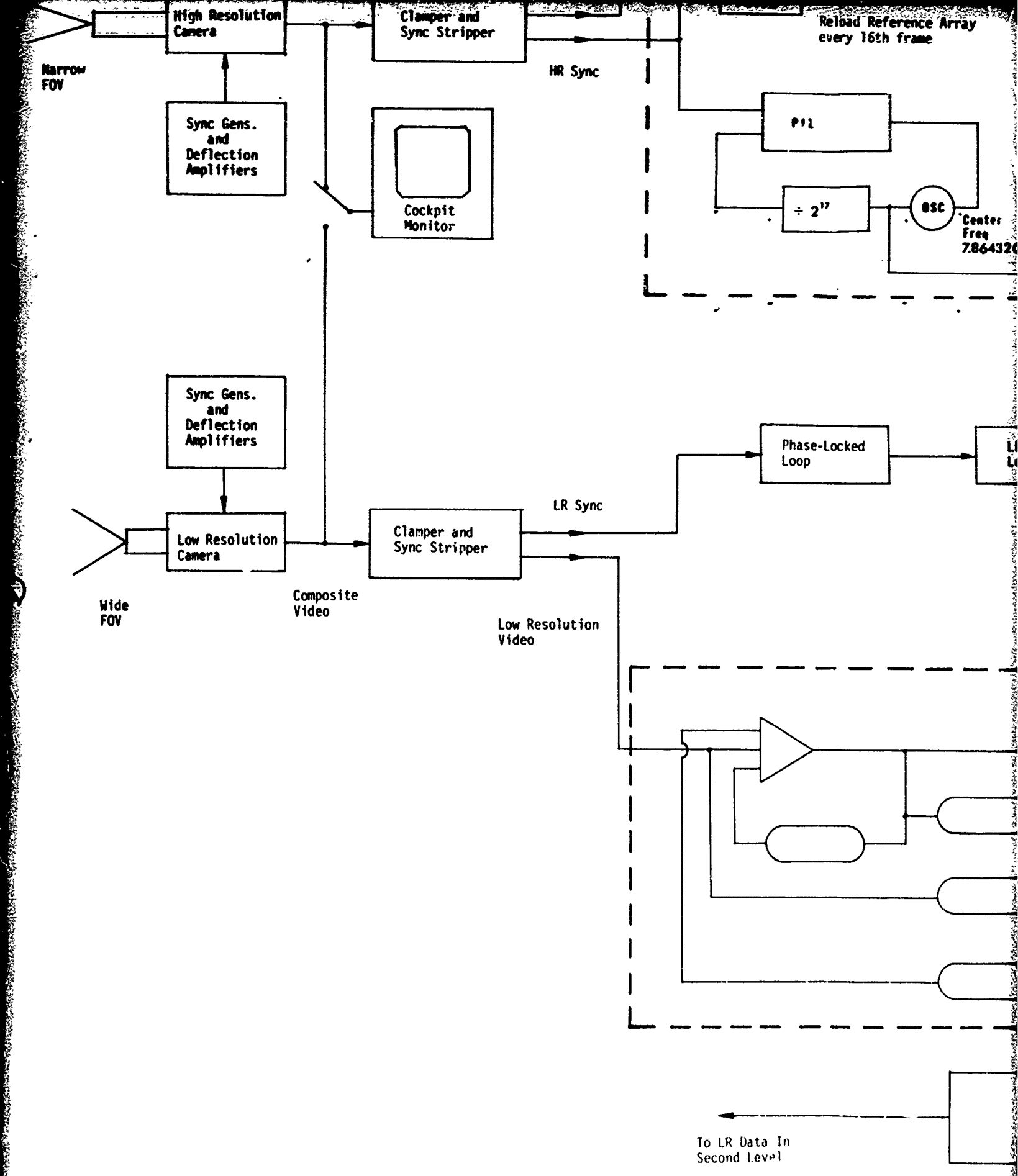
High Resolution Camera
Narrow FOV
Sync Gens. and Deflection Amplifiers
Clamper and Sync Stripper
HR Sync
Cockpit Monitor
Reload Reference Array every 16th frame
PLL
÷ 2^17
OSC
Center Freq
Sync Gens. and Deflection Amplifiers
Low Resolution Camera
Wide FOV
Composite Video
Clamper and Sync Stripper
LR Sync
Phase-Locked Loop
Low Resolution Video
To LR Data In Second Level

Figure 49

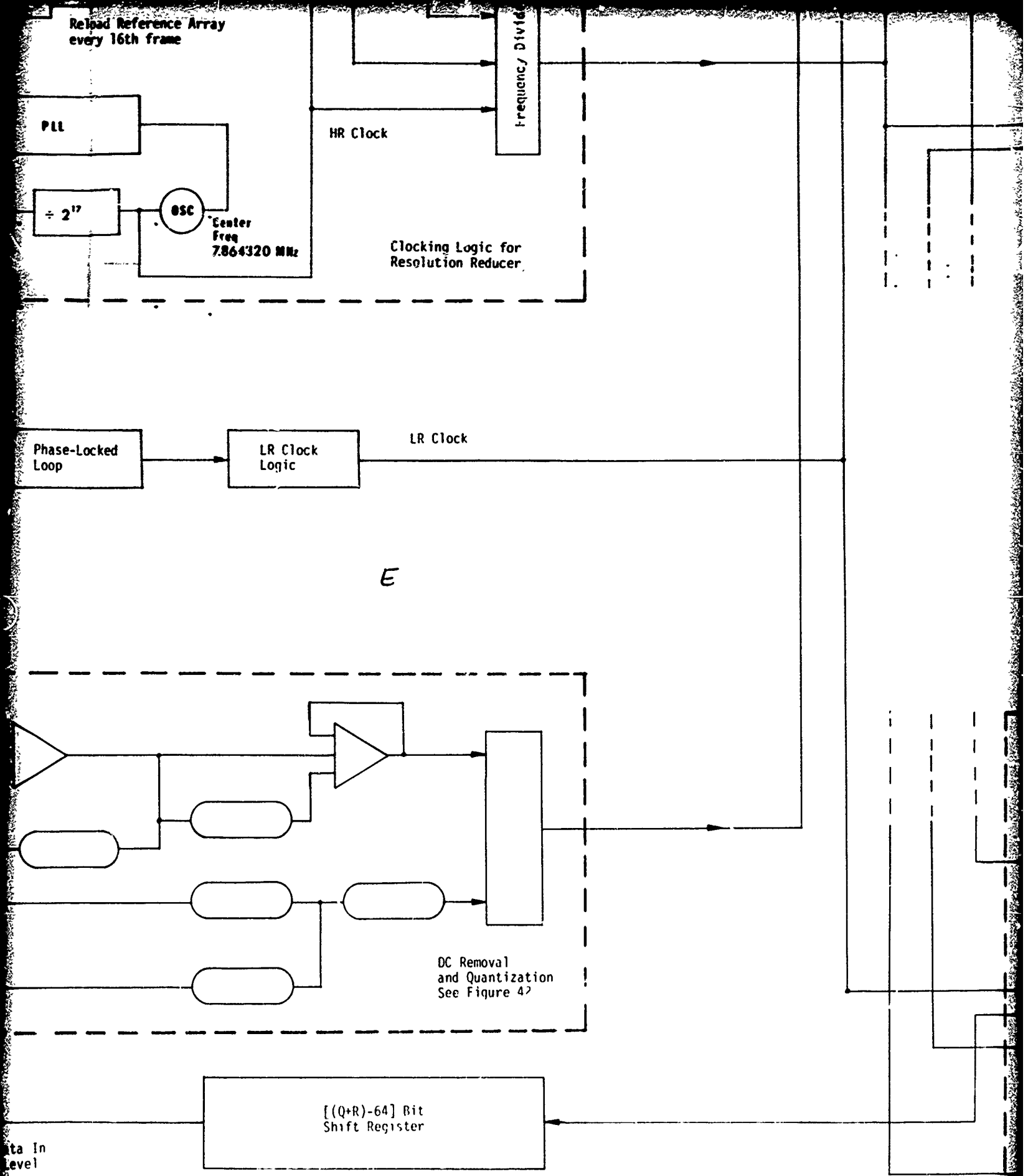

Figure 49 (Part 1). Complete digital correlator circuit.

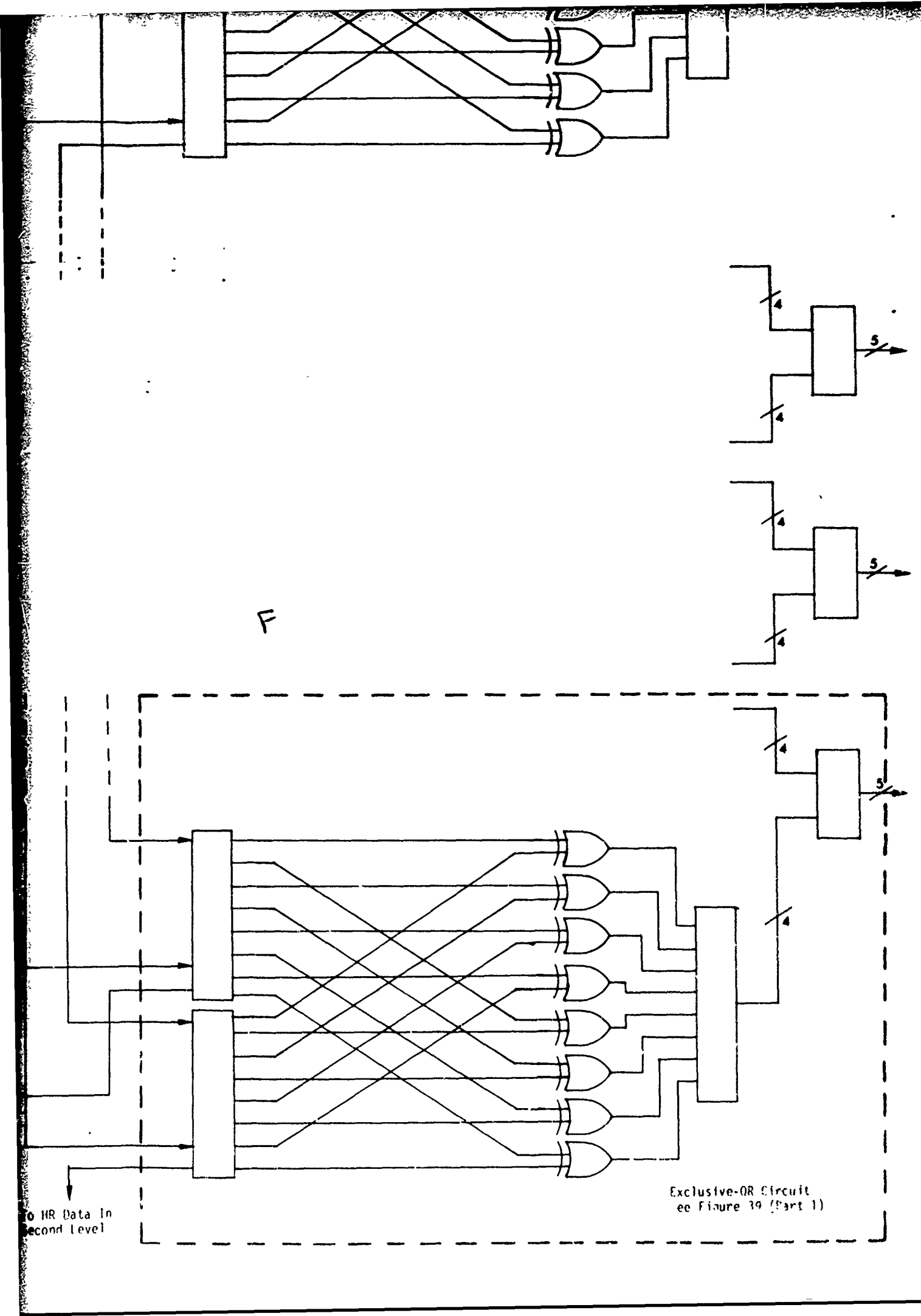
4
5
4
4
5
4
4
5
4
Exclusive-OR Circuit
ee Figure 39 (Part 1)
o HR Data In
econd Level

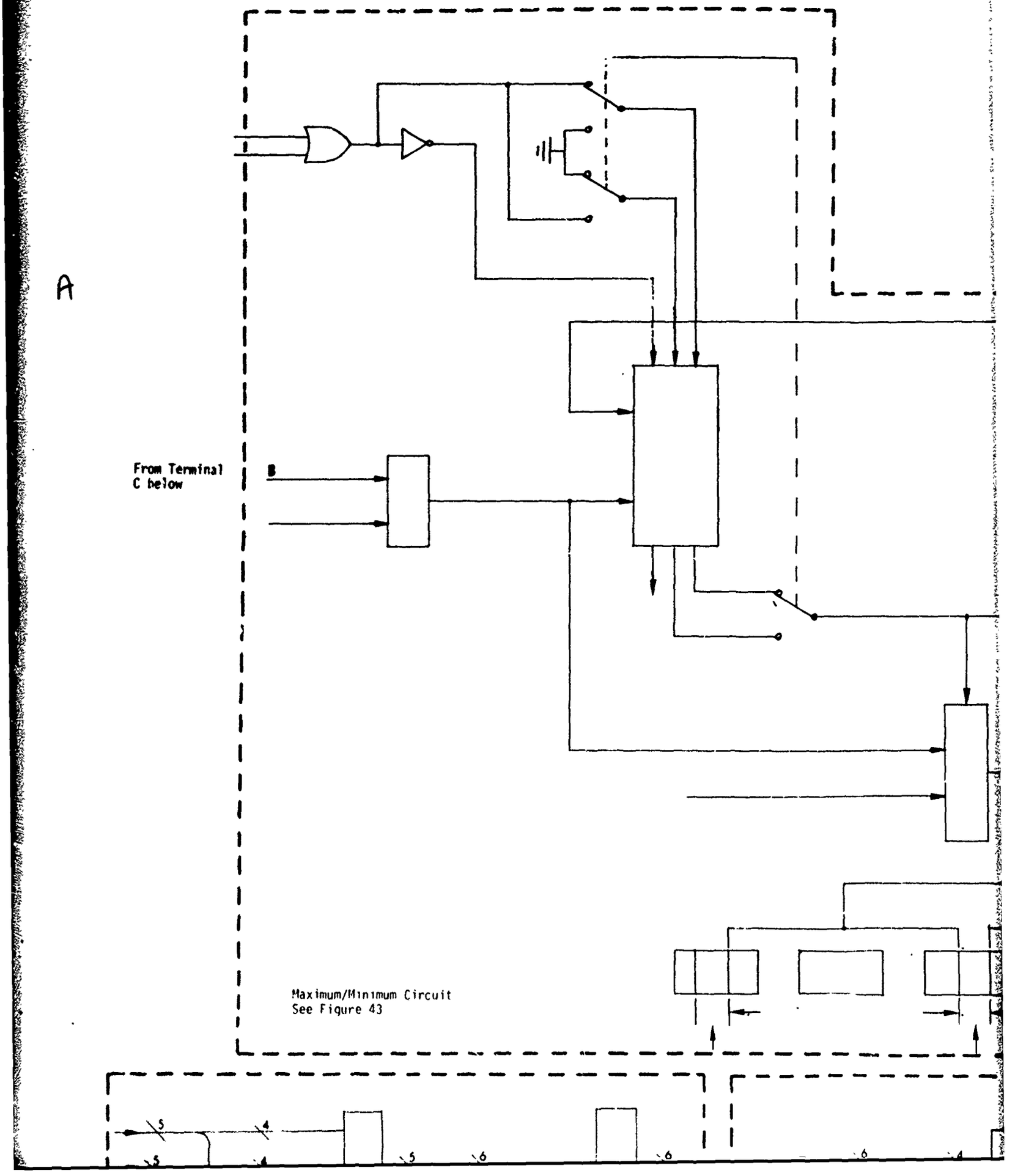
A
From Terminal
C below
B
Maximum/Minimum Circuit
See Figure 43
5
4
5
4
5
6
6
6
4

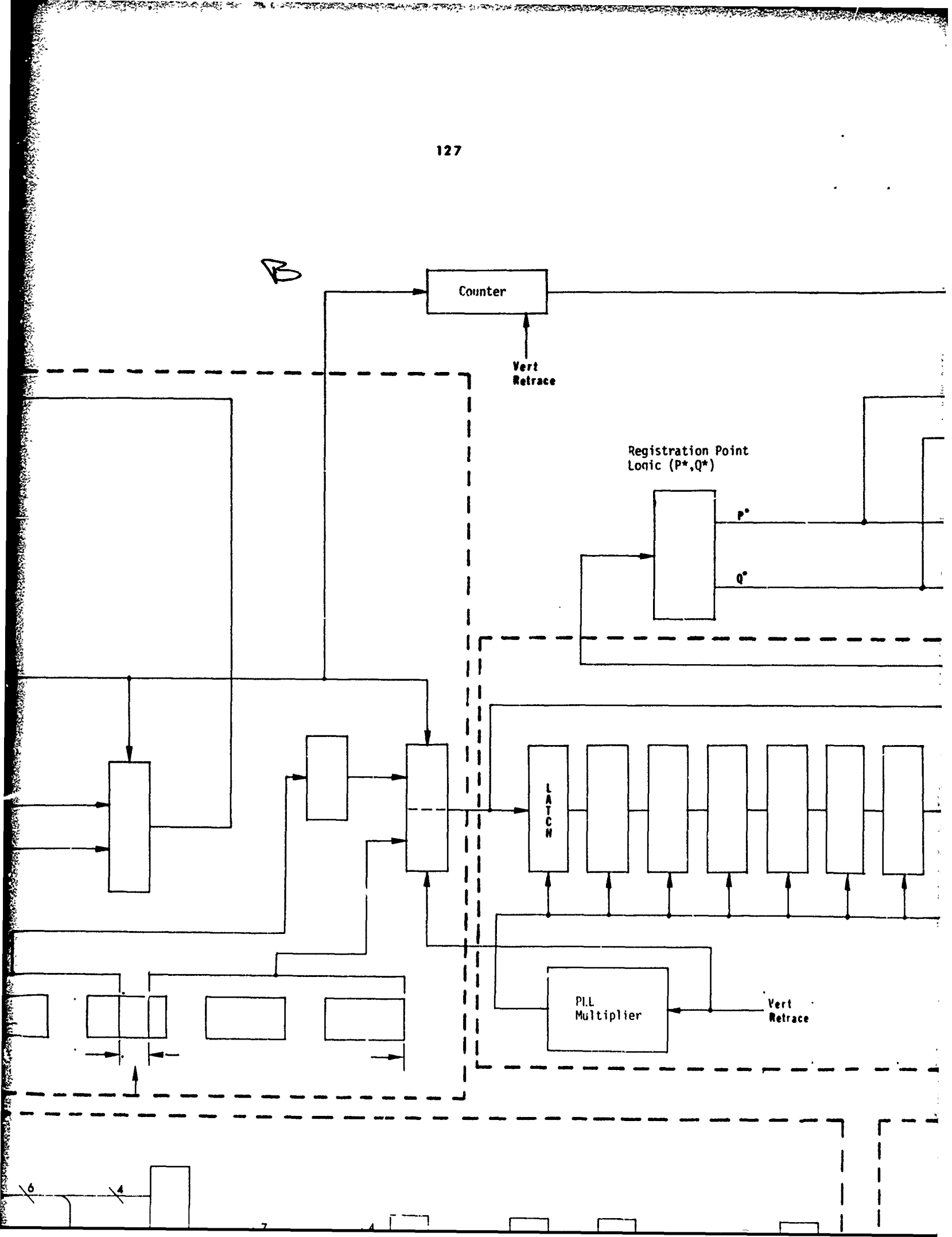
Counter
Vert
Retrace
Registration Point
Logic (P*,Q*)
P*
Q*
LATCH
PLL
Multiplier
Vert
Retrace
6
4

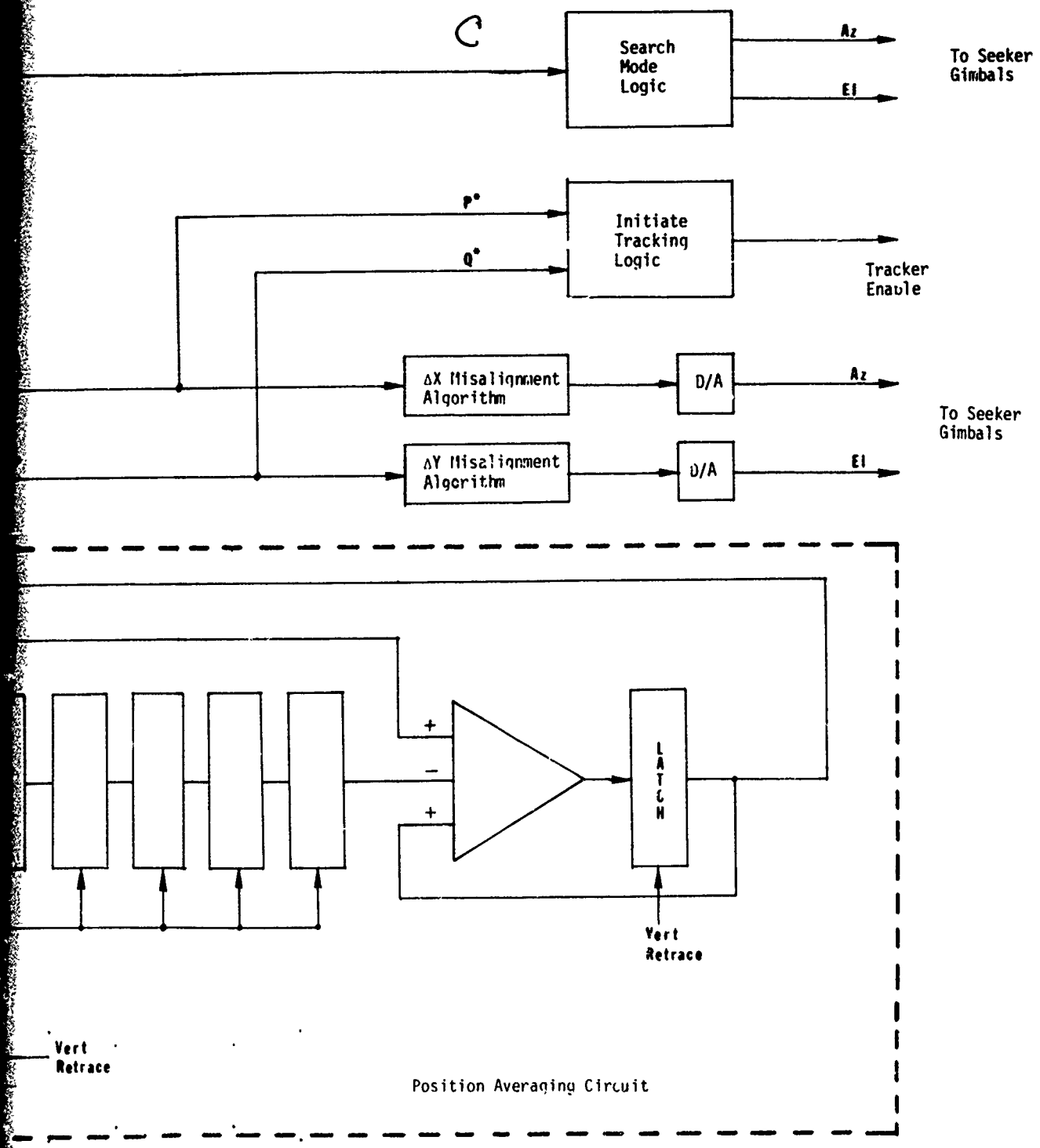
Search Mode Logic
Az
El
To Seeker Gimbals
P*
Q*
Initiate Tracking Logic
Tracker Enable
ΔX Misalignment Algorithm
D/A
Az
To Seeker Gimbals
ΔY Misalignment Algorithm
D/A
El
+
−
+
LATCH
Vert Retrace
Vert Retrace
Position Averaging Circuit

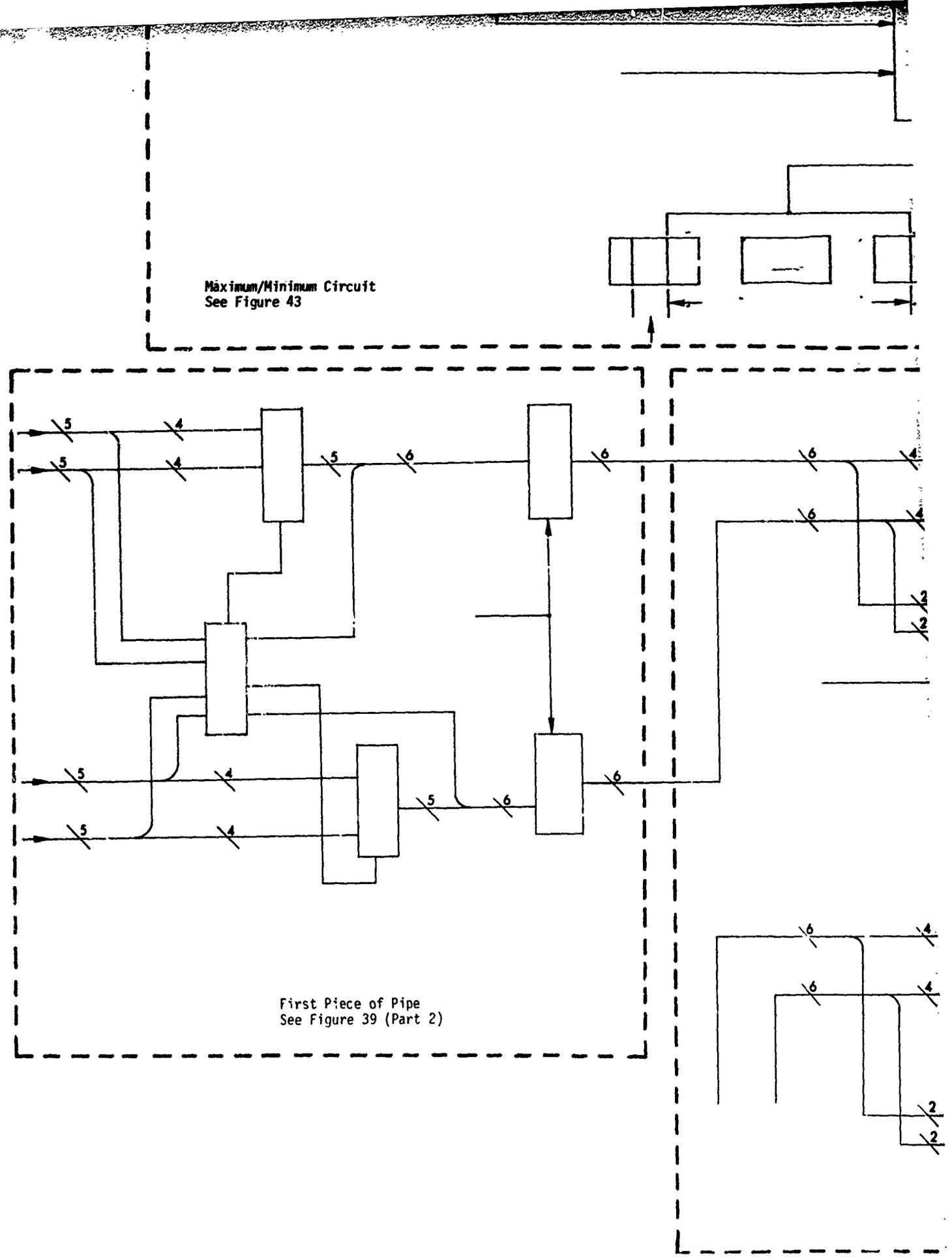
Maximum/Minimum Circuit
See Figure 43
First Piece of Pipe
See Figure 39 (Part 2)

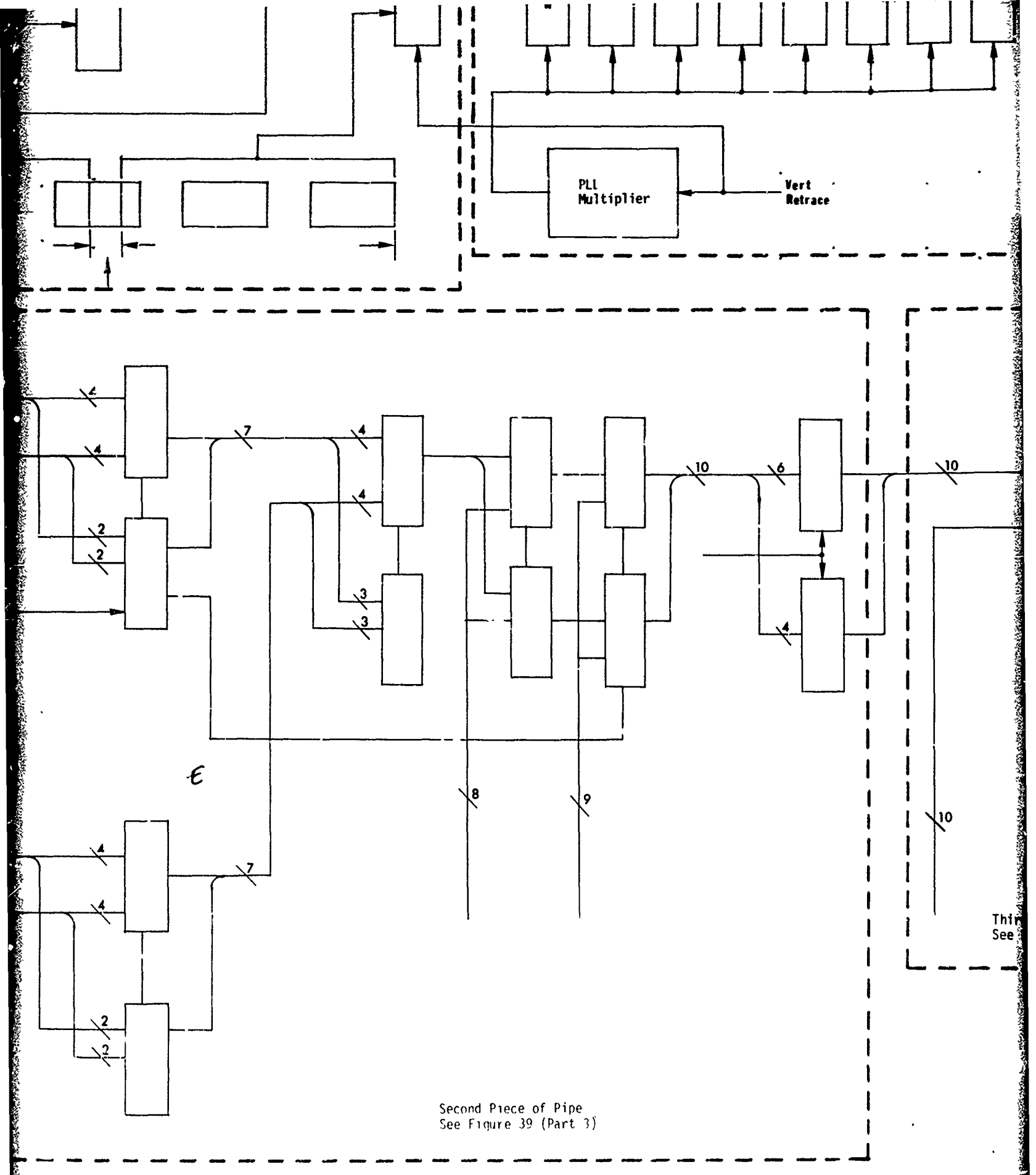

Figure 49 (Part 2) Complete digital correlator circuit

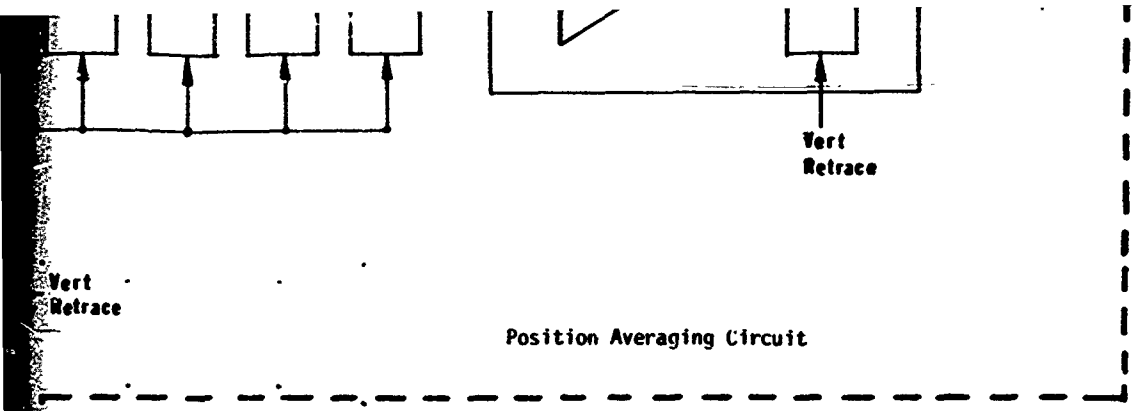

Position Averaging Circuit

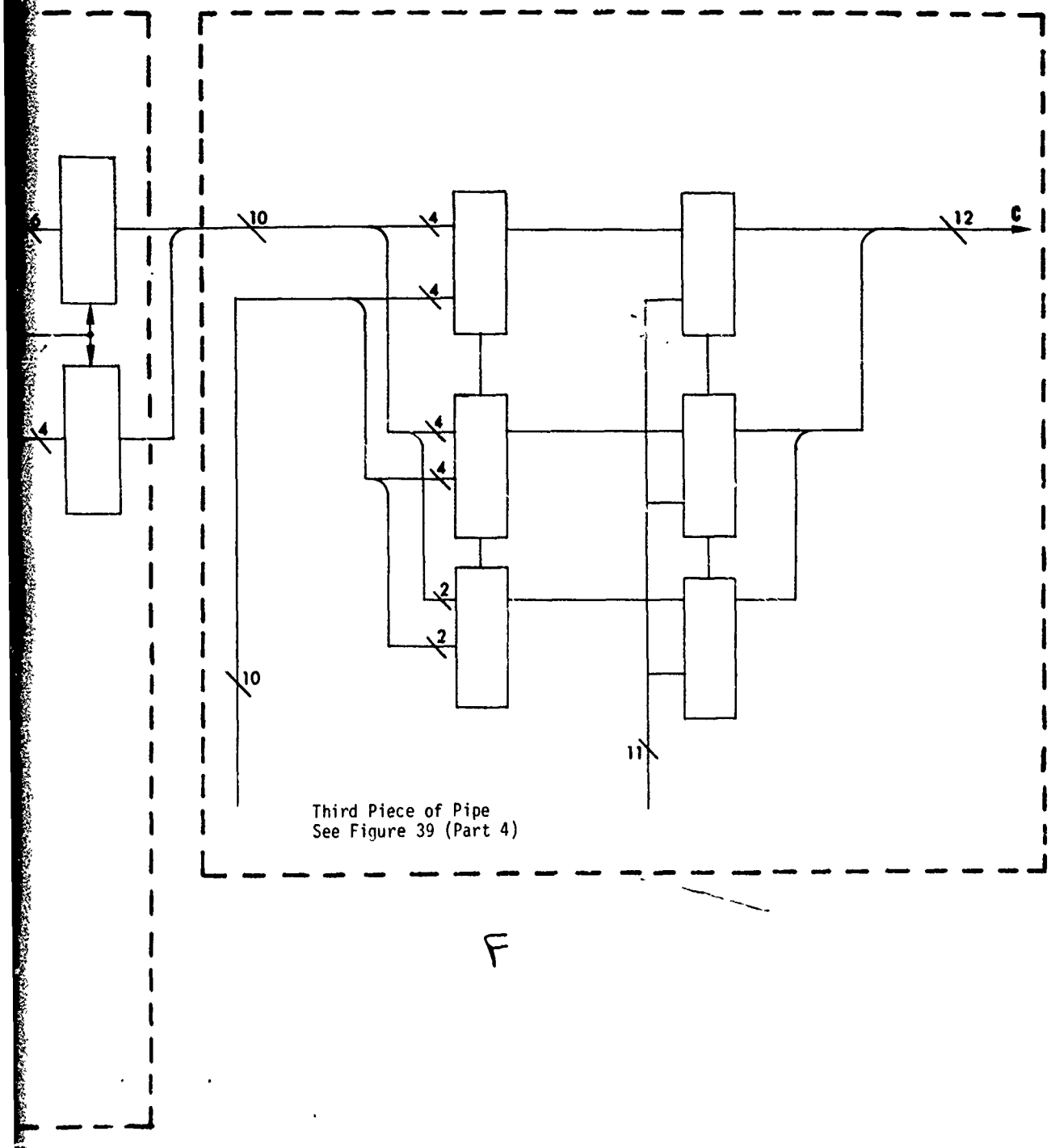

F

resolution signal is separated into video and sync components. The vertical sync is used as a reference to a phase-locked loop circuit (PLL) to provide the HR clock which is used to control the HR sample interval. The HR video is conditioned by a high pass filter to remove the mean or dc component of that signal. The HR signal is then spatially averaged in a field of varying size to reduce resolution to that compatible with the LR image. Selected pulses from the HR clock (again to reduce resolution) are used to load the HR portion of the correlator. The HR buffer is not loaded on every HR frame but at a slower rate. This rate may be target dependent. The LR sync is used as a reference PLL circuit in a manner similar to the HR sync. DC removal is accomplished on a pixel basis by using an approximate local averaging technique. This processed video is sent to the LR correlator buffer. The correlator produces correlation signals at the LR clock rate. The peak of this signal is passed to a peak averaging circuit that reduces the probability of false registration. The y coordinate is adjusted on odd frames. If the maximum detector fails to find a maximum above the specified threshold in a specified number of consecutive fields, the search mode signal is activated in an attempt to locate the target. The correlator speed is the limiting factor in this implementation.

The speed of the correlator is limited by the fan-in at each step of the adder tree. The investigators have recently learned of an integrated circuit available from TRW that forms the XOR of 64 pairs of numbers and sums the resulting products by analog means. (The summing is done by adding currents at a node.) The speed of this device is quoted

in the 5-10 MHz range. It may be possible to employ this device in a correlator implementation that does not require pipeline techniques. The power requirements for this device are also well below the full digital implementation. The analog adder is less precise than the digital one but the system should perform well in either approach. The investigators recommend the analog approach in view of present available information.

5. CONCLUSIONS AND RECOMMENDATIONS

Most of the conclusions and recommendations resulting from the work on this contract have been given and justified within the first four chapters of this report. For compactness they are given again in this chapter.

A. Conclusions

1. A one-bit by one-bit correlator using exclusive OR gate or exclusive NOR gate realization should be used in a hand-off technology program.
2. The one-bit correlator may be either an implementation of the Direct Summation Method (search for a maximum) or the Sequential Simularity Detection Algorithm (search for a minimum) since they are equivalent in a one-bit by one-bit correlator.
3. In a technology program the reference array size should be variable in order to investigate the trade-off of reference array size vs. correlation accuracy using typical military targets and scenes. The size of the reference array in the correlator should be variable up to at least 32 x 64 or 2048 elements. The statistical reliability of the correlator improves as the number of elements increases.
4. The adder tree may be either digital or analog. The digital adder is more accurate but requires more hardware than the analog implementation. There exists more clock timing problems with the digital adder tree.

5. The exclusive OR gates in the correlator should be in special purpose chips, like the one developed by TRW and reported in Chapter Four of this report. These special chips reduce the amount of hardware significantly. Other companies may manufacture similar chips but they are unknown to these investigators.
6. The 32 x 64 correlator should operate on 32 succeeding lines in each TV field rather than 16 lines from one field and the 16 interlaced lines from the next TV field. This implementation is referred to as a half-frame correlator and reduces the required hardware and minimizes the effects of vibration.
7. Some form of image normalization is required to prevent false registration points. For the one-bit by one-bit correlator no normalization is required since the images are already normalized.
8. If a higher level quantizer is desired, there is not much point in using more than four levels from a S/N point of view. If more than two levels are used, care should be taken in how the quantization step levels are obtained. Inaccuracies in the quantization levels between the two video signals could cause a larger reduction in the S/N ratio than that gained by going to more levels. Using more than two levels can cause further degradation because fewer picture elements can be processed in a given time.
9. At the ranges at which the correlator will be operating, it is actually correlating on an area and not the target since the target represents only a small portion of the reference image.

10. **With a 32 x 64 or 2048 pixel reference array, the performance of the correlator will depend almost entirely on the goodness of the preprocessing of the two images. The various preprocessing design parameters should be investigated in a technology program. Realistic sensor differences should be included in this investigation.**
11. **The search pattern shown in Figure 32(b) is recommended if the target is not found in the initial missile seeker FOV.**

B. Objectives of a Technology Program

From the results of this study it is concluded that hand-off of a target from a pointing and tracking system to a missile seeker using a correlator is not only feasible but an attractive option. It is recommended that a correlator be built and used in a technology program to demonstrate this feasibility and to study the various trade-offs discussed in this report. The following are some recommended objectives of such a technology program.

1. Determine overall performance of correlator. Performance criteria include average time for target lock-on, percentage of false lock-ons, percentage of missed targets, etc.
2. Investigate the accuracy of the correlator vs. the size of reference array used. This might be scene dependent.
3. Determine the optimal threshold value to use in the correlator. This is also scene dependent to some extent.
4. Determine the effects of varying the TV signal sampling rate from approximately 3.5 MHz to 8 MHz.

5. Investigate sensitivity of correlation algorithm to quantization about incorrect dc level.
6. Investigate sensitivity of correlation algorithm to errors in W_H and W_V in reducing the resolution of the PTS video to that of the seeker video.
7. Investigate effects of vibration on the correlator accuracy.
8. Determine sensitivity of correlator to sensors with differing spectral responses.
9. Determine rate at which HR reference image must be up-dated with typical moving targets.
10. Investigate sensitivity of correlator to various video S/N ratios.

REFERENCES

1. J. E. Tillery and J. A. Stanford, "Terminal Homing Engineering Flight Test T7/Current Optical Contrast Seeker Missile," Technical Report RG-7T-11, U. S. Army Missile Research, Development and Engineering Laboratory, U. S. Army Missile Command, Redstone Arsenal, AL, 2 September, 1976.

2. A. Papoulis, Probability, Random Variables, and Stochastic Processes, McGraw-Hill Book Company, 1965 (pp. 226-227).

3. R. Price, "A Useful Theorem for Nonlinear Devices Having Gaussian Inputs," IRE Transactions on Information Theory, Vol. IT-4, 1958.

4. "Spatial Frequency Analysis of Vehicle Targets," Delco Electronics, General Motors Corporation, Santa Barbara Operations, 1970.

5. Jan F. Andrus, C. Warren Campbell, and Robert R. Jayroe, "Digital Image Registration Method Using Boundary Maps," IEEE TRANSACTIONS ON COMPUTERS, Vol. C-24 No. 9, pp. 935-940, Sept. 1975.